AD-A174 442 A SELF CONSISTENT ESTIMATE OF THE ELASTIC CONSTANTS OF A RANDOM ARRAY OF..(U) RENSSELAER POLYTECHNIC INST TROY NY DEPT OF CIVIL ENGINEERING.. E PETRAKIS ET AL. 1/2

UNCLASSIFIED JUL 86 RPI-CE-86-04 AFOSR-TR-86-1050 F/G 8/13 NL

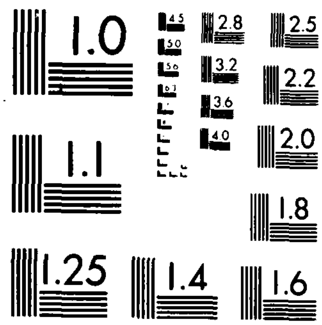

MICROCOPY RESOLUTION TEST CHART
NATIONAL BUREAU OF STANDARDS-1963-A

SECURITY CLASSIFICATION OF THIS PAGE

REPORT DOCUMENTATION PAGE

1a. REPORT SECURITY CLASSIFICATION	1b. RESTRICTIVE MARKINGS
2a. SECURITY CLASSIFICATION AUTHORITY	3. DISTRIBUTION/AVAILABILITY OF REPORT Approved for Public Release; Distribution Unlimited
2b. DECLASSIFICATION/DOWNGRADING SCHEDULE	
4. PERFORMING ORGANIZATION REPORT NUMBER(S) CE-86-04	5. MONITORING ORGANIZATION REPORT NUMBER(S) AFOSR-TR- 86-1050
6a. NAME OF PERFORMING ORGANIZATION Rensselaer Polytechnic Inst. Civil Engineering Dept. 6b. OFFICE SYMBOL (If applicable)	7a. NAME OF MONITORING ORGANIZATION Air Force Office of Scientific Research
6c. ADDRESS (City, State and ZIP Code) Troy, NY 12180-3590	7b. ADDRESS (City, State and ZIP Code) Bldg 410 Bolling AFB, DC 20332-6448
8a. NAME OF FUNDING/SPONSORING ORGANIZATION AFOSR 8b. OFFICE SYMBOL (If applicable) NA	9. PROCUREMENT INSTRUMENT IDENTIFICATION NUMBER ~~SFR Contract No~~. F49620-85-K-~~011~~ 0011
8c. ADDRESS (City, State and ZIP Code) Same as 7B	10. SOURCE OF FUNDING NOS.

PROGRAM ELEMENT NO.	PROJECT NO.	TASK NO.	WORK UNIT NO.
61102F	2302	C1	

11. TITLE (Include Security Classification) A Self Consistent Estimate of the Elastic Constants of a Random Array of Equal Spheres with Application to Granular Soil Under Isotropic Conditions

12. PERSONAL AUTHOR(S) Emmanual Petrakis and Ricardo Dobry

13a. TYPE OF REPORT	13b. TIME COVERED	14. DATE OF REPORT (Yr., Mo., Day)	15. PAGE COUNT
Final	FROM 85/05/06 TO 86/05/05	July 1986	112

16. SUPPLEMENTARY NOTATION

17. COSATI CODES FIELD	GROUP	SUB. GR.

18. SUBJECT TERMS (Continue on reverse if necessary and identify by block number)
Particulate Mechanics; Stress-Strain Relationships; Regular Arrays of Spheres; Isotropy/Transverse Isotropy; Self Consistent Method; Small Strains; Small Modulus

19. ABSTRACT (Continue on reverse if necessary and identify by block number)

The need for a micromechanical approach to modelling the stress-strain response of granular soil is discussed and justified. The report focuses on the small shear strain ($\gamma \leq 0.01\%$) behavior, and investigates the validity of analytically modelling uniform, rounded-grained quartz sands by arrays of identical elastic quartz spheres. As a first step, the stress-strain properties of six regular arrays of spheres are studied in some detail, with focus on isotropic and transversely isotropic boundary loading.

An analytical procedure is established for determining the elastic moduli of a random assemblage of equal elastic spheres of arbitrary mean porosity, subjected to isotropic confining pressure. The procedure uses the properties of the regular arrays already described, it accounts for the spatial distribution of porosity, and it calculates the macroscopic moduli through the Self Consistent Method. The procedure was applied to compute the shear and bulk moduli of assemblages of quartz spheres, which were then

20. DISTRIBUTION/AVAILABILITY OF ABSTRACT UNCLASSIFIED/UNLIMITED ☒ SAME AS RPT. ☐ DTIC USERS ☐	21. ABSTRACT SECURITY CLASSIFICATION
22a. NAME OF RESPONSIBLE INDIVIDUAL Spiro T. Wu	22b. TELEPHONE NUMBER (Include Area Code) 767-4935 | 22c. OFFICE SYMBOL NA

DD FORM 1473, 83 APR EDITION OF 1 JAN 73 IS OBSOLETE.

SECURITY CLASSIFICATION OF THIS PAGE

compared with static and dynamic measurements on quartz sands from the literature. The theoretical sands are significantly stiffer than the actual soils due to the lower number of effective contacts in actual sands. However, excellent agreement was found with resonant column shear modulus measurements on Ottawa sand, after subjecting it to a large number of cycles of shear prestraining, which increased the number of contacts toward the theoretical value.

CE Report No. CE-86-04

A SELF CONSISTENT ESTIMATE OF THE ELASTIC CONSTANTS OF A RANDOM ARRAY OF EQUAL SPHERES WITH APPLICATION TO GRANULAR SOIL UNDER ISOTROPIC CONDITIONS

by

Emmanuel Petrakis and Ricardo Dobry

Prepared under Contract No. F49620-85-K-0011
United States Air Force
Office of Scientific Research
Bolling Air Force Base

Department of Civil Engineering
Rensselaer Polytechnic Institute
Troy, NY 12180-3590

July 1986

FOREWORD

This is one of the two Final Reports of a research sponsored by the Air Force Office of Scientific Research, and it corresponds to the analytical part of the investigation. The second Final Report, corresponding to the experimental part, is being issued separately by the Geotechnical Engineering Center of the University of Texas at Austin, as follows:

"Investigation of Low-Amplitude Compression Wave Velocity in Anisotropic Material," by Shannon H.H. Lee and Kenneth H. Stokoe, II, Report GR86-6, August 1986, 320 pages.

TABLE OF CONTENTS

List of Symbols

Greek Letters:

α^*	: constant; value of the Eshelby S-tensor
α	: relative vertical displacement between the centers of two spheres in contact
$\alpha_{sc}, \alpha_{bcc}, \alpha_{fcc}$	: length of edge of representative volume of the sc, bcc and fcc arrays respectively
β	: constant (= dT/dN)
β^*	: constant; value of the Eshelby S-tensor
γ	: engineering shear strain
$\bar{\gamma}_i$	: average shear strain experienced by inclusion i
γ_t	: threshold strain
γ_{ij}	: engineering shear strains (components of the strain tensor)
δ_{ij}	: Kronecker delta
δ_{ij}	: displacement
δ	: horizontal displacement between the centers of two spheres in contact
ε_{ij}	: strain tensor
$\varepsilon^e_i, \varepsilon^p_{ij}$	: elastic and plastic strains respectively
$\bar{\varepsilon}_{v_i}$	: average volumetric strain experienced by inclusion i
$\bar{\varepsilon}_v$	: average macroscopic volumetric strain
θ	: constant (=f/β)
θ_z	: angle of incidence of S-wave
λ	: coefficient of proportionality in plastic flow rule
λ	: constant, parameter of the probability density function of the void ratio, p(e)
ν	: Poisson's ratio

ν^*	:	macroscopic Poisson's ratio
ν_s	:	Poisson's ratio of the spheres
π	:	3.14159
ρ	:	mass density
σ_{ii} (i=1,2,3)	:	normal stress applied to regular array
σ_{ij}	:	stress tensor
σ_{ij} (i,j=1,2,3)	:	shear stress applied to regular array
σ_a	:	axial stress
σ_a, σ_b	:	principal stresses in directions of propagation and polarization
σ_c	:	principal stress in direction of no propagation/no polarization
σ_o	:	isotropic confining pressure
$\bar{\sigma}_o$	:	mean effective stress
σ_i (i=1,2,3)	:	principal stress
$\bar{\sigma}_i$ (i=1,2,3)	:	effective principal stress
$\bar{\sigma}_o^i$	:	istropic stress experienced by inclusion i
σ_o^o	:	applied isotropic stress
τ^o	:	applied shear stress
τ	:	shear stress
τ^*	:	shear stress at failure ($=f\sigma_o$)
σ_v,σ_n	:	vertical and horizontal stresses
Latin Letters	:	
A	:	area of face of elementary volume
a	:	constant ($0.15 \leq a \leq 0.23$)
a	:	radius of area of contact between two spheres in contact
C	:	constant

$C_{ijk\ell}$	: Compliance Matrix
C_n, C_t	: Normal and Tangential Compliance respectively
C_n	: Uniformity Coefficient
c_i	: volume concentration
D	: Constrained Modulus
$\overline{D}, D$	: Displacement between centers fo two spheres in contact
D_{10}	: percent passing
$\overline{dD}, dD$	: Displacement increment
E	: Young's Modulus
E_s	: Young's Modulus of the spheres
e	: void ratio
e_{min}, e_{max}	: minimum and maximum void ratio respectively
$\overline{e}$	: mean void ratio
F	: constant
$f(\sigma_{ij})$	: yield function
f	: friction coefficient
FEM	: finite element method
G_i	: shear modulus of inclusion i
G^*	: macroscopic shear modulus
G	: shear modulus, secant shear modulus
G_s	: shear modulus of the spheres
$\overline{G}$	: normalized shear modulus
G_{max}	: shear modulus at very small strains
$g(\sigma_{ij})$	: plastic potential
H, H_o, H_e	: tangential elastoplastic and elastic moduli
I_1	: first invariant of the stress tensor
K_i	: Bulk Modulus of inclusion i

K^*	: macroscopic Bulk modulus
K	: stress ratio ($K = \sigma_z/\sigma_o$)
k	: constant $[k = (2-\nu_s)/2(1-\nu_s)]$
L	: constant $(= T/fN_o)$
L^*	: constant $(= T^*/fN_o)$
M	: constant
m	: constant
ma, mb, mc	: constants
n	: constant
n	: porosity
$\overline{n}$	: mean porosity, macroscopic porosity
n_{min}, n_{max}	: minimum and maximum porosity respectively
N	: Number of cycles
N	: Number of phases or materials
N	: Normal force
N'_{ij}	: Contact forces at local coordinate system
N_{ij}	: Contact forces
N_o	: Normal contact force due to application of σ_o
N	: constant
$\overline{N}, N$	: contact normal force
P	: constant
$\overline{P}, P$	: contact force
P_a	: atmospheric pressure
P_{ij}	: applied forces
$p(x)$	: probability density function of x
R	: radius of spheres

S_x, S_y, S_z	:	elastic constants
$S_{ijk\ell}$	:	Stiffness matrix
T_x, T_y	:	Tangential contact forces in x and y directions
dT_n, dT_t	:	outward normal and tangential components to the yield surface of the applied tangential force increment
t, t_o, t_1	:	time
x_i	:	coordinate
$\overline{T}, T$	:	tangential force
T^*	:	tangential force at failure (= fN_o)
V_p, V_s	:	P and S wave velocities
V_L	:	rod wave velocity

ACKNOWLEDGEMENTS

The authors wish to acknowledge the following people and organizations for their valuable assistance in this project.

The Air Force Office of Scientific Research (AFOSR), Bolling Air Force Base, Washington, D.C. for sponsoring the research (Contract No. F49620-85-K-0011); and Lieutenant Colonel Lawrence Hokanson, project manager, for his warm support and encouragement.

The Dept. of Civil Engineering of the University of Texas at Austin, for the warm hospitality and support provided to the two authors during their stay in Austin in 1985.

Professor Kenneth H. Stokoe, II of the University of Texas at Austin (UT), for his wholehearted support, hospitality, encouragement, cooperation and many stimulating discussions, and Dr. Shannon H.H. Lee, also of UT, for sharing with us some of his valuable experimental data.

Professor George Dvorak of Rensselaer Polytechnic Institute (RPI), for his suggestions, which were most valuable in developing the analytical model of Section 6.

Professor Mark S. Shephard, also of RPI, and the staff of RPI's Interactive Computer Graphics Center, for their ideas and work related to the use of computer graphics in modelling granular arrays.

ABSTRACT

The need for a micromechanical approach to modelling the stress-strain response of granular soil is discussed and justified. The report focuses on the small shear strain ($\gamma \leq 0.01\%$) behavior, and investigates the validity of analytically modelling uniform, rounded-grained quartz sands by arrays of identical elastic quartz spheres. ~~As a first step,~~ the stress-strain properties of ~~six~~ regular arrays of spheres are studied ~~in some~~ detail, with focus on isotropic and transversely isotropic boundary loading.

An analytical procedure is established for determining the elastic moduli of a random assemblage of equal elastic spheres of arbitrary mean porosity, subjected to isotropic confining pressure. The procedure uses the properties of the regular arrays already described, it accounts for the spatial distribution of porosity, and it calculates the macroscopic moduli through the Self Consistent Method. The procedure was applied to compute the shear and bulk moduli of assemblages of quartz spheres, which were then compared with static and dynamic measurements on quartz sands from the literature. The theoretical sands are significantly stiffer than the actual soils due to the lower number of effective contacts in actual sands. However, excellent agreement was found with resonant column shear modulus measurements on Ottawa sand, after subjecting it to a large number of cycles of shear prestraining, which increased the number of contacts toward the theoretical value.

Section 1

INTRODUCTION

The main objective of this report is to present a simple, yet rigorous, particulate mechanics model of the stress-strain response of granular soil under isotropic boundary loading at very small shear strains, γ, of the order of 10^{-4}% or less. The proposed model idealizes sand as a combination of regular arrays of elastic, rough spheres and uses Mindlin's formulation for the contacts. In turn, this is the first stage of a long-term attempt to model sands as 3-D spatial arrangements of regular arrays at both small strains ($\gamma \leq \gamma_t \simeq 0.01\%$) and large strains ($\gamma > \gamma_t \simeq 0.01\%$), where $\gamma_t \simeq 0.01\%$ is the threshold strain for densification and pore water pressure buildup(*). A second stage will include anisotropically loaded granular media, and the ultimate goal is to perform 2-D and 3-D computer simulations of arrays of spheres at different small and large strain ranges, including analytical modelling of densification under boundary cyclic loading.

This is a final report of a research on the subject performed by the authors in cooperation with a U. of Texas team headed by Prof. Stokoe.

"Elastic constants" of interest at very small strains include the shear and bulk moduli and the Poisson's Ratio(s). Experimental results and basic considerations indicate that these "constants" depend on both the void ratio of the soil and the state of confining stresses. The variations of these moduli and of the damping of the soil with an applied shear strain up to the threshold are also of interest, as is the value of the threshold strain itself at which

(*) The concepts of small and large shear strains as used here are consistent with usual Soil Dynamics terminology, but they do not coincide with that of traditional Soil Mechanics, where much greater strains, about 1% or larger are usually of interest.

gross sliding occurs at the grains' contacts.

These small strain soil parameters are very important in geotechnical engineering problems involving cyclic loading or wave propagation in the soil, such as: ocean wave loading, soil structure interaction, site response, ground settlement and liquefaction during earthquakes. Due to this, a great number of experimental studies of small strain behavior have been performed, and correlations have been developed for practical use. Especially important are the equations for the shear modulus at very small strains, G_{max}, in sands developed by Hardin and Richart (1963) and Seed and Idriss (1970) on the assumption that these soils can be treated as elastic isotropic solids. In both correlations, discussed in more detail in Section 2, $G_{max} = A \cdot (\bar{\sigma}_o)^{0.5}$, with $\bar{\sigma}_1$, $\bar{\sigma}_2$, $\bar{\sigma}_3$ being the effective principal stresses, $\bar{\sigma}_o = (\bar{\sigma}_1 + \bar{\sigma}_2 + \bar{\sigma}_3)/3$ is the mean effective stress and A is a soil constant which depends on void ratio or relative density. Both correlations assume that G_{max} (and thus, also, the shear wave velocity, $V_s = (G_{max}/\rho)^{1/2}$), is the same for isotropically or anisotropically loaded sand, provided that the mean stress $\bar{\sigma}_o$ is the same; also, both correlations assume that for the anisotropic loading case G_{max} and V_s do not change with direction.

These assumptions for G_{max} in sands have been challenged more recently by the experimental results obtained by Roesler (1979), Knox et al. (1982) and Yu and Richart (1984), as discussed in Section 2. Therefore, a main motivation for this work was the need, suggested by those experimental findings, for a fresh approach to our basic understanding of G_{max} and other small-strain soil parameters. Some preliminary analytical results previously obtained by the senior author (Dobry et al., 1982) had shown that a particulate mechanics approach was very well suited to this purpose, and should be the basis of this fresh approach.

The large strain ($0.01\% \leq \gamma \leq 1\%$) behavior of granular soils is also very important in engineering problems involving cyclic loading, and especially those related to earthquakes. At these strains, the stress-strain behavior becomes strongly nonlinear and hysteretic, and rearrangement of particles take place producing phenomena such as densification and pore water pressure build-up (Silver and Seed, 1971; Youd, 1972; Dobry et al., 1982; National Research Council, 1985). A number of continuum mechanics models, based mostly on the Incremental Theory of Plasticity, try to simulate this behavior and have been proposed for soils, as discussed in Section 3.

A summary literature review of previous relevant particulate mechanics studies is presented in Section 4. Many of these past investigations have focused on the very large strain ($\gamma > 1\%$) and strength behavior of granular soils; at those very large strains, gross sliding and rolling of the grains are main contributors to the overall strain, while the elasticity of the particles and contacts play a minor or negligible role. On the other hand, for the small to large strain ranges of interest of the proposed research, the elasticity of the particles and the details of the force-displacement response at the contacts are very significant factors. The discussion in Section 4 includes a general model recently proposed for the force-displacement response at the contact between two identical elastic spheres (Seridi and Dobry, 1984).

The results of the present research are discussed in Sections 5 and 6. Section 5 presents a detailed study of the differential stress-strain relations for various regular arrays of spheres. Section 6 describes an application of these findings, using the Self-Consistent Method, to a random arrangement of regular arrays subjected to isotropic boundary loading, and with the arrangement having an arbitrary macroscopic void ratio.

Section 2

LABORATORY MEASUREMENTS ON SANDS AT SMALL STRAINS

Starting around 1960, a number of cyclic and dynamic laboratory measurements have been performed to determine the stress-strain behavior of granular arrays and of natural sands at small strains. Properties studied have included: i) maximum shear modulus at very small strains, G_{max}; ii) the variation of secant modulus, G, with shear strain, γ; iii) the Poisson's ratio of the soil; iv) the variation of shear damping ratio with strain; and v) the threshold shear strain, γ_t, at which densification and pore pressure buildup start. Many of these tests have been conducted in a triaxial cell, on sand specimens isotropically or anisotropically consolidated under a biaxial stress state ($\sigma_2 = \sigma_3$ or $\sigma_2 = \sigma_1$), with the small strain measurements performed using the pulse method, the resonant column or cyclic torsional techniques, and with particular emphasis on shear modulus determinations. Important results and state-of-the-art summaries of these modulus measurements have been presented by Duffy and Mindlin (1957), Hardin and Richart (1963), Lawrence (1965), Richart et al. (1970), Seed and Idriss (1970), Hardin and Drnevich (1972), Woods (1978), Iwasaki et al. (1978), and Tatsuoka et al. (1979).

As mentioned before, "small strains" are defined here by the condition $\gamma < \gamma_t$, as in this range the original geometry of the granular array or sand remains essentially unchanged, with very few or no particles experiencing gross sliding or rolling, and, thus, with the macroscopic strain of the array being controlled by the elastic deformations of the particles and by localized slips within the areas of contact areas between particles. In many sands, $\gamma_t \approx 10^{-4} = 10^{-2}\%$; measurements and studies of γ_t have been presented by Drnevich and Richart (1970), Youd (1972), Pyke (1973), Dobry et al. (1980, 1981, 1981a,

1982), Dyvik et al. (1982), Oner (1984) and National Research Council (1985).

On the basis of laboratory measurements, Hardin and Richart (1963) proposed the following expression for G_{max}:

$$G_{max} = f(e)(\bar{\sigma}_o)^{0.5} \tag{1}$$

where e = void ratio, $f(e) = 2630(2.17-e)^2/(1+e)$ for round-grained sands, and $f(e) = 1230(2.97-e)^2/(1+e)$ for angular-grained sands; both G_{max} and $\bar{\sigma}_o$ are in psi in Eq. 1.

Seed and Idriss (1970) proposed the alternative expression:

$$G_{max} = 1{,}000\ K_{2max}\ (\bar{\sigma}_o)^{0.5} \tag{2}$$

where G_{max} and $\bar{\sigma}_o$ are in psf, and K_{2max} is a function of relative density.

Eqs. 1-2 reflect the conclusion of these and other studies, that G_{max} and V_s are mainly a function of void ratio or relative density, and of the mean effective normal stress $\bar{\sigma}_o$. Other variables, such as static shear stresses, stress history, stress path (compression versus extension loading), frequency of cyclic loading, degree of saturation, were found to have, either a small effect or no effect at all (Richart et al., 1970, Yu and Richart, 1984). One exception is that a large number of shear prestraining cycles at strains larger than the threshold was found to increase G_{max} significantly (Drnevich and Richart, 1970).

It is useful to make explicit some of the implications of Eqs. 1-2 for anisotropically loaded dry sand, either for the general "triaxial" case in which $\sigma_1 \neq \sigma_2 \neq \sigma_3$ or, as is very usually the case in the field, or for the "biaxial" case, $\sigma_1 \neq \sigma_2 = \sigma_3$. (The bars have now been dropped from the stresses, as for a dry sand, $\bar{\sigma} = \sigma$). These implications are:

i) G_{max} and V_s depend equally on σ_1, σ_2 and σ_3.

ii) For a shear wave propagating in the sand, the value of V_s is the same whatever the directions of propagation and polarization of the wave.

Implication ii) is equivalent to assume that, at very small strains, the anisotropically loaded sand can be modeled as an isotropically elastic material, defined by the two elastic constants G_{max} and Poisson's Ratio, ν. Under the usual additional assumption that for a dry sand, $\nu \approx 0.3$ to 0.4 is a constant independent of confining stresses, a set of implications similar to i) and ii) can be obtained, but now for a dilational, P-wave, travelling in this dry sand. If we call D, V_p the constrained modulus and P-wave velocity, the corresponding implications are:

iii) D and V_p depend equally on σ_1, σ_2 and σ_3, with D $\alpha(\sigma_o)^{0.5}$ and V_p $\alpha(\sigma_o)^{0.25}$.

iv) The value of V_p is the same whatever the direction of propagation of the P-wave.

Five recent experimental studies have attempted to verify in detail this formulation by Hardin/Richart and Seed/Idriss, and specifically the validity of implications i) through iv) above for anisotropically loaded dry sand.

Schmertmann (1978) measured V_p and V_s in several directions in a large dry sand specimen (4 ft diameter by 4 ft high). In these tests, a biaxial state of stress could be achieved, $\sigma_1 = \sigma_v \neq \sigma_2 = \sigma_3 = \sigma_h$, with σ_v, σ_h = vertical, horizontal stresses, with the stresses varying between 5 to 20 psi, and with a stress ratio, $\sigma_1/\sigma_3 = 1$ to 3. He found that there was a slight amount of inherent anisotropy (different wave velocities in the horizontal and vertical directions when $\sigma_v = \sigma_h$). He also found that for constant $\sigma_o = 1/3(\sigma_v + 2\,\sigma_h)$ and variable σ_1/σ_3, V_s varied less than 10%, thus verifying the basic Hardin/Richart assumption as a first approximation for V_s in this biaxial case. However, V_p

was strongly affected by σ_1/σ_3. The results suggested that, for P-waves propagating in the vertical direction, V_p depended more on σ_v than on σ_o.

Roesler (1979) measured V_s using a 1 ft^3 cubical dry sand sample. In these tests, a true triaxial state of stresses was achieved. Test pressures ranged from 5.8 psi to 23 psi, with σ_1/σ_3 = 1 to 1.8. He propagated the shear waves along either of the principal stress directions (σ_a), with particle motions polarized in another principal direction (σ_b). The third principal direction, or out-of-plane direction, is neither a direction of propagation nor polarization (σ_c). Roesler found that his results followed the law:

$$V_s = B\ \sigma_a^{0.149}\ \sigma_b^{0.107}\ \sigma_c^{0} \tag{3}$$

where B = constant. These results are illustrated in Fig. 1. For isotropic confinement ($\sigma_o = \sigma_a = \sigma_b = \sigma_c$) they do confirm the Hardin-Richart law that G_{max} $\alpha(\sigma_o)^{0.5}$ and V_s $\alpha(\sigma_o)^{0.25}$, as 1.49 + 0.107 = 0.256. However, for the general case, Eq. 3 contradicts Eqs. 1-2, in that now V_s is completely independent of σ_c. Also, Roesler's results for this case indicate that V_s is a function of direction and the sand cannot be treated as an isotropic elastic material; therefore, more than two elastic constants are necessary to define it.

Stokoe et al. (1980) developed at the University of Texas at Austin (U.T.) a large scale, 7 ft^3 cubical triaxial facility, for the specific purpose of measuring V_s and V_p in dry sand. In this facility, a triaxial state of stress, $\sigma_1 \neq \sigma_2 \neq \sigma_3$ can also be achieved. All tests performed to date at U.T. have used a local medium to fine, washed mortar sand classified as SP, with effective grain size, D_{10} = 0.28 mm and a uniformity coefficient C_u = 1.7. The sand is placed by the raining technique and is tested dry. Values of principal stresses used have ranged between 10 psi and 40 psi, with the stress ratio, σ_1/σ_3 = 1 to 4. Knox et al. (1982) used this facility to study V_s and,

similarly to Roesler, they propagated the shear waves along one of the principal stresses (σ_a), and polarized parallel to another principal stress (σ_b). They expressed V_s as:

$$V_s = F \; \sigma_a^{ma} \; \sigma_b^{mb} \; \sigma_c^{mc} \tag{4}$$

where F = constant. They found values of ma ≈ mb = 0.09 to 0.12, and mc ≈ 0 to 0.01. Except for some minor differences, these results are identical to those of Roesler, including the independence of V_s on σ_c. Kopperman et al. (1982) used the same U.T. facility and sand to study P-waves and concluded that:

$$V_p = L \; \sigma_a^{0.22} \tag{5}$$

where L = constant. The insensitivity of V_p to variations in the stresses σ_b and σ_c perpendicular to wave propagation is illustrated by Fig. 2. Again, and similar to Schmertmann's findings, these results indicate that V_p is strongly dependent on direction of propagation when the sand is anisotropically loaded.

Yu and Richart (1984) performed resonant column tests on three sands subjected to a biaxial state of stress. Their results essentially agreed with those of Roesler and Knox; however, they found some effect of the stress ratio on the results. They proposed for G_{max} the expression:

$$G_{max} = CP_a^{0.49} \; \sigma_v^{0.26} \; \sigma_h^{0.25} \; (1-a \; K_n^2) \tag{6}$$

where C=constant, P_a=atmospheric pressure, a=0.15 to 0.23, with a mean value of 0.18, $K_n=(\sigma_1/\sigma_3-1)/[(\sigma_1/\sigma_3)_{max}-1]$, and $(\sigma_1/\sigma_2)_{max}$ corresponds to shear failure of the sand. Except for the factor $1-a \; K_n^2$, which is usually between 0.8 and 1, Eq. 6 is consistent with Eqs. 3 and 4 proposed by Roesler and Knox.

Therefore, all of these results clearly indicate that implications i) through iv) above, associated with the currently used correlations for V_p and

V_s in sands, need to be revised and upgraded. In most cases of practical interest, sands are anisotropically loaded, and thus more than two elastic constants may be needed to specify the behavior of the soil at very small strains. For the typical biaxial state of stresses existing in the field under geostatic conditions, for which all horizontal normal stresses are equal but different from the vertical stress, the sand will behave as a cross-anisotropic elastic solid and 5 elastic constants will be generally needed (Love, 1927, Sokolnikoff, 1956). In the more general case of $\sigma_1 \neq \sigma_2 \neq \sigma_3$, as it may happen in the soil under a structure, the sand can be described as an orthotropic elastic solid, with three planes of elastic symmetry, and a total of 9 elastic constants are needed (Sokolnikoff, 1956).

The previous discussion focused on the elastic properties of sand at very small strains, $\gamma \approx 10^{-4}\%$, and especially on V_p and V_s measurements. If larger loads and strains are applied to a dry granular soil, compression-wave type loading induces a nonlinear locking stress-strain response, while shear-wave type loading induces a yielding response (see Fig. 3). This behavior is obviously associated with the particulate nature of the soil (Seed and Idriss, 1970; Hardin and Drenvich, 1972). During cyclic shear loading in sand, stress-strain hysteresis loops are generated such as shown in Fig. 4; these loops are essentially strain-rate and frequency independent. For small strains, $\gamma < \gamma_t \approx 10^{-2}\%$, the hysteretic loop repeats itself cycle after cycle, and no permanent volumetric strain is observed, thus suggesting an essentially non-destructive though nonlinear behavior, controlled mainly by the response of the contacts between the grains, and with no coupling between shear and volumetric strains. At shear strains, $\gamma > \gamma_t$, although the overall behavior remains approximately the same, densification occurs, and there is also some increase in stiffness, with the shear stress-strain curve and the tips of the loop going up a little

as the number of cycles increases (see Fig. 4). For the strain range $0.01\% < \gamma < 0.1\%$ to 1%, the monotonic and cyclic behavior of the sand is always contractive, that is, shear strains generate exclusively compressive volumetric strains, independently of the density of the sand. However, for strains larger than about $\gamma \simeq 1\%$, a mixture of contractive and dilative behavior is measured in dense sands, with expansion of the soil occurring during part of the cycle in cyclic shear loading (Youd, 1972). At all strains, and for both shear and compression-type cyclic loading, the stress-strain response of dry granular soil is strongly dependent on the level of normal stresses acting on it.

Section 3

STRESS-STRAIN MATHEMATICAL MODELLING

A significant amount of research has been directed to obtain stress-strain constitutive relations for cyclic and dynamic loading of soil. Most of these studies have modelled the soil as an elastic-plastic material, using as a basis tool the Incremental Theory of Plasticity. In this type of model, which is particularly appropriate for dry granular soil, the total strain increment is equal to the sum of elastic and plastic strain increments, $d\varepsilon_{ij} = d\varepsilon_{ij}^{e} + d\varepsilon_{ij}^{p}$, with all $d\varepsilon$ being strain rate independent (Drucker and Prager, 1952; Reyes, 1966; Chen, 1975; Lade and Duncan, 1975; Prevost, 1978; Hardin, 1978). Based on the V_p measurements by Roesler previously described in Section 2, Hardin (1980) suggested the following expressions for $d\varepsilon_{ij}^{e}$ in dry granular soil:

$$\left.\begin{aligned} d\varepsilon_x^e &= \frac{F(e)}{P_a^{1-n}} * \left(\frac{d\sigma_x}{S_x \sigma_x{}^n} - \nu\,\frac{d\sigma_y}{S_y \sigma_y{}^n} - \nu\,\frac{d\sigma_z}{S_z \sigma_z{}^n}\right) \\ d\gamma_{xy}^e &= \frac{2(1+\nu)F(e)}{P_a{}^{1-n}\, S_{xy}} * \left(\frac{d\tau_{xy}}{(\sigma_x\sigma_y)^{n/2} - \dfrac{\tau_{xy}{}^{2+n}}{\sigma_x\sigma_y}}\right) \end{aligned}\right\} \qquad (7)$$

where ε_x^e = normal strain, $\gamma_{xy}^e = 2\varepsilon_{xy}^e$ = engineering shear strain, and four additional equations are obtained by permutation of subscripts. In these equations, σ_x, σ_y and σ_z = normal stresses; τ_{xy} = a shear stress; P_a = atmospheric pressure; and $F(e) = 0.3 + 0.7\ e^2$, where e = void ratio. Eqs. 7 contain five elastic constants (S_x, S_y, S_z, S_{xy} and ν); based on Roesler's experimental V_p results, a power of stress n = 0.5 was proposed.

A variety of associated and nonassociated flow roles have been proposed for the plastic strain increment, of the form:

$$d\varepsilon_{ij}^{p} = \lambda \frac{\partial g}{\partial \sigma_{ij}} \qquad (8)$$

where λ = coefficient of proportionality, and $g(\sigma_{ij})$ is the plastic potential function, which may or may not coincide with the yield function $f(\sigma_{ij})$ at which plastic strains develop. Figure 5 shows the shapes of a number of plastic potential surfaces proposed for soil by different authors.

In the simplest type of elastic-plastic model, there is only one yield (failure) surface. For stresses below that surface, the behavior is assumed to be perfectly elastic. However, granular and other soils develop plastic strains even at the small shear strains of interest to this report. To allow for this behavior, a wide variety of strain-hardening laws have been proposed, including families of yield surfaces and specific strain-hardening yield rules. In some of these models, the elastic region is completely eliminated, thus allowing for plastic flow at very low levels of stress and strain (Mroz, 1967; Prevost, 1977). One of the earliest developments included various cap models, based on the work done at Cambridge University by Roscoe and his co-workers (i.e., Roscoe, 1970). This includes the models proposed in several papers by DiMaggio and Sandler (1971), which have been widely used for dynamic analyses of soil response to explosions. Several capped yield models are included in Fig. 5.

An important aspect of the development of elastic-plastic models is the definition of the strain-hardening law, which defines the modifications of the yield surface(s) in the course of the plastic flow. This is especially critical for cyclic loading, where the type of strain-hardening determines the stress-strain behavior after load reversals. In most of the models described above, which were originally developed for monotonic loading, isotropic strain-hardening is assumed (Hill, 1950), with the yield surfaces expanding as the

stresses increase (Fig. 6). When isotropic hardening is assumed, a large amount of load reversal is required for additional yielding to occur, in contradiction with the observed behavior of experimental hysteresis loops such as shown in Fig. 4.

A better alternative for earthquake loading is provided by the kinematic strain-hardening law, sketched in Figure 7. The kinematic model was originally proposed by Ishlinsky (1954) and Prager (1955). Iwan (1967) proposed a reological representation for the stress-strain model, constituted by infinite elasto-plastic elements, placed in series or in parallel. This model is a nonfrictional one, with all the nested yield surfaces being circular cylinders in principal stress space. Mroz (1967, 1969) proposed a general model for elastic-plastic materials, composed also of a field of yield surfaces, with a combination of kinematic and isotropic strain-hardening laws. Prevost (Prevost and Hoeg, 1975; Prevost, 1977, 1978), Mroz, Norris and Zienkiewicz (1978, 1979) and Vicente and Dobry (1985), have proposed to use this model to predict static and cyclic behavior of soils. The model is flexible enough to allow its adaptation to the cases of drained and undrained loading, and to incorporate important large strain cyclic phenomena such as densification, liquefaction and stiffness degradation. Anisotropically loaded soils are represented by nonsymmetric nested surfaces in stress space. Under cyclic shear loading, the strain-hardening behavior is basically kinematic for the reasons described above. A simultaneous isotropic hardening (or softening) is allowed with the corresponding expansion or contraction of the yield surfaces as cyclic loading develops. This isotropic expansion (contraction) thus could simulate in dry granular soil the observed increase of stiffness caused by cyclic loading above $\gamma_t \simeq 10^{-2}\%$.

Section 4

THE MICROMECHANICAL APPROACH

Eqs. 1-2 for G_{max} and similar expressions for other small strain moduli in dry sands assume that the controlling normal stress parameter is the mean stress σ_o: $G_{max} = f(\sigma_o)$. This functional relationship, selected on the basis of limited experimental evidence, was no doubt influenced by a continuum mechanics view of the situation, as σ_o is proportional to the first invariant of the stress tensor. As discussed in Section 2, more detailed measurements have revealed the elastic anisotropy of a dry sand subjected to different principal stresses, and they have also shown that the functional relationship between principal stresses σ_1, σ_2, σ_3, on one hand, and G_{max} and other elastic constants on the other, is not $G_{max} = f(\sigma_o)$ but rather $G_{max} = f(\sigma_a, \sigma_b)$; similarly, for the constrained modulus, $D = f(\sigma_a)$. Derivations shown later in Section 5.1 for a simple cubic regular array of elastic rough spheres match very well with those recent experimental findings in sands. This strongly suggests that a micromechanical (particulate mechanics) approach should be used to analytically simulate and generalize the experimental observations.

A great number of studies have been performed using particulate models to understand and model the behavior of cohesionless soils and other granular materials. Most of these investigations have been analytical, but they have also included measurements in actual granular soils, as well as in regular or random arrays of spheres (3-D) or disks/rods (2-D); a number of them have dealt with the load-deformation characteristics at the contact between two elastic bodies possessing friction (Mindlin's problem). State-of-the-art summaries have been presented by Deresiewicz (1958, 1973), Mogami (1965), Scott and Ko (1969), Richart et al. (1970), White (1965), Harr (1977), and

Dobry and Grivas (1978), between others. The proceedings of two US/Japan seminars on the mechanics of granular materials contain excellent papers on the subject (Cowin and Satake, 1978; Jenkins and Satake, 1983).

A number of these studies have focused on the probabilistic aspects and statistical distributions of different parameters within the soil or granular medium, and their effect on the mechanical behavior of the array. These have included investigations of the orientations of the individual particles, of the spatial distribution of porosity, and of the distribution of number, orientation and levels of force transmitted by the contacts, conducted between others by Smith et al. (1929), Dantu (1957), Field (1963), Mogami (1965), Grivas and Harr (1974), Oda (1974), Yanagisawa (1978), Shahinpoor and Shahrpass (1982), Nemat-Nasser and Mehrabadi (1983), and Dobry and Petrakis (1984).

Many of those analytical investigations, computer simulations and observations have focused on the stress-strain behavior at very large strains and on the failure of dry granular media. Because of this very large strain nature of the phenomena, the load-deformation characteristics of the particles' contacts have played a minor or negligible role, and the emphasis has been on changes in the geometric arrangement of the grains due to their sliding and rolling. In some of these investigations the compliance of the contacts has been eliminated altogether by assuming perfectly rigid particles. Some important references here are Rowe (1962), Morgenstern (1963), Horne (1965), Konishi (1978), and Oda et al. (1983). Cundall and Strack (1983) performed numerical experiments of 2-D random arrays of disks using an explicit finite difference procedure (see Fig. 8). In these, the authors successfully simulated "compression triaxial" loading to failure, and studied in detail the spatial distribution of contact forces and the distribution and relative contributions of sliding and rolling to macroscopic strain, during anisotropic

deviatoric loading with constant σ_3. One of their conclusions for this deviatoric loading is that the major principal stress σ_1 is transmitted mainly by a few "stiff chains" of particles having large contact forces, with the particles in between chains being lightly loaded; sliding and rolling occurs mainly in those lightly loaded regions. Oner (1984) worked with a similar numerical scheme to predict the observed threshold strain γ_t at which sliding and rolling starts, while Dobry et al. (1982) used a regular simple cubic array of spheres for the same purpose.

Of special interest are the investigations which have studied the stress-strain behavior of granular arrays considering the elasticity of the particles and the corresponding compliances at the contacts. Most of these studies have assumed spherical grain shapes and elastically isotropic grains characterized by three material constants (two elastic and one friction coefficient). All of these investigations have used the normal and tangential compliances at the contact between two elastic bodies, derived by Hertz (1882), Cattaneo (1938), and Mindlin and his co-workers (Mindlin, 1949, Mindlin et al. 1951, Mindlin and Deresiewicz, 1953). Figures 9 and 10 show, respectively, the distorsion of two spheres subjected to normal (N) and tangential (T) contact loads, and the tangential load-displacement curve for constant N. As noted in the summary reviews of the contact theory by Deresiewicz (1958, 1973) and Dobry and Grivas (1978), Mindlin and his co-workers developed the basic theoretical framework of the contact problem, and solved it for some special force time histories; however, the general problem of computing the displacements for a contact force $\vec{P} = \vec{N} + \vec{T}$, whose magnitude and direction change arbitrarily, remained unsollved. Only very recently, Seridi and Dobry (1984) provided a general and practical solution to this general problem, thus making it possible the use of direct stiffness and finite difference techniques to simulate the 3-D response

of granular array at small strains. A more detailed discussion of this general solution is presented in Section 4.1.

The contact theory has been repeatedly used to predict the elastic stress-strain properties of granular arrays of spheres. Several authors calculated the influence of isotropic confining pressure on V_p and V_s for various arrays of smooth and rough spheres, and concluded that both velocities increase proportionally to $(\sigma_o)^{1/6}$ (Hara, 1935, Takahashi and Sato, 1950, Gassman, 1951, White and Sengbush, 1953, Brandt, 1955). Of special interest here are some detailed analytical and experimental investigations of regular arrays of equal spheres. Deresiewicz (1958) lists the five stable regular arrays included in Table 1 and sketched in Fig. 11, which range from the loosest simple cubic, (void ratio, e = 0.91) to the densest pyramidal (also called face centered cubic array) and tethraedral (also called hexagonal close packed), both with e = 0.35. More complete lists and descriptions of feasible regular arrays have been presented by Filep (1936), Brown (1978) and Shahinpoor (1981). Table 2 reproduces one of these lists containing 31 arrays, while Fig. 12 presents elevation and plane views for one of the loosest arrays of Table 2 (Cell No. 2 with e = 1.94). Deresiewicz (1958a) investigated in detail the simple cubic array subjected to an initial isotropic loading followed by an arbitrary stress history. He found that the array is statically determinate in this case, provided that the stress field is uniform, with a one-to-one correspondence between the nine components of the stress tensor and the nine independent components of the contact forces. Whitman et al. (1964) studied a 2-D version of the simple cubic array subjected to triaxial and confined compression. Duffy and Mindlin (1957), Duffy (1959) and Hendron (1963) investigated the densest arrays of Fig. 11 and Table 1, which are statically indeterminate, including some measurements of compressional (rod) wave velocity, V_L, in stainless steel

granular bars loaded isotropically (see Fig. 13). As shown in the figure, the measured values of V_L are somewhat smaller than predicted, with the difference being greater at small values of σ_o, and with this difference increasing for the low tolerance balls; at high pressures the measured V_L approach the predicted one. As a result, the observed $V_L \; \alpha (\sigma_o)^m$, where $m > 1/6 = 0.167$ predicted by the theory. This difference is explained by Deresiewicz (1958), by the small differences in size between the actual spheres, which results in the number of actual, load-transmitting contacts being smaller than predicted; thus, the array is less stiff than calculated. When the tolerance becomes higher or the pressure increases, the number of these actual contacts also increases and approaches the theoretical value, and thus the measured velocity also approaches the prediction. As discussed in Section 2, values of $m \simeq 0.25 > 0.167$ have also been measured for V_s in isotropically loaded sands, most probably due to the same reason: an increase in the number of actual contacts as σ_o increases.

Several approaches have been used to model the effect of deviations from regularity in arrays of equal or unequal spheres. Smith et al. (1929) proposed considering a random array as formed by clusters of loose and dense regular arrays, each present in such proportion as to yield the overall void ratio or porosity; this idea was generalized by Munro and Jowitt (1974) and Brown (1978), who used the concept of maximum entropy to find the contribution of each regular array. Ko and Scott (1967) used a similar procedure to investigate the stress-strain behavior under isotropic compression; in this study, "holey" models were used in which some of the spheres in both the loose and the dense regular component array, are slightly smaller than the other spheres. In this way the effect on the bulk modulus of the increased number of contacts caused by an increasing pressure, was incorporated into the model. Perry and

Brown (1981) studied the influence of having different size spheres on the compliance of the array. Davis and Deresiewicz (1977) investigated the compressibility of a 3-D random array of smooth equal spheres subjected to isotropic loading. Serrano and Rodrigues-Ortiz (1973) suggested a method for generating random configurations of unequal disks or spheres having a prescribed grain size distribution; their work was continued by the 2-D numerical simulations by Cundall and by Oner, previously discussed.

4.1 General Solution of the Contact Problem

As previously discussed, Mindlin and Deresiewicz studied the problem of the load-displacement behavior of two spheres in contact. In its most general formulation, the problem is to relate an arbitrary force time history $\vec{P}(t) = T_x(t)\hat{i} + T_y(t)\hat{j} + N(t)\hat{k}$, transmitted through the contact (no twisting moments are considered), to the corresponding displacement time history $\vec{D}(t) = \delta_x(t)\hat{i} + \delta_y(t)\hat{j} + \alpha(t)\hat{k}$ of center O of one sphere relative to center O' of the other sphere (see Figs. 9 and 14). T_x, T_y, δ_x, δ_y are tangential forces and displacements, while N and α are the normal force and displacement. Mindlin and Deresiewicz established the general framework for the solution of this problem, and they obtained closed form solutions for the following particular cases: i) normal load only, $N \neq 0$, $T_x = T_y = 0$ (Hertz problem); ii) N constant and T_x increasing or decreasing with $T_y = 0$; and iii) a normal load N followed by an oscillating oblique force of constant dT_x/dN and $T_y = 0$. However, the general problem of obtaining $\vec{D}(t)$ for an arbitrary, monotonically or cyclically varying $\vec{P}(t)$ was not solved until very recently by Seridi and Dobry (1984). This solution of the contact problem, which has been implemented by means of currently available computer code CONTACT, is an elastic-plastic incremental model, where all yield surfaces are cones of angle f in force space (N, T_x,

T_y), see Fig. 14. The cones translate without rotation and without changing their shape or size (kinematic strain-hardening), and the current positions of the apexes of the cones reflect the prior force history $\vec{P}(t)$. A modified form of the normality rule is applicable, and the displacement increment $d\vec{D}$ is computed as:

$$d\vec{D} = \frac{dN(1-\nu_s^2)a}{E_s} \hat{k} + f \frac{dN}{H_o} \hat{n} + \frac{dT_t}{H_e} \hat{t} \tag{9}$$

where E_s, ν_s, f are the material properties of the spheres, a = radius of contact area between the two spheres, H, H_o, H_e are tangential elastic and elasto-plastic moduli, and dT_n, dT_t are the outward normal and tangential components (with respect to the yield surface) of the applied tangential force increment $d\vec{T} = d\vec{T}_n + d\vec{T}_t$. As demonstrated by Seridi and Dobry (1984), this elastic-plastic general model reproduces identically all equations developed by Mindlin and Deresiewicz for all their particular cases of loading, and allows computing $\vec{D}(t)$ for any arbitrary $\vec{P}(t)$.

The availability of this general solution to the contact problem is critical to the mathematical modelling of the small strain stress-strain response of a granular soil by models of spheres. The existing program CONTACT relating $\vec{P}$ and $\vec{D}$ can now be used as a basic tool, in conjunction with direct stiffness or finite difference techniques, to study the behavior of either regular or random arrays of spheres.

Section 5

DIFFERENTIAL STRESS-STRAIN RELATIONS FOR REGULAR ARRAYS OF SPHERES

The general solution of the problem of the contact between two spheres can be used to derive incremental stress-strain relationships for regular arrays of spheres. These stress-strain relationships are discussed in this section, with particular emphasis on the behavior under isotropic loading followed by very small but arbitrary stress and strain increments, and for the following regular arrays:

i) simple cubic array (sc, see Figs. 11a and 17), discussed in Section 5.1

ii) body centered cubic array (bcc, see Fig. 15); discussed in Section 5.2

iii) face centered cubic or pyramidal array (fcc, see Figs. 11d and 16); discussed in Section 5.3

iv) cubical tetrahedral (ct, see Fig. 11b) and tetragonal-sphenoidal arrays (ts, see Fig. 11c); discussed in Section 5.4.

Most of these incremental stress-strain relations were taken from Deresiewicz (1958), Duffy and Mindlin (1957) and Moklhouf and Stewart (1967). However, some are new; in particular, the body centered cubic array is discussed here for the first time.

In addition to the five regular arrays listed above, a sixth regular array is the hexagonal closed packed or tetrahedral array (hcp, see Fig. 11e, see also Deresiewicz, 1958). Table 1 lists the most important parameters of all six arrays. A comparison of the behavior of the sc, bcc and fcc cubic arrays is presented in Section 5.5.

5.1 Simple Cubic Array (sc)

The simple cubic array sketched in Figs. 11a and 17 is the simplest of all regular arrays of equal spheres. One sphere of radius R represents the whole array, and for a uniform stress field this is a statically determinate system with a one-to-one correspondence between the array's stresses and the contact forces (Deresiewicz, 1958). If the normal stresses parallel to the axes of the array are σ_{ii} ($i = 1,2,3$, see Fig. 17), the normal contact forces N_i are: $N_i = 4R^2\ \sigma_{ii}$(*). If the shear stresses parallel to the axes of the array are σ_{ij} ($i,j = 1,2,3$ and $i \neq j$), the corresponding tangential contact forces and $T_{ij} = 4R^2\ \sigma_{ij}$. These relations occur due to equilibrium and are independent of the previous history of stresses. Therefore, they are also valid for any stress and force increments at any stage during the loading, provided that no gross sliding of the contact has taken place $dN_i = 4R^2\ \sigma_{ii}$, $dT_{ij} = 4R^2\ d\sigma_{ij}$. Figure 17 illustrates the case in which an anisotropic state of stresses is applied first, with all $\sigma_{ij} = 0$, followed by small arbitrary increments $d\sigma_{ii}$ and $d\sigma_{ij}$.

A similar set of simple relations is valid in this case between the array strains and the displacements between spheres; these relations are obtained for a uniform strain field based on simple geometric considerations. If α_i = normal relative displacement of centers of the two adjacent spheres separated by contact i, and δ_{ij}, δ_{ik} = tangential relative displacements between the same two centers, then: $\varepsilon_{ii} = \alpha_i/(2R)$; and $\gamma_{ij} = 2\varepsilon_{ij} = (\delta_{ij} + \delta_{ji})/(2R)$, where ε_{ii} = normal strain, and γ_{ij} = engineering shear strain of the array. Again, all these relations are independent of the prior history of strains and are valid for incremental displacements and strains.

(*) Indicial tensor notation is not used here, that is, σ_{ii} does not imply a sum of several terms.

The elastic stiffnesses corresponding to small stress and strain increments applied to the array subsequent to an isotropic stress state, $\sigma_{11} = \sigma_{22} = \sigma_{23} = \sigma_o$, $\sigma_{ij} = 0$ are:

$$\begin{bmatrix} d\sigma_{11} \\ d\sigma_{22} \\ d\sigma_{33} \\ d\sigma_{12} \\ d\sigma_{13} \\ d\sigma_{23} \end{bmatrix} = \begin{bmatrix} S_{1111} & 0 & 0 & 0 & 0 & 0 \\ 0 & S_{2222} & 0 & 0 & 0 & 0 \\ 0 & 0 & S_{3333} & 0 & 0 & 0 \\ 0 & 0 & 0 & S_{1212} & 0 & 0 \\ 0 & 0 & 0 & 0 & S_{1313} & 0 \\ 0 & 0 & 0 & 0 & 0 & S_{2323} \end{bmatrix} \begin{bmatrix} d\varepsilon_{11} \\ d\varepsilon_{22} \\ d\varepsilon_{33} \\ d\varepsilon_{12} \\ d\varepsilon_{13} \\ d\varepsilon_{23} \end{bmatrix} \quad (10)$$

$$\left.\begin{aligned} &\text{where} \quad S_{1111} = S_{2222} = S_{3333} = \left(\frac{3}{2}\right)^{1/3} (1-\nu_s)^{-2/3} (\sigma_o G_s^2)^{1/3} \\ &S_{1212} = S_{1313} = S_{2323} = \left(\frac{3}{2}\right)^{1/3} \frac{2(1-\nu_s)1/3}{(2-\nu_s)} (\sigma_o G_s^2)^{1/3} \end{aligned}\right\} \quad (11)$$

Notice that the stiffness matrix is diagonal, and therefore the Poisson's ratio of the array, $\nu = d\varepsilon_{22}/d\varepsilon_{11} = 0$, for "triaxial" loading corresponding to increasing σ_{11} and constant $\sigma_{22} = \sigma_{33} = \sigma_o$. The array has a $\nu = 0$ quite independently of the values of σ_o and ν_s (see Fig. 20).

Note that, for a given σ_o, Eqs. 10-11 describe a linearly elastic <u>anisotropic</u> medium. The necessary and sufficient conditions for this medium to be isotropic are of the type $S_{1111} - S_{1122} = S_{1212}$. These are satisfied only for a Poisson's ratio of the spheres, $\nu_s = 0$. This assumption results in an <u>isotropic</u> medium with $\nu = 0$.

For the case of an anisotropic state of stress, $\sigma_{11} \neq \sigma_{22} \neq \sigma_{33}$, $\sigma_{ij} = 0$,

the coefficients become:

$$\left.\begin{aligned} S_{1111} &= \left(\frac{3}{2}\right)^{1/3} (1-\nu_s)^{-2/3} \left(\sigma_{11}G_s^2\right)^{1/3} \\ S_{2222} &= \left(\frac{3}{2}\right)^{1/3} (1-\nu_s)^{-2/3} \left(\sigma_{22}G_s^2\right)^{1/3} \\ S_{3333} &= \left(\frac{3}{2}\right)^{1/3} (1-\nu_s)^{-2/3} \left(\sigma_{33}G_s^2\right)^{1/3} \end{aligned}\right\} \qquad (12)$$

$$S_{ijij} = 4\left(\frac{3}{2}\right)^{1/3} * \frac{(1-\nu_s)1/3}{2-\nu_s} * \frac{G_s^{2/3}}{\left(\frac{1}{\sigma_{ii}}\right)^{1/3} + \left(\frac{1}{\sigma_{jj}}\right)^{1/3}}\ ; \qquad i \neq j \qquad (13)$$

where G_s and ν_s are the shear modulus and Poisson's Ratio of the material of the spheres.

The array locks under "triaxial" conditions (σ_{11} increasing with $\sigma_{22} = \sigma_{33} = \sigma_o$ = constant), while it fails in pure shear (σ_{12} increasing with all other $d\sigma = 0$). Because the stiffness matrix, [S], in Eq. 10 is diagonal, the corresponding diagonal compliance matrix is $[C] = [S]^{-1}$, with each compliance being the reciprocal of the corresponding diagonal stiffness term. That is, $C_{iiii} = 1/S_{iiii}$ and $C_{ijij} = 1/S_{ijij}$, and $\{d\varepsilon\} = [C]\ \{d\sigma\}$.

In this simple cubic array, and again for the case of isotropic loading, $\sigma_{ii} = \sigma_{jj} = \sigma_{kk} = \sigma_o$; for P- and S-waves propagating along principal axis i of the array (and, for the S-wave, polarized parallel to principal axis j), the wave propagation velocities V_p and V_s are proportional to $(\sigma_o)^{1/6}$, and thus, the corresponding constrained and shear moduli, $D = \rho V_p^2 = d\sigma_{ii}/d\varepsilon_{ii}$ and, $G_{max} = \rho V_s^2 = d\sigma_{ij}/d\gamma_{ij}$, are both proportional to $(\sigma_o)^{0.33}$. As discussed in Section 4, a similar dependence of modulus on $(\sigma_o)^{0.33}$ is also predicted for other regular arrays, while laboratory measurements on regular arrays and

soils indicate that $G_{max}\ \alpha(\sigma_o)^{0.5}$.

For this same case of isotropic loading and for a cubic array of quartz spheres, and if the array is loaded in pure shear, $d\sigma_{ij} = d\sigma_{ji}$, then a threshold shear strain, $\gamma_t = 4.5 \times 10^{-3}.\ \ (\sigma_o)^{2/3}$ is predicted (see Appendix B). This expression was obtained using the properties of quartz listed in Table 3 with σ_o in psi and γ_t in inches/inch, at which gross sliding occurs at contacts i and j, and there is a tendency for a change in the geometric arrangement of the spheres. This predicted relation between γ_t and σ_o for a sc array of quartz spheres is plotted in Fig. 21 while Fig. 22 shows the detailed shear stress-strain plots up to the threshold (failure). In the range of practical interest for soils, 500 psf < σ_o < 2000 psf, the expression gives $\gamma_t \simeq 10^{-4}\% = 10^{-2}\%$, which agrees very well with the measured γ_t in sands as discussed in Section 2. Expressions for the secant modulus reduction, G/G_{max}, and for the damping ratio of the array, versus strain increment $\gamma = d\gamma_{ij}$ were also obtained for a cubic array of quartz spheres (Dobry et al., 1982), and were compared with actual measurements in sands, with good agreement. The corresponding comparison for G/G_{max} versus γ is reproduced in Fig. 18 for an assumed $\gamma_t = 1.5 \times 10^{-2}\%$.

The more general case of anisotropic loading of the cubic array, with $\sigma_{11} \neq \sigma_{22} \neq \sigma_{33}$, is very interesting, as this model crudely simulates the laboratory measurements of V_p and V_s on anisotropically loaded sands discussed in Section 2. For a P-wave propagating parallel to the i-axis of the array, the predicted expressions for $D = d\sigma_{ii}/d\varepsilon_{ii}$ and V_p are:

$$\left.\begin{aligned} D &= [(3)^{1/3}/2]\,[E_s/(1-\nu_s^2)]^{2/3}\,(\sigma_{ii})^{1/3} \\ V_p' &= (D/\rho)^{1/2} \end{aligned}\right\} \qquad (14)$$

where E_s, ν_s = elastic constants of the spheres. Therefore, both D and V_p are functions only of the normal stress σ_{ii} in the direction of propagation, and do <u>not depend</u> on the other two array stresses σ_{jj} and σ_{kk}.

For an S-wave propagating parallel to the i-axis of the anisotropically loaded array and with motions polarized parallel to the j-axis of the array, the corresponding expressions for $G_{max} = d\sigma_{ij}/d\gamma_{ij}$ and V_s are:

$$\left.\begin{aligned} G_{max} &= \frac{[3(1-\nu_s^2)]^{1/3}(E_s)^{2/3}}{(2-\nu_s)(1+\nu_s)} \; \frac{\sigma_{ii}^{1/3}\sigma_{jj}^{1/3}}{\sigma_{ii}^{1/3}+\sigma_{jj}^{1/3}} \\ V_s &= (G_{max}/\rho)^{1/2} \end{aligned}\right\} \tag{15}$$

G_{max} and V_s are functions only of the normal stresses in the direction of propagation (σ_{ii}) and polarization (σ_{jj}), and <u>do not depend</u> on the third, out of plane array stress σ_{kk}. Furthermore, as Eqs. 15 are symmetric with respect to σ_{ii} and σ_{jj}, the values of V_s and G_{max} do not change if the directions of propagation and polarization are interchanged.

These conclusions for the simple cubic array, that V_p depends only on σ_{ii}, and V_s depends only on σ_{ii} and σ_{jj}, are identical to the experimental findings of Roesler, Knox et al., Kopperman et al., and Yu and Richart on anisotropically loaded sands, previously discussed in Section 2. The symmetry of σ_{ii} and σ_{jj} in Eq. 15 is also present as a symmetry of σ_a and σ_b in empirical Equation 4, obtained by Knox et al. from their sand measurements.

Of course, Eqs. 14 and 15 cannot be used directly for quantitative predictions in sands, as they give $D \propto \sigma_o^{1/3}$ and $G_{max} \propto \sigma_o^{1/3}$ for the isotropic case, while D and $G_{max} \propto (\sigma_o)^{1/2}$ in actual sands. It is interesting to modify Eq. 15 to make it consistent with this empirical fact, by replacing $\sigma_{ii}^{1/3}$, $\sigma_{jj}^{1/3}$ by $\sigma_{ii}^{1/2}$, $\sigma_{jj}^{1/2}$, and then comparing measurements and predictions. The

new equation is $G_{max} = M\sigma_{ii}^{0.5}\sigma_{jj}^{0.5}/(\sigma_{ii}^{0.5}+\sigma_{jj}^{0.5})$, where M = constant. It is useful to specialize this expression for the biaxial case, $\sigma_{ii} = \sigma_{11} = \sigma_v$, $\sigma_{jj} = \sigma_{kk} = \sigma_{33} = \sigma_h$, to be able to compare it with the empirical Eq. 6 obtained by Yu and Richart for sand. If $K = \sigma_{ii}/\sigma_{jj} = \sigma_{11}/\sigma_{33}$, the new equation becomes: $G_{max} = N\sigma_v^{0.25}\sigma_h^{0.25}[2K^{0.25}/(1+K^{0.5})]$, where N = 0.5M. It is convenient to define the normalized parameter $\overline{G} = G_{max}/(N\sigma_v^{0.25}\sigma_h^{0.25})$, where $\overline{G} = 1$ for K = 1. The theoretical expression $G = 2K^{0.25}/(1+K^{0.5})$ has been plotted in Fig. 19. The corresponding empirical expression $\overline{G} = 1-0.18\ K_n^2$, obtained from Eq. 6, has also been superimposed on Fig. 19 for typical values $K_{max} = 3$ and 4. The trends of the predicted and measured curves are the same in Fig. 19, with the laboratory results showing a somewhat faster decrease in G as K_n increases.

The fact that the crude particulate model used here is capable of predicting the lack of influence of the two stresses perpendicular to propagation on V_p (Eq. 14), and of the out-of-plane stress on V_s and G_{max} (Eq. 15), as well as the general trend of the relationship between G_{max} and the in-plane stresses (Fig. 19), is extremely encouraging. The main advantage of the cubic array used here is its simplicity, but of course this model is still far from representing real sand. One deficiency (which it shares with other regular arrays), is that in the general case the array itself is inherently anisotropic even when isotropically loaded (crystal-type behavior); that is, G_{max} and other "elastic" stress-strain parameters are somewhat different for shear stresses corresponding to axes which are different from the structural axes (axes of symmetry of the array 1, 2, 3 selected in Fig. 17). However, when the material of the spheres has $\nu_s = 0$, the array is isotropic when isotropically loaded. Also, the array locks when a "triaxial" test is conducted on it along any of its structural axes, instead of yielding and eventually failing in shear as it happens with actual granular materials.

5.2 Body Centered Cubic Array (bcc)

The body centered cubic array, sketched in Fig. 15, was the next regular array studied. It is also represented by one sphere, and the relations between stress and contact forces can be easily determined for one uniform stress field of interest: isotropic loading followed by small stress increments. The coordination number (number of contacts/sphere) is now eight instead of six for the simple cubic array, and, thus, the computations are somewhat more involved. A procedure analogous to that used for analyzing the simple cubic array can be followed, except that it is now easier to work directly with the compliance matrix, $C_{ijk\ell}$, $[C] = [S]^{-1}$, instead of the stiffness matrix $[S]$ used before in Eq. 10.

For the case of isotropic loading, followed by small stress increments, $[C]$ has the following form:

$$\begin{bmatrix} d\varepsilon_{11} \\ d\varepsilon_{22} \\ d\varepsilon_{33} \\ d\varepsilon_{12} \\ d\varepsilon_{13} \\ d\varepsilon_{23} \end{bmatrix} = \begin{bmatrix} C_{1111} & C_{1122} & C_{1133} & 0 & 0 & 0 \\ C_{2211} & C_{2222} & C_{2233} & 0 & 0 & 0 \\ C_{3311} & C_{3322} & C_{3333} & 0 & 0 & 0 \\ 0 & 0 & 0 & C_{1212} & 0 & 0 \\ 0 & 0 & 0 & 0 & C_{1313} & 0 \\ 0 & 0 & 0 & 0 & 0 & C_{2323} \end{bmatrix} \begin{bmatrix} d\sigma_{11} \\ d\sigma_{22} \\ d\sigma_{33} \\ d\sigma_{12} \\ d\sigma_{13} \\ d\sigma_{23} \end{bmatrix} \qquad (16)$$

where

$$C_{1111} = C_{2222} = C_{3333} = \frac{2}{\sqrt{3}} * \frac{1}{(4\sqrt{3}\ G_s{}^2\sigma_o)^{1/3}} * \left[(1-\nu_s)^{2/3} + \frac{2-\nu_s}{(1-\nu_s)^{1/3}} \right] \qquad (17)$$

$$C_{1122} = C_{1133} = C_{2233} = \frac{1}{\sqrt{3}} * \frac{1}{(4\sqrt{3}\ G_s{}^2\sigma_o)^{1/3}} * \lfloor 2(1-\nu_s)^{2/3} \quad \frac{2-\nu_s}{(1-\nu_s)^{1/3}} \rfloor \tag{18}$$

$$C_{1212} = C_{1313} = C_{2323} = \frac{4}{\sqrt{3}} * \frac{1}{(4\sqrt{3}\ G_s{}^2\sigma_o)^{1/3}} * \lfloor (1-\nu_s)^{2/3} + \frac{1}{4}\,\frac{2-\nu_s}{(1-\nu_s)^{1/3}} \rfloor \tag{19}$$

Notice that, unlike Eq. 10 for the sc array, the compliance matrix [C] in Eq. 16 is not diagonal. However, it becomes diagonal and it corresponds to an isotropic elastic medium with $\nu = 0$, if $\nu_s = 0$ similarly to that found for the sc in Section 5.1. For an initial cross-anisotropic or biaxial loading, $\sigma_{33} = \sigma_o + \sigma_a$ and $\sigma_{11} = \sigma_{33} = \sigma_o$, followed byarbitrary, small stress increments*, the form of [C] is still that of Eq. 16, and the compliances in Eq. 16 are:

$$C_{1111} = C_{2222} = C_{3333} = \frac{2}{3\sqrt{3}} * \frac{1}{4\sqrt{3}\ G_s{}^2\sigma_o}^{1/3} * \left[1 + \frac{1}{3}\left(\frac{\sigma_a}{\sigma_o}\right)\right]^{-1/3} * \lfloor (1-\nu_s)^{2/3} + \\ + \frac{2-\nu_s}{(1-\nu_s)^{1/3}} \rfloor \tag{20}$$

$$C_{1122} = C_{1133} = C_{2233} = \frac{-2}{\sqrt{3}} * \frac{1}{4\sqrt{3}\ G_s{}^2\sigma_o}^{1/3} * \left[1 + \frac{1}{3}\left(\frac{\sigma_a}{\sigma_o}\right)\right]^{-1/3} * \left[(1-\nu_s)^{2/3} - \right. \\ \left. - \frac{2-\nu_s}{2(1-\nu_s)} \right] \tag{21}$$

---

* See footnote, Appendix A.3.

$$C_{1212} = C_{1313} = C_{2323} = \frac{1}{3\sqrt{3}} * \frac{1}{4\sqrt{3}\, G_s^2 \sigma_o}^{1/3} * \left[1 + \frac{1}{3}\left(\frac{\sigma_a}{\sigma_o}\right)\right]^{-1/3} * (1-\nu_s)^{2/3} + \\ + \frac{2-\nu_s}{(1-\nu_s)^{1/3}}\Big] \tag{22}$$

As it can be seen in the above equations 17-22, V_s and V_p are again proportional to $(\sigma_o)^{1/6}$ for the body centered cubic array, since the corresponding moduli are proportional to $(\sigma_o)^{1/3}$; this is a characteristic common to all regular cubic arrays (Duffy and Mindlin, 1957, Duffy, 1959, Makhlouf and Stewart, 1967). However, again it is possible to modify the exponents empirically, and $(\sigma_o)^{1/3}$ can be replaced by $(\sigma_o)^{1/2}$ when measurements and predictions are compared.

Threshold strain calculations were performed for this body-centered array for the case of triaxial loading, starting from an isotropic pressure σ_o, for which the array yields and fails (as the array tends to lock under pure shear loading). Again, the threshold strain, γ_t, obtained for the array was a function of the confining pressure, $(\sigma_o)^{2/3}$, and for an array of quartz spheres (using properties for quartz in Table 3), $\gamma_t = 3.44 \times 10^{-3}\ \sigma_o^{2/3}$, with σ_o in psi and γ_t in inches/inch. This gives slightly lower values of γ_t than obtained from the simple cubic array of quartz spheres in Section 5.1, $\gamma_t = 4.53 \times 10^{-3}\ \sigma_o^{2/3}$. The plots for these two expressions of γ_t are compared in Fig. 21, while Fig. 23a) presents detailed axial stress-strain curves up to the threshold (failure). For the usual range of values of confining pressure for soils, both of them agree well with $\gamma_t \simeq 10^{-2}\%$ experimentally observed in sands.

The body centered cubic array also has some deficiencies when compared to the behavior of actual sands. First, it remains isotropic even when loaded under anisotropic loads, as shown in Appendix A. Second, in this anisotropic

loading case the wave propagation velocities are not proportional to the product of the principal stresses in the directions of propagation and polarization (as measured in sands), but rather they are proportional to the mean effective stress, as can be verified from Eqs. 20-22. Finally, this array locks under pure shear loading, and in fact it locks under a number of different shear loading paths depending upon their orientations and initial stress state. However, the bcc array adds to our understanding of the general problem, as it is a medium dense (e = 0.47) array, located within the range between the densest face centered cubic array (e = 0.35) and the loosest simple cubic array (e = 0.91).

5.3 Face Centered Cubic Array (fcc)

The Face Centered Cubic Array sketched in Fig. 16 is one of the two densest arrays, and it has been investigated by several researchers (Duffy and Mindlin 1957, Ko and Scott 1969, Hendron 1963). The differential stress-strain relationship for this medium was derived by Duffy and Mindlin (1957). The array has 12 contacts per sphere, and unfortunately it is statically indeterminate for most loading situations; as a consequence, closed form solutions are available only for the case of isotropic confining pressure. In the case of transversely isotropic loading a qualitative solution does exist, but the compliances at the contacts have not yet been evaluated. Computation of these compliances is a formidable task due to the indeterminacy of the problem and the variation of the forces from contact to contact.

The incremental constitutive law under isotropic confining pressure was used by Duffy and Mindlin (1957) to compare the theoretical and experimental rod wave velocities through a bar composed of face centered cubic arrays of spheres (Fig. 13).

For the case of isotropic loading $\sigma_{ii} = \sigma_o$, followed by small stress increments, $d\sigma_{ii}$, $d\sigma_{ij}$, the stiffness matrix has the form shown below:

$$\begin{bmatrix} d\sigma_{11} \\ d\sigma_{22} \\ d\sigma_{33} \\ d\sigma_{12} \\ d\sigma_{13} \\ d\sigma_{23} \end{bmatrix} = \begin{bmatrix} S_{1111} & S_{1122} & S_{1133} & 0 & 0 & 0 \\ S_{2211} & S_{2222} & S_{2233} & 0 & 0 & 0 \\ S_{3311} & S_{3322} & S_{3333} & 0 & 0 & 0 \\ 0 & 0 & 0 & S_{1212} & 0 & 0 \\ 0 & 0 & 0 & 0 & S_{1313} & 0 \\ 0 & 0 & 0 & 0 & 0 & S_{2323} \end{bmatrix} \begin{bmatrix} d\varepsilon_{11} \\ d\varepsilon_{22} \\ d\varepsilon_{33} \\ d\varepsilon_{12} \\ d\varepsilon_{13} \\ d\varepsilon_{23} \end{bmatrix} \quad (23)$$

$$S_{1111} = S_{2222} = S_{2323} = \left[\frac{3G_s^2\ \sigma_o}{2(1-\nu_s)^2}\right]^{1/3} * \frac{4-3\nu_s}{2-\nu_s} \quad (24)$$

$$S_{1122} = S_{1133} = S_{2233} = \left[\frac{3G_s^2\ \sigma_o}{2(1-\nu_s)^2}\right]^{1/3} * \frac{\nu_s}{2(2-\nu_s)} \quad (25)$$

$$S_{1212} = S_{1313} = S_{2323} = \left[\frac{3G_s^2\ \sigma_o}{2(1-\nu_s)^2}\right]^{1/3} * \frac{4-3\nu_s}{(2-\nu_s)} \quad (26)$$

Similar to that discussed previously for Eq. 16 and the bcc array, the stiffness matrix [S] in Eq. 23 becomes isotropic and diagonal only if $\nu_s = 0$. In that case, all diagonal terms are identical and equal to:

$$2\left(\frac{3G_s^2\ \sigma_o}{2}\right)^{1/3} \quad (27)$$

and the Poisson's ratio of the array is $\nu = 0$.

If the face centered cubic array is consolidated under a transversely isotropic state of stress with $\sigma_{11} = \sigma_o + \sigma_a$, $\sigma_{22} = \sigma_{33} = \sigma_o$, and $\sigma_{12} = \sigma_{13} = \sigma_{23} = 0$, the situation becomes more complicated, since in the case of a non isotropic loading the forces vary from contact to contact and each compliance is different. To obtain a stress-strain relation for an anisotropic loading path, the derivation must be performed anew, distinguishing between contacts with different loading histories.

The differential stress strain law for this case appears in great detail in the original paper by Duffy and Mindlin (1957); it is identical in form to Eq. 23 , except that now the expressions for $S_{ijk\ell}$ are not known. Thurston (1958) extended the results of Duffy and Mindlin to a set of 18 equations and 18 unknowns.

The fcc array was subjected analytically to the conditions of a triaxial test by Brauns (1968) and Brauns and Leussink (1970), who derived theoretical expressions between stress and strain at finite levels for an array of glass spheres (Fig. 23b). These expressions were later compared to experimental data obtained in triaxial tests on regular fcc packings of glass and steel spheres (see Appendix B3).

Thurston and Deresiewicz (1959) derived expressions for the uniaxial compression of an fcc array when applied concurrently with a related isotropic pressure. Again, the theoretical results were compared with experimental results obtained through compression of bars of steel bearing spheres arranged in fcc array, with good agreement.

5.4 Cubical-Tetrahedral (ct) and Tetragonal-Sphenoidal (ts) Arrays

The elastic constants relating stress to strain increments for the Cubical Tetrahedral and Tetragonal Sphenoidal arrays that have been consolidated

isotropically were derived by Makhlouf and Stewart (1967). The procedure for determining those constants is the same as in the other arrays described in detail by Duffy and Mindlin (1957).

The corresponding constitutive law for the Cubical Tetrahedral array has the same form as Eq. 23, but now

$$S_{1111} = S_{2222} = \frac{3^{1/3}(1+3k)}{4k} * \left[\frac{3}{2}\frac{G_s^2\sigma_o}{(1-\nu_s^2)}\right]^{1/3} \tag{28}$$

$$S_{3333} = \left(\frac{4}{2}\right)^{1/3} * \left[\frac{3}{2}\frac{G_s^2\sigma_o}{(1-\nu_s^2)}\right]^{1/3} \tag{29}$$

$$S_{1122} = \frac{3^{1/3}\ (1-k)}{4k} * \left[\frac{3}{2}\frac{G_s^2\sigma_o}{(1-\nu_s^2)}\right]^{1/3} \tag{30}$$

$$S_{1212} = \frac{\sqrt{3}\ (1+k)}{5k}\ 3^{1/3}*2* \left[\frac{3}{2}\frac{G_s^2\sigma_o}{(1-\nu_s^2)}\right]^{1/3} \tag{31}$$

$$S_{1313} = S_{2323} = \frac{2*3^{1/3}}{5k} * \left[\frac{3}{2}\frac{G_s^2\sigma_o}{(1-\nu_s^2)}\right]^{1/3} \tag{32}$$

where $k = \dfrac{2 - \nu_s}{2(1-\nu_s)}$ (33)

As we can see from the above equations, the Cubical-Tetrahedral array differs from the simple cubic, the body centered cubic and the force centered cubic arrays in that it does not exhibit cubic anisotropy, but rather transverse or hexagonal anisotropy, as is also the case of the Hexagonal Close Packed

array (Duffy, 1959) and of the Tetragonal-Sphenoidal Array.

The constitutive law for the Tetragonal-Sphenoidal array appears also in Makhlouf and Stewart (1967). However, not enough detail is provided in this reference for a full understanding of the results, which are quite complex, as the representative unit prism is not symmetric. Unfortunately, the original reference (Makhlouf, 1963) could not be found by the authors*, thus preventing a better understanding of this array.

5.5 Comparison of Different Cubic Arrays

The analytical results on the three regular cubic arrays discussed in Sections 5.1-5.2-5.3: simple cubic, body centered cubic and face centered cubic, were compared as part of the current research. This was done to gain further insight into the behavior of granular media, and as a necessary intermediate step toward the investigation of more elaborated and realistic particulate models.

All these arrays generally exhibit cubic anisotropy (crystal-type behavior) under an isotropic confining pressure σ_o. In the three arrays, it was found that the necessary and sufficient condition for the array to become isotropic under σ_o is for the Poisson's ratio of the spheres, ν_s, to be equal

---

*The differential constitutive laws for the cubical-tetrahedral and the tetragonal-sphenoidal arrays are either not applicable to our research or they are erroneous. As one can see from Eqs. 28-31, contrary to general belief (Duffy 1959), the cubical tetrahedral array does not become isotropic under isotropic loading. This is a serious deficiency vis-a-vis our research, as sands are isotropic under isotropic load. Consequently, the cubical tetrahedral array will not be used here. As for the tetrogonal sphenoidal array, the results are not complete, and since the representative volume element of this array is not symmetric, completion of the stress strain relation in Makhlouf and Stewart (1967) appears to be a major task. The inexistence of the primary source for this array, Makhlouf (1963), made it impossible for the authors to clarify the above aspects; therefore no results will be used here for the cubical-tetrahedral and tetragonal-sphenoidal array.

to zero. If $\nu_s = 0$, the incremental stiffness (and compliance) matrix for the three arrays is diagonal. Although the Poisson's Ratio of quartz is $\nu_s \approx 0.15$, (Table 3), is certainly different from zero, it is low enough to make this "$\nu_s = 0$ assumption", needed for isotropy, a reasonable one for quartz sands, at least as a first approximation. If $\nu_s = 0$ is assumed, the Poisson's Ratio of the array is also computed to be $\nu = 0$ for the same three arrays. It must be note that for the range $0 \leq \nu_s \leq 0.5$, values up to $\nu \approx 0.13$ are computed for the same arrays (see Fig. 20). Therefore, the fact that a value $\nu = 0$ results for the array as soon as $\nu_s = 0$ is assumed does not seem to be so far off either. It is interesting to note that measurements of V_p and V_s by Stokoe and his coworkers on an actual sand consolidated isotropically also provided a similarly low value of $\nu \approx 0.10$ (Knox et al. 1982, Kopperman et al. 1982, Lee 1985). In any case, even with $\nu_s \neq 0$, the cubic anisotropy of these expressions for ν arrays is not pronounced; the error resulting from computing the moduli between the extreme values of ν_s is smaller than 3.3% (Duffy, 1959).

The above three cubic arrays starting from an isotropic σ_o state, were loaded statically in triaxial compression or pure shear up to failure, that is up to gross sliding, and computations were performed and are displayed here for their stress-strain curves and threshold/failure strains (Figs. 21-23). A graph of obliquity, σ_{22}/σ_o at failure versus the intergranular friction coefficient between spheres, f, was also computed and is plotted in Fig. 24. The curves obtained for the arrays in this figure were also compared to the obliquity obtained assuming the Mohr-Coulomb Failure law:

$$\frac{\sigma_{22}}{\sigma_o} = \frac{1+\sin\phi}{1-\sin\phi} = \tan^2(45 + \frac{\phi}{2}), \text{ with } \tan\phi = f$$

To be able to fail the simple cubic array in triaxial compression, this medium was compressed by a force parallel to one of the face diagonals of the unit volume of the array, that is along a [110] direction (Deresiewicz, 1959).

The same cubic arrays also give excellent results when predicting the influence of anisotropic consolidation on shear wave velocity; this is shown in Fig. 25 by a plot of normalized shear wave velocity vs stress ratio $K = \sigma_{22}/\sigma_o$. In this plot, $V_s(K)$ and $V_s(1)$ are the values of the shear wave velocity, V_s, computed for the anisotropic case (K) and for the isotropic loading condition (K=1), respectively, for direction of propagation and polarization parallel or perpedicular to σ_{22}. The same plot includes data measured by Stokoe et al. (1985) and Lee (1985) on dry sand in the large cubic testing facility at the University of Texas, with excellent agreement between the analytical predictions and experimental data.

The shear modulus at very small strains, G_{max}, computed for these same three cubic arrays under a given isotropic stress, σ_o, is plotted in Fig. 26 as a function of the coordination number (= number of contacts/sphere). As expected, the higher the coordination number, the stiffer the array, with essentially a linear relation between the two parameters; it is interesting that for a given σ_o the straight lines in Fig. 26 extrapolate down to zero, suggesting that G_{max} is essentially proportional to the coordination number (a similar plot appears in Yanagisawa, 1983). Therefore, adding contacts to the spheres has the same effect on the stiffness of the arrays as increasing the number of springs in a system of equal, parallel, elastic springs. A derived plot is the graph between the shear wave velocity, $V_s = (G_{max}/\rho)^{1/2}$ versus void ratio and isotropic pressure σ_o (Fig. 27a) for the same three arrays. This last figure is especially interesting, as the trend observed in actual sands is very similar (compare analytical curves with measured data in sands in Fig. 27b),

except that the absolute values of V_s in the real soils are much smaller, by a factor of two or three. For example, for e = 0.47, corresponding to the bcc array, and σ_o = 30 psi = 4,320 psf, $V_s \simeq$ 1,800 fps is predicted by the analytical model in Fig. 27a , while $V_s \simeq$ 1,100 fps has been measured in rounded grained sands. Therefore, Figs. 26 and 27 strongly suggest that the dependency of G_{max} and V_s on void ratio observed in real soils is explained mainly by the increase in the number of contacts as the void ratio decreases.

Even though the above results are encouraging, the regular arrays are still very crude analytical models of actual granular soils, and results such as shown in Fig. 27a are not easy to interpolate to intermediate void ratios. A significant improved model is discussed in the following section.

Section 6

A MODEL OF GRANULAR SOIL OF ARBITRARY VOID RATIO

Smith et al. (1929) found experimentally that a random arrangement of equal spheres, after enough shaking and tapping has been applied to it, seems to be composed of regular arrays, representing dense and loose clusters distributed within the random grandular medium. The measurements showed that all spheres had between 6 and 12 contacts per sphere, which corresponds exactly to the theoretical range for regular arrays.

Additional experimental work by Bernal and Mason (1960), Bernal et al. (1964), Scott (1960), Scott et al. (1964), Davis (1974) and Shahinpoor and Shahrpass (1982), Finney (1983), Figs. 28 and 29, has confirmed that 2-D and 3-D random assemblages of equal spheres tend to crystalize. Consequently, at the present time, it is generally accepted that an assemblage of equal spheres can be modelled by a combination of regular arrays, Finney (1983), Backman et al. (1983).

In this section, a model of granular soil is proposed which consists of clusters of the three cubic arrays discussed in Section 5.5, with the additional assumption that the spheres have $\nu_s = 0$. In this model, the three cubic arrays, having different void ratios and inherent stiffnesses, occur in proportions such as to give the desired macroscopic void ratio of the "soil". In Section 6.3, the relation between G_{max}, void ratio and σ_o applied to the "soil" is calculated using the self consistent method, and the results are compared with G_{max} measured in actual sands.

6.1 The Self Consistent Method

One of the most commonly used procedure for describing the behavior of macroscopically isotropic composite elastic media is the "Self Consistent

Scheme".

This "Self Consistent Scheme" was first devised by Hershey (1954) and Kroner (1958) as a means to model the behavior of isotropic and anisotropic polycrystalline materials. Such materials are just one phase media, but because of the random or partially random orientation of the crystals. They are heterogeneous, the elastic properties vary with position within the medium and discontinuities in properties exist across some crystal interfaces.

In these original applications of the method to polycrystalline aggregates, a single anisotropic crystal was viewed as a spherical or ellipsoidal inclusion within an infinite medium; this infinite medium had the (still unknown) isotropic elastic properties of the aggregate. Then the medium, with the inclusion in it, was subjected to a uniform stress or strain field applied at large distances from the inclusion. Next, the orientation average of the stress or strain in the inclusion was assumed to be equal to ("consistent with") the corresponding applied value of stress or strain. Thus the "self-consistent" name of the method. This formulation provided enough equations to solve for the isotropic effective properties of the medium (Christensen, 1979).

Improvement of this self consistent scheme and its extension to multiphase media are due to Hill (1965) and Budiansky (1965), who developed the method to be used here. This improved method represents an approximate analysis for the prediction of the overall (macroscopic) elastic moduli of a multiphase medium composed of a coherent mixture of several isotropic, linearly elastic materials or phases. The medium is assumed to consist of contiguous, irregular zone continuing these constituent materials, and the shapes of these zones are assumed not to deviate much from spherical. The spatial distribution of the phases is assumed to be such that the composite medium is macroscopically (i.e. at a scale much larger than the dimensions of the zones), both homogeneous and

isotropic. Now, if an N-phase medium of total volume V is defined, such that the aggregate volume of all zones containing the i^{th} phase is V_i, the volume concentration is $c_i = V_i/V$ and c_i is also equal to the probability that any arbitrary point within the medium is located within a zone of the i^{th} material. It should be noted that in the limiting case of very small concentrations, c_1, c_2, ... c_{N-1}, the first N-1 phases will tend to appear as isolated inclusions in a matrix consisting of the Nth phase.

In order to obtain to effective overall (macroscopic) shear, G^*, and bulk, K^*, moduli of the medium, a uniform stress field is applied at its boundaries. Then, the stress and strain field, in each of the phases is evaluated as explained in the next paragraph. Once the fields are determined for all materials, the effective moduli, G^* and K^*, can be calculated by equating the strain energies of the macroscopic medium and of the phases. Again, the problem reduces to a number of coupled equations for K^* and G^*, which are in terms of the properties of the individual materials and of their volume concentrations (Budiansky, 1965). This method has been severely critized for taking enormous liberties with the geometrical arrangement of the phases (Christensen, 1979). To calculate the elastic field in each material, the geometry of the different zones containing the phase is successively rearranged to view the phase as a single inclusion. However, the method is relatively simple and in many instances, when used with caution, gives very good results. Furthermore, it has been proven by Hill (1965) that this "Self Consistent Method" yields results for G^* and K^* which always lie between the Voigt and Reuss bounds, that is, the spatial average of the moduli of the phases (Voigt bound, springs-in-parallel) and of the reciprocal of the moduli, or compliances of the phases (Reuss bound, springs-in-sands).

The evaluation of the stress and strain fields in each of the phases is

performed for the isotropic case by the solution of the problem of the fields of an ellipsoidal elastic inclusion (Eshelby, 1957). It was shown by Eshelby that the fields inside an ellipsoidal isotropic elastic inclusion embedded in an isotropic elastic medium is uniform; this is an extremely important conclusion as it eliminates the need for averaging the fields within the inclusion phase and simplifies enormously the formulation. Later, it was shown that the stress and strain fields inside an orthotropic inclusion embedded in an orthotropic medium are also uniform, as long as the cross section of the inclusion is quadratic (Kinoshita and Mura, 1971).

The averaging of the shear moduli of all phases by a strain energy balance between the medium and the inclusions yields:

$$\frac{1}{G^*} = \frac{1}{G_N} + \sum_{i=1}^{N-1} c_i\left(1 - \frac{G_i}{G_N}\right)\left(\frac{\overline{\gamma}_i}{\tau^\circ}\right) \tag{34}$$

$$\frac{1}{K^*} = \frac{1}{K_N} + \sum_{i=1}^{N-1} c_i\left(1 - \frac{K_i}{K_N}\right)\left(\frac{\overline{\varepsilon}_{v_i}}{\sigma_o^\circ}\right) \tag{35}$$

where G^*, K^* are the desired macroscopic moduli; K_i, G_i ($i = 1,2,\ldots N$) are the moduli of the i^{th} phase, $c_i = V_i/V$ is the volume concentration, and $\overline{\gamma}_i$, $\overline{\varepsilon}_{v_i}$ are the values of the average shear strain and volumetric strain respectively, inside the phase. The parameters τ° and σ_o° are the shear stress and isotropic pressure applied at the boundary of the medium.

The Elshelby (1957) solution gives

$$\overline{\gamma}_i = \frac{\tau^\circ}{G^*+\beta^*(G_i-G^*)} \tag{36}$$

$$\overline{\varepsilon}_{v_i} = \frac{\sigma^\circ}{K^*+a^*(K_i-K^*)} \tag{37}$$

where α^*, β^* are components of the Eshelby S-tensor; for the case of spherical inclusions are:

$$\alpha^* = \frac{1+\nu^*}{3(1-\nu^*)} \tag{38}$$

$$\beta^* = \frac{2}{15}\frac{(4-5\nu^*)}{(1-\nu^*)} \tag{39}$$

where ν^* is the macroscopic Poisson's ratio of the medium:

$$\nu^* = \frac{3K^*-2G^*}{6K^*+2G^*} \tag{40}$$

By "smearing out", that is, by replacing the matrix surrounding each inclusion (phase) by the desired resultant macroscopic medium, equations 32 and 33 reduce to:

$$\sum_{i=1}^{N} \frac{c_i}{1+\beta^*(\frac{G_i}{G^*} - 1)} = 1 \tag{41}$$

$$\sum_{i=1}^{N} \frac{c_i}{1+\alpha^*(\frac{K_i}{K^*} - 1)} = 1 \tag{42}$$

which are symmetrical for the various phases. Therefore, Budiansky (1965) has suggested to use equations 41 and 42 for arbitrary concentrations of the constituents of the composite medium as described previously. Furthermore, Budiansky (1965) simplified equations 36 and 37 to:

$$\overline{\gamma}_i = \frac{\tau^\circ}{G^*}\left[\frac{1}{1+\beta^*(\frac{G_i}{G^*} - 1)}\right] \tag{43}$$

$$\bar{\varepsilon}_{v_i} = \frac{\sigma_o^o}{K^*}\left[\frac{1}{1+\alpha^*\left(\frac{K_i}{K^*} - 1\right)}\right] \tag{44}$$

A comparison of Eq. 43 with results obtained through statistical finite element methods, suggests that the above equations do indeed model the continuum described previously, including the assumption that the stress and strain fields of the phases are approximately independent of location (Fig. 30, see Petrakis, 1983).

Finally, Equations 38-42 have to be solved simultaneously to yield the desired values of the macroscopic elastic moduli, G^*, K^*. These resultant macroscopic moduli are estimates of the overall elastic constants of the multiphase medium, and, as mentioned before, they invariably lie between the Reuss and Voigt bounds. Other solutions may provide narrower bounds for the actual solution (Hashin and Shtrikman, 1963); however, the Self Consistent solution, in certain cases, also falls between these narrower bounds, thus shwoing its capability for providing accurate results (Hill 1965).

6.2 The Model

The Self Consistent Method is applied here to evaluate the elastic constants of a random assemblage of equal, rough elastic spheres that has been consolidated isotropically and has a prescribed mean void ratio $\bar{e}$. The spheres are assigned the elastic properties of quartz, and the assemblage is assumed to be composed of random zones, with each zone consisting of a large number of spheres arranged in either of three regular cubic arrays.

Recently, Shahinpoor (1981) modelled a random 2-D array of equal steel spheres as a combination of Voronoi cells, derived an expression for the probability density function of the void ratio, p(e), and checked experimentally this analytical p(e) by means of an optical scanning technique, Fig. 28

(see also Shahinpoor and Shahrpass, 1982). The expression for p(e) is:

$$p(e) = \frac{\lambda \exp(-\lambda e)}{\exp(-\lambda e_{min}) - \exp(-\lambda e_{max})} \tag{45}$$

where $$\bar{e} = \frac{1}{\lambda} + \frac{e_{min} \exp(-\lambda e_{min}) - e_{max} \exp(-\lambda e_{max})}{\exp(-\lambda e_{min}) - \exp(-\lambda e_{max})} \tag{46}$$

λ is obtained from the mean void ratio, $\bar{e}$, of the distribution p(e). As mentioned before, it is reasonable to model a uniform, rounded-grained sand as a random combination of zones corresponding to regular cubic arrays, and this was the approach taken in this work. The sand medium is assumed to be composed of regular arrays in the fashion of Figs. 28 and 29, where each randomly oriented Voronoi polyhedron is one of these zones, and contains a regular array with many spheres. A cross section of this 3-D medium could be visualized approximately by the actual photograph of the 2-D medium in Fig. 28b; in this, the black spots are spheres and the white are voids, and zones of regular packings can be clearly observed. The macroscopic moduli of the whole medium will be determined from the properties of these zones through the self consistent scheme.

As a first step, the probability density function of the void ratio, p(e), Eq. 45, was transformed to the probability density function of the porosity, p(n), with the basic equation (Benjamin and Cornell, 1970):

$$p(n) = \left|\frac{de}{dn}\right| p(e)$$

as the mean of the porosity distribution, $\bar{n}$, coincides with the macroscopic (measured) porosity of the "soil", unlike the mean void ratio $\bar{e}$, which is not identical to the macroscopic void ratio (Petrakis, 1983).

Then, the probability density function of the porosity, p(n), was discretized into three segments of influence, corresponding respectively to the porosities of the three regular cubic arrays (see Fig. 31): sc (n = 0.48), bcc (n = 0.32) and fcc (n = 0.26). The values of n_{min} and n_{max} used for all calculations were those of the sc and fcc arrays.

For example, for a prescribed macroscopic porosity $\bar{n}$ = 0.35 corresponding to a mean void ratio $\bar{e}$ = 0.54, the calculation illustrated in Fig. 31 allowed determining the following three volume concentrations, c_i:

Array	n_i	c_i
sc	0.48	0.1934
bcc	0.32	0.5921
fcc	0.26	0.2143

The medium with these three phases was then subjected to an isotropic boundary confining pressure, σ_o°, and subsequently subjected to small boundary stress increments $d\sigma_{ij}$, from which the corresponding elastic, very small strain increments at the boundaries, and the mean cubic medium moduli K^* and G^* were evaluated.

If we now assume that the phases are quadratic (elliptical or circular) in cross section we can apply the Self Consistent method. The assumption that the "zones" are quadratic in cross-section is important, since if the resulting stress and strain fields are uniform (see Section 6.1) within each "zone", the "zone" can be replaced by the representative cube of each cubic array (Figs. 15-17) and the corresponding constitutive laws are given by Eqs. 10, 16 and 23. Since in turn these relations depend upon the pressure acting on each inclusion or phase, the value of the stress field at the boundary of each of these phases and inside it can be readily obtained from Eshelby's

(1957), and Budiansky's (1965) results:

$$\bar{\sigma}_o^i = \sigma_o^o \frac{K_i}{K^*} \left[\frac{1}{1 + \alpha^* \left(\frac{K_i}{K^*} - 1 \right)} \right] \tag{47}$$

where the value of α^* depends upon the shape of the zone, (Eshelby, 1957), which here has been assumed to be spherical for simplicity. Note that this value of $\bar{\sigma}_o^i$ is independent of the location of the zone, and is thus the same for all zones containing the same regular cubic array or phase.

Equation 47 is then replaced into Eqs. 10, 16 and , and the problem finally reduces to the solution of the following equations for the three phases:

$$\bar{\sigma}_o^i = \sigma_o^o \frac{K_i}{K^*} \left[\frac{1}{1 + \alpha^* \left(\frac{K_i}{K^*} - 1 \right)} \right] \quad ; \ i = 1,2,3 \tag{48}$$

$$\sum_{i=1}^{3} \frac{C_i}{1 + \beta^* \left(\frac{G_i}{G^*} - 1 \right)} = 1.0 \tag{49}$$

$$\sum_{i=1}^{3} \frac{C_i}{1 + \alpha^* \left(\frac{K_i}{K^*} - 1 \right)} = 1.0 \tag{50}$$

$$\alpha^* = \frac{1+\nu^*}{3(1-\nu^*)} \tag{51}$$

$$\beta^* = \frac{2}{15} \frac{(4-5\nu^*)}{(1-\nu^*)} \tag{52}$$

$$\nu^* = \frac{3K^*-2G^*}{6K^*+2G^*} \tag{53}$$

where $K_i = K_i(\overline{\sigma}_o^i)$, $G_i = G_i(\overline{\sigma}_o^i)$ for the three phases are obtained with Eqs. 10, 16 and 23 for $i = 1, 2, 3$, corresponding, respectively, to the simple cubic, body centered cubic and face centered cubic regular arrays.

6.3 Application to Quartz Sand

The proposed model was evaluated using as input the elastic parameters of quartz for the individual spheres, which are $E_s = 11.0 \times 10^6$ psi and $\nu_s = 0.15$ (White, 1965, Ko & Scott, 1967, Lambe and Whitman, 1969, see Table 3), and for a wide range of isotropic confining pressures. The values of the computed shear modulus G^* are plotted on solid lines in Figs. 32 and 33 versus confining pressure $\sigma_o = \sigma_o^o$ for e = 0.54 and e = 0.46, respectively. The values of the bulk modulus, K^*, were also computed, and Fig. 34 contains a plot of confining pressure versus volumetric strain predicted by the model for e = 0.54, where the volumetric strain was derived from this computed bulk modulus, $\overline{\varepsilon}_v = \sigma_o^o/K^*$.

As mentioned before in connection with Fig. 27, regular arrays are much stiffer, up to 3.5 times stiffer, than actual uniform, rounded sands, and this constitutes a serious defficiency of the model. However, Drnevich and Richart (1970) have suceeded in increasing significantly the shear stiffness of dry, rounded, uniform Ottawa quartz sand by applying millions of cycles of a shear strain slightly greater than the threshold strain in a resonant column device.

Figures 32 and 33 also include as data points the resonant column experimental results obtained by Drenvich and Richart, for macroscopic void ratios, e = 0.54 and e = 0.46, respectively. The lower dotted line in each figure corresponds to virgin or uncycled sand as predicted by the Hardin and Black (1966)

correlation, which is essentially identical to the Hardin and Richart correlation depicted in Fig. 27(b). In both figures, two trends may be clearly observed: a) as the number of cycles, N, increases, the test results steadily approach the model values until, at $N = 22 \times 10^6$ cycles, in Fig. 32, the agreement becomes excellent; and b) the slope of the line of shear modulus vs confining pressure decreases from about 1/2 in the uncycled state to about 1/3 after, approximately, 1×10^6 cycles. The reason for some of the points showing more scatter is probably because those points were cycled more than others with the same void ratio, or because their void ratios were slightly differed.

In the above tests, the sand specimens were cycled at strains which, although larger than the threshold strain, were small enough so that no significant densification occurs, and indeed the change in measured (macroscopic) void ratios between virgin and cycled specimens was very little or negligible; thus, densification is certainly not the explanation in the observed threefold increase in the sand stiffness. Drnevich and Richart (1970) speculated in their paper that the above behavior could be due to wearing of the contacts, increase of the contact areas or <u>formation of additional contacts</u>. The authors think that this third reason explains the phenomenom completely, as illustrated by the comparison with the model in Figs. 32-33, and by the relation between stiffness and number of contacts in Fig. 26. It is known that in a random array of spheres there may be less contacts than in regular packings (see Smith et al., 1929) and, furthermore, it is possible to have contacts which do not transmit any load (dead contacts). By continuous cycling such as performed by Drnevich and Richart in their tests these contacts were made load-transmitting and new ones were formed until all or most possible contacts were created and the stiffness of the sand coincided with that predicted by the model. It is interesting that the creation of contacts can also be achieved by high

isotropic confining pressures (Duffy and Mindlin, 1958, Deresiewicz 1958, see also Fig. 13).

The analytical model proposed herein describes exactly this: since it assumes that the sand is a random assemblage of regular arrays of spherical grains, it implies that the number of contacts is the maximum possible. Furthermore, as shown by Duffy and Mindlin (1958) and Deresiewicz (1959), and as illustrated by Fig. 13, when the number of contacts increases the pressure dependency of the moduli tends to change from 1/2 to 1/3. All of this is interpreted by the model, which is shown here to represent the limiting state, in terms of number of contacts and of stiffness, that a sand can reach.

Figure 34 shows the confining pressure σ_o^o vs. volumetric strain, $\bar{\varepsilon}_v$, measured by Drnevich and Richart on the same Ottawa sand specimens discussed above, for a virgin specimen and for a specimen after 1 x 10^6 cycles of shear strain. Unfortunately, no data is available for sand specimens cycled with more than 1 x 10^6 cycles. In the figure, lines have been passed which approximately represent these experimental data. The line predicted by the model is also plotted, and again it is clear that the cycling is increasing the bulk modulus of the soil, thus making it approach the curve predicted by the model, as the number of contacts increases toward the theoretical, maximum value. It would be interesting to compare the difference between the analytical results and the experimental values for both moduli, K^* and G^* at a given cycling state. The experimental values for the case of hydrostatic compression (Fig. 34) are closer to the model predicted curve than the measurements with shear (Figs.32-33), for a comparable number of cycles. This is explained by the fact that, once the spheres have approached each other due to the cycles of shearing, an increase in σ_o^o can complete the formation of many contacts, thus further increasing the stiffness of the soil.

Section 7

CONCLUSION

A particulate mechanics (micromechanical) model has been developed for describing the elastic response of assemblages of identical elastic spheres of arbitrary macroscopic porosity, $\bar{n}$, subjected to an arbitrary isotropic boundary pressure, σ_o. The model is based on the Mindlin-Deresiewicz theory of bodies in contact and takes into account the spatial variation of porosity. The model assumes that the assemblage is composed of random clusters of several regular arrays of various porosities and it computes the macroscopic moduli by means of the Self Consistent Method.

The predictions of the model, specialized for the case of quartz spheres, were compared to measurements of shear modulus, G_{max} on uniform quartz sands, with good qualitative agreement; however, the analytical "sands" were as much as 3.5 times stiffer than the actual soils. This is explained by the fact that sands have less effective contacts per grain than theoretically predicted for a given porosity $\bar{n}$. However, when the sand is prestrained by millions of shearing cycles slightly above the threshold strain, G_{max} approaches the theoretical value without changing $\bar{n}$, as the theoretical number of contacts is realized. Thus, the model exhibits excellent agreement with results on heavily prestrained sand, and it also provides upper bounds for small strain shear and bulk moduli for all rounded uniform sands.

REFERENCES

Backman, B.F., Brown, C.B., Jowitt, P.W. and Munro, J. (1983), "Statistical Mechanics of Granular Materials," <u>Advances in the Mechanics and the Flow of Granular Materials</u>, Vol. I, M. Shahinpoor, ed., Trans. Tech. Publications, Clansthal-Zellerfeld, Fed. Republic of Germany.

Benjamin, J.R. and Cornell, C.A. (1970), <u>Probability, Statistics and Decision for Civil Engineers</u>, McGraw Hill.

Bernal, J.D. and Mason, J. (1960), Co-ordination of Randomly Packed Spheres, Nature, Vol. 188, pp. 910-911.

Bernal, J.D., Knight, K.R. and Cherry, I. (1964), Growth of Crystals from Random Close Packing, Nature, Vol. 202, pp. 852-854.

Brandt (1955), "A Study of the Speed of Sound in Porous Media," J. Appl. Mech. 22, pp. 479-486.

Brauns, J. (1968), Uber den Einfuss des Einzelkornbruches auf die Belastbarkeit von Haufwerken, besonders von regelmassigen kugelpackugen, im Dreiaxialversuch, PhD Dissertation, Univ. Karlsruhe.

Brauns, J. and Leussnink (1970), Uber mechanische Eigenschaften von Kugelpackungen, verfahrenstechnik 4, 1, S.5-8.

Brown, C.B. (1978), "The Use of Maximum Entropy in the Characterization of Granular Media," <u>Proceedings US-Japan Seminar on Continuum Mechanical and Statistical Approaches in the Mechanics of Granular Materials</u>, Cowin and Satake, editors, pp. 98-109.

Budiansky, B. (1965), "On the Elastic Moduli of Some Heterogeneous Materials," JMPS 1965, Vol. 13, pp. 223-227.

Cattaneo, C. (1938), "Sul contatto di due corpi elastici," Atti Acad. naz. Lincei Rc., Ser. 6, 27, 342-348, 434-436, 474-478.

Chen, W.F. (1975), <u>Limit Analysis and Soil Plasticity</u>, Elsevier Scientific Publishing Co., Amsterdam, The Netherlands.

Christensen, R.M. (1979), <u>Mechanics of Composite Materials</u>, John Wiley & Sons, Inc. New York.

Cowin and Satake, editors (1978), <u>Continuum Mechanical and Statistical Approaches in the Mechanics of Granular Materials</u>, Proceedings of US-Japan Seminar, Sendai, Japan, June 1978.

Cundall, P.A. and Strack, P.A. (1983), "Modeling of Microscopic Mechanisms in Granular Material," in <u>Mechanics of Granular Materials: New Models and Constitutive Relations</u>, Jenkins and Satake, editors, pp. 137-149.

Dantu, P. (1957), "Contribution a l'Etude Mechanique et Geometrique des Millieux Pulverulents," Proc. of the 4th Int. Conf. on Soil Mech. and Found. Eng., London.

Davis, R.A. (1974), "A Discrete Probabilistic Model for Mechanical Response of a Granular Medium," Ph.D. Dissertation, Columbia Univ.

Davis, R.A. and Deresciewicz, H. (1977), "A Discrete Probabilistic Model for Mechanical Response of a Granular Medium," Acta Mechanica, 27, pp. 69-89.

Deresciewicz (1958), "Mechanics of Granular Matter," Advances in Applied Mechanics, V, pp. 233-306, New York: Academic Press Inc.

Deresciewicz, H. (1958a), "Stress-Strain Relations for a Simple Model of a Granular Medium," J. Appl. Mech., Trans. ASME, Sept., pp. 402-406.

Deresciewicz, H. (1973), "Bodies in Contact with Applications to Granular Media," included in R.D. Mindlin and Applied Mechanics, G. Herrmann, Editor, Pergamon Press, New York.

DiMaggio, F.L. and Sandler, I.S. (1971), "Material Model for Granular Soils," Journal of the Engineering Mechanics Division, ASCE, Vol. 97, pp. 935-950.

Dobry, R. and Anthanasiou-Grivas, D. (1978), "Stress-Strain Relation for Soils Under Earthquake Loading: Technical Background," Report No. 78-2, Department of Civil Engineering, Rensselaer Polytechnic Institute, Troy, NY.

Dobry, R., Powell, D.J., Yokel, F.Y. and Ladd, R.S. (1980), "Liquefaction Potential of Saturated Sand - The Stiffness Method," Proc. Seventh World Conference on Earthquake Engineering, Istanbul, Turkey, September, Vol. 3, pp. 25-32.

Dobry, R., Stokoe, K.H. II, Ladd, R.S. and Youd, T.L. (1981), "Liquefaction Susceptibility from S-Wave Velocity," Proc. Session on In Situ Tests on Evaluate Liquefaction Susceptibility, ASCE National Convention, St. Louis, Missouri, October.

Dobry, R., Yokel, F.Y. and Ladd, R.S. (1981a), "Liquefaction Potential of Overconsolidated Sands in Moderately Seismic Areas," Proc. Conf. on Earthquake and Earthquake Engineering in the Eastern U.S., Knoxville, TN, September.

Dobry, R., Ladd, R.S., Yokel, F.Y., Chung, R.M. and Powell, D. (1982), "Prediction of Pore Water Pressure Buildup and Liquefaction of Sands During Earthquakes by the Cyclic Strain Method," Building Science Series 138, National Bureau of Standards.

Dobry, R. and Petrakis, E. (1984), "Sand Compaction in Cyclic Shear - A Statisti- Model," Proceedings 5th ASCE-EMD Specialty Conference, Laramie, Wyoming, August.

Drenevich, V.P. and Richart, F.E., Jr. (1970), "Dynamic Prestraining of Dry Sand," Journal of the SMFD, ASCE, 96, SM2, March, pp. 453-469.

Drucker, D.C. and Prager, W. (1952), "Soil Mechanics and Plastic Analysis or Limit Design," Quarterly of Applied Mathematics, Vol. 10, pp. 157-165.

Duffy, J. and Mindlin, R.D. (1957), "Stress-Strain Relations of a Granular Medium," J. Appl. Mech., Trans. ASME, Dec., pp. 585-593.

Duffy, J. (1959), "A Differential Stress-Strain Relation for the Hexagonal Close-Packed Array of Elastic Spheres," J. Appl. Mech., 26, pp. 88-94.

Dyvik, R., Dobry, R., Thomas, G.E. and Pierce, W.G. (1982), "Influence of Consolidation Shear Stresses and Relative Density on Threshold Strain and Pore Pressure During Cyclic Straining of Saturated Sand," Research Report No. CE-82-11, Department of Civil Engineering, Rensselaer Polytechnic Institute, Troy, NY.

Eshelby, J.D. (1957), "The determination of the elastic field of an ellipsoidal inclusion and related problems," Proc. R. Soc. London, vol. A241, 376.

Field, W.G. (1963), "Towards the Statistical Definition of a Granular Mass," 4th Australia - New Zealand Conf. on Soil Mech. and Found. Eng., pp. 143-148.

Filep, L. (1936), "Egynelo qom bokol allo halmozok, Vizugyi Kolzlemenyek, Budapest.

Finney, J.L. (1985), "Structure and Properties of Granular Materials: Guidelines from Modelling Studies of Liquids and Amorphos Solids," Advances in the Mechanics and the Flow of Granular Materials,, Vol. I, M. Shahinpoor, ed., Trans. Tech. publications, Clansthal-Zellerfeld, Fed. Republic of Germany.

Gassmann, F. (1951), "Elastic Waves Through a Packing of Spheres," Geophysics, 16, pp. 673-685 and (1953) 18, p. 269.

Grivas, D. and Harr, M.E. (1974), "Particle Contacts in Discrete Materials," Indiana Academy of Science, Engineering Division.

Hara, G. (1935), "Theorie der Akustischen Schwingungsausbreitung in Gekornten Substanzen und Experimentelle Untersuchungen an Kohlepulver," Elektrische Nachrichten-Technik 12, pp. 191-200.

Hardin, B.O. and Richart, F.E., Jr. (1963), "Elastic Wave Velocities in Granular Soils," Journal of the Soil Mechanics and Foundations Division, ASCE, Vol. 89, No. SM1, February, pp. 33-65.

Hardin, B.O. and Black, W.L. (1966), "Sand Stiffness Under Various Triaxial Stresses," J. Soil Mechanics and Foundation Div. Proc. ASCE, Vol. 94, No. SM2, pp. 27-42.

Hardin, B.O. and Drnevich, V.P. (1972), "Shear Modulus and Damping in Soils: Measurements and Parameter Effects," Proc. ASCE, 98, No. SM6, June, pp. 603-624.

Hardin, B.O. (1978), "The Nature of Stress-Strain Behavior of Soils," Proc. ASCE Specialty Conference on Earthquake Engineering and Soil Dynamics, Pasadena, California, Vol. 1, pp. 3-90.

Hardin, B.O. (1980), "Discussion to 'Anisotropic Shear Modulus Due to Stress Anisotropy' by S.K. Roesler," Journal of the Geotechnical Engineering Division, ASCE, Vol. 106, No. GT8, August, pp. 956-958.

Harr, M.E. (1977), Mechanics of Particulate Media - A Probabilistic Approach, McGraw Hill, N.Y.

Hashin, Z. and Shtrikman, S. (1963), "A Variational Approach to the Theory of the Elastic Behaviour of Multiphase Materials," JMPS, Vol. 11, 127.

Hendron (1963), "The Behavior of Sand in One-Dimensional Compression," Ph.D. Thesis, University of Illinois, Dept. of Civil Engineering.

Hershey, A.V. (1954), "The Elasticity of an Isotropic Aggregate of Anisotropic Cubic Crystals," J. Appl. Mechanics, Vol. 21, 236.

Hertz, H. (1882), "Ueber die Beruhrungfester Elastischer Korper," J. renie angew. Math. 92, pp. 156-171.

Hill, R. (1950), The Mathematical Theory of Plasticity, Clarendon Press, Oxford.

Hill, R. (1965), "A Self-Consistent Mechanics of Composite Materials," JMPS, Vol. 13, pp. 213-222.

Horne, M.R. (1965), "The Behavior of an Assembly of Rotund, Rigid, Cohesionless Particles," Proc. Royal Society, Series A., Vol. 286.

Ishlinsky, A. Iu. (1954), Ukr. Mat. Zhurnal, 6, 314.

Iwan, W.D. (1967), "On a Class of Models for the Yielding Behavior of Continuous and Composite Systems," Journal of Applied Mechanics, Vol. 34, pp. 612-617.

Iwasaki, T., Tatsuoka, F. and Takagi, Y. (1978), "Shear Moduli of Sands Under Cyclic Torsional Shear Loading," Soils and Foundations, Vol. 18, No. 1, March, pp. 39-56.

Jenkins and Satake, editors (1983), Mechanics of Granular Materials: New Models and Constitutive Relations, Proceedings of US-Japan Seminar, Ithaca, New York, August 1982.

Kinoshita, N. and Mura, T. (1971), Elastic Fields of Inclusions in Anisotropic Media Physica status solidi (a)5, 759.

Knox, D.P., Stokoe, K.H., II and Kopperman, S.E. (1982), "Effect of State of Stress on Velocity of Low-Amplitude Shear Waves Propagating Along Principal Stress Directions in Dry Sand," Geotechnical Engineering Report GR82-23, Civil Engineering Department, The University of Texas at Austin.

Ko, H.Y. and Scott, R.F. (1967), "Deformation of Sand in Hydrostatic Compression," J. Soil Mech. Found. Div., Proc. ASCE, 93, pp. 137-156.

Konishi, J. (1978), "Microscopic Model Studies on the Mechanical Behavior of Granular Materials," Proceedings US-Japan Seminar on Continuum Mechanical and Statistical Approaches in the Mechanics of Granular Materials, Cowin and Satake, editors, pp. 27-46.

Kopperman, S.E., Stokoe, K.H., II and Knox,D.P. (1982), "Effect of State of Stress on Velocity of Low-Amplitude Compression Waves Propagating Along Principal Stress Directions in Sand," Research Report GR22-22, Department of Civil Engineering, University of Texas at Austin.

Kroner, E. (1958), Berechnung der Elastischen Kanstauten des Vielkristalls ones den Konstanten des Einkristalls. Zeitschrift fur Physik, Bd 151, S504-518.

Lade, P.V. and Duncan, J.M. (1975), "Elastoplastic Stress-Strain Theory for Cohesionless Soil," Journal of Geotechnical Engineering Division, ASCE, Vol. 101, No. GT10, pp. 1037-1053.

Lambe, T. and Whitman, R. (1969), Soil Mechanics, John Wiley & Sons, New York.

Lawrence, F.V. (1965), "Ultrasonic Shear Wave Velocities in Sand and Clay," Massachusetts Institute of Technology, Department of Civil Engineering, Research Report R65-05, January.

Lee, S.H.H. (1985), "Investigation of Low Amplitude Shear Wave Velocity in Anisotropic Material," Ph.D. Dissertation, Univ. Texas at Austin, TX.

Love, A.E.H. (1927), A Treatise on the Mathematical Theory of Elasticity, Cambridge University Press.

Makhlouf, H. (1963), "Stress-Strain Relation and Irrotational Wave Motion of Granular Media," Doctoral Thesis, Carnegie Institute of Technology.

Makhlouf, H. and Stewart (1967), "Elastic Constants of Cubical-Tetrahedral and Tetragonal Sphenoidal Arrays of Uniform Spheres," Proc. Intl. Symposium on Wave Propagation and Dynamic Properties of Earth Materials, Albuquerque, NM, Aug.

Mindlin, R.D. (1949,) "Compliance of Elastic Bodies in Contact," Journal of Applied Mechanics, Sept., pp. 259-268.

Mindlin, R.D., Mason, W.P., Osmer, T.F. and Deresiewicz, H. (1951), "Effects of an Oscillating Tangential Force on the Contact Surfaces of Elastic Spheres," Proc. 1st U.S. National Congress of Appl. Mech., ASME, pp. 203-208.

Mindlin, R.D. and Deresiewicz, H. (1953), "Elastic Spheres in Contact Under Varying Oblique Forces," J. Appl. Mech., Trans. ASME, Sept., pp. 327-344.

Mogami, T. (1965), "A Statistical Theory of Mechanics of Granular Materials," J. Fac. Engng., Univ. of Tokyo (B), Vol. 28, pp. 65-79.

Morgenstern, M. (1963), "Maximum Entropy of Granular Materials," Nature, Vol. 200, pp. 559-560.

Mroz, Z. (1967), "On the Description of Anisotropic Workhardening," Journal of Mechanics and Physics of Solids, Vol. 15, pp. 163-175.

Mroz, Z. (1969), Acta Mech., 7 (2-3), (199-212).

Mroz, Z., Norris, V.A. and Zienkiewicz, O.C. (1978), "An Anistropic Hardening Model for Soils Its Applications to Cyclic Loading," International Journal for Numerical and Analytical Methods in Geomechanics, Vol. 2, pp. 203-221.

Mroz, Z., Norris, V.A. and Zienkiewicz, O.C. (1979), "Application of an Anisotropic Hardening Model in the Analysis of Elasto-Plastic Deformation of Soils," Geotechnique, Vol. 29, No. 1, pp. 1-34.

Munro, J. and Jowitt, P.W. (1974), "Information Theory and Granular Materials," Civil Eng. Dept., Imperial College of Science and Techn., London.

National Research Council (1985), Report on "Liquefaction of Soils," Washington, D.C.

Nemat-Nasser, S. and Mehrabadi, M. (1983), "Stress and Fabric in Granular Masses," in Mechanics of Granular Materials: New Models and Constitutive Relations, Jenkins and Satake, editors, pp. 1-8.

Oda, M. (1974), "A Mechanical and Statistical Model of Granular Material," Soils and Found., Japanese Soc. of S.M. & F.E., Vol. 14, No. 1, pp. 13-27.

Oda, M., Konishi, J. and Nemat-Nasser, S. (1983), "Experimental Micromechanical Evaluation of the Strength of Granular Materials; Effects of Particle Rolling," in Mechanics of Granular Materials: New Models and Constitutive Relations, Jenkins and Satake, editors, pp. 21-30.

Oner, M. (1984), "Analysis of Fabric Changes During Cyclic Loading of Granular Soils," Proc. 8th World Conf. on Earthquake Engineering, San Francisco, July.

Perry, D.C. and Brown, C.B. (1981), "Compliance of Assemblage of Unlike Elastic Spheres," Journal of the Engineering Mechanics Division, ASCE, Vol. 107, No. EM1, February, pp. 149-167.

Petrakis, E. (1983), "A Statistical Model to Predict Compaction of Dry Sand During Cyclic Simple Shear Loading: Model and Applications," M.S. thesis, Rensselaer Polytechnic Institute, Troy, NY.

Prager, W. (1955), Proc. Institution of Mechanical Engineers, Vol. 169, pp. 44-57.

Prevost, J.H. (1977), "Mathematical Modelling of Monotonic and Cyclic Undrained Clay Behavior," International Journal for Numerical and Analytical Methods in Geomechanics, Vol. 1, pp. 195-216.

Prevost, J.H. (1978), "Plasticity Theory for Soil Stress-Strain Behavior," Journal of the Engineering Mechanics Division, ASCE, Vol. 104, No. EM5, pp. 1177-1194.

Prevost, J.H. and Hoeg, K. (1975), "Effective Stress-Strain-Strength Model for Soils," Journal of the Geotechnical Engineering Division, ASCE, Vol. 101, No. GT3, pp. 259-278.

Pyke, R.M. (1973), "Settlement and Liquefaction of Sands under Multi-Directional Loading," Ph.D. Dissertation, University of California, Berkeley.

Reyes, S.F. (1966), "Elastic-Plastic Analysis of Underground Openings by the Finite Element Method," Ph.D. Thesis, University of Illinois, Urbana, Ill.

Richart, F.E., Hall, J.R. and Woods, R.D. (1970), Vibrations of Soils and Foundations, Prentice-Hall Inc., New Jersey.

Roesler, S.K. (1979), "Anisotropic Shear Modulus Due to Stress Anisotropy," Journal of the Geotechnical Engineering Division, ASCE, Vol. 105, No. GT5, July, pp. 871-880.

Roscoe, K.H. (1970), "The Influence of Strains in Soil Mechanics," Geotechnique, 20, 129-170.

Rowe, P.W. (1962), "The Stress-Dilatancy Relation for Static Equilibrium of an Assembly of Particles in Contact," Proc. Roy. Soc., A269, pp. 500-527.

Schmertmann, J.H. (1978), "Effect of Shear Stress on Dynamic Bulk Modulus of Sand," U.S. Army Engineering Waterways Experiment Station, Technical Report S-78-16, October.

Scott, G.D. (1960), Packing of Equal Spheres, Nature, Vol. 188, pp. 908-909.

Scott, R. and Ko, H. (1969), "Stress-Deformation and Strength Characteristics," State-of-the-Art Report, Proceedings Seventh Int. Conf. on Soil Mechanics and Foundation Engineering, Mexico City, pp. 1-47.

Seed, H.B. and Idriss, I.M. (1970), "Soil Moduli and Damping Factors for Dynamic Response Analyses," Earthquake Engineering Research Center Report No. EERC 70-10, University of California, Berkeley.

Seridi, A. and Dobry, R. (1984), "An Incremental Elastic-Plastic Model for the Force-Displacement Relation at the Contact Between Two Spheres," Research Report, Dept. of Civil Engineering, Rensselaer Polytechnic Institute, Troy, N.Y.

Serrano, A.A. and Rodrigues-Ortiz, J.M. (1973), "A Contribution to the Mechanics of Heterogeneous Granular Media," Symp. on Plast. and Soil Mech., Cambridge, England.

Shahinpoor, M. (1981), "Statistical Mechanical Considerations on Storing Bulk Solids," Bulk Solids Handling, Vol. 1, February, pp. 31-36.

Shahinpoor, M. and Shahrpass, A. (1982), "Frequency Distribution of Voids in Monolayers of Randomly Packed Equal Spheres," Bulk Solids Handling, Vol. 2, 4, pp. 825-838.

Silver, M.L. and Seed, H.B. (1971), "Volume Changes in Sands during Cyclic Loading," JSMFD, ASCE, Vol. 97, No. SM-9, pp. 1171, Sept.

Smith, W.O., Foote, P.D. and Busang, P.F. (1929), "Packing of Homogeneous Spheres," Phys. Rev., 34, pp. 1271-1274.

Sokolnikoff, I.S. (1956), Mathematical Theory of Elasticity, McGraw Hill, New York.

Stokoe, K.H. II, Roesset, J.M., Knox, D.P., Kopperman, S.E. and Suddhiprakarn, C. (1980), "Development of a Large-Scale Triaxial Testing Device for Wave Propagation Studies," Geotechnical Engineering Report GR80-10, University of Texas at Austin.

Stokoe, K.H. II, Lee, S.H.H. and Knox, D.P. (1985), "Shear Moduli Measurements under True Triaxial Stresses," Advances in the Art of Testing Soils Under Cyclic Conditions, Khoslo Vijay, ASCE, Detroit, MI.

Takahashi, T. and Sato, Y. (1950), "On the Theory of Elastic Waves in Granular Substance," Bulletin Earthquake Research Institute Tokyo University, 28, pp. 37-43.

Vicente, E. and Dobry, R. (1983), "Pore Water Pressure Increase in Loose Saturated Sand at Level Sites During Three Directional Earthquake Loading," Report CE-83-9-1, Dept. of Civil Engineering, Rensselaer Polytechnic Institute, Troy, NY.

Tatsuoka, F., Iwasaki, T., Fukushima, S. and Sudo, H. (1979), "Stress Conditions and Stress Histories Affecting Shear Modulus and Damping of Sand under Cyclic Loading," Soil and Foundations, Japanese Society of Soil Mechanics and Foundation Engineering, Vol. 19, No. 2, pp. 29-43.

Thurston, C.W. and Deresiewicz, H. (1959), "Analysis of a Compression Test of a Model of a Granular Medium," Journal Applied Mechanics, June, pp. 251-158.

Thurston, C.W. (1958), "Stress Strain Relations and Vibration of a Granular Medium," Discussion, Journal of Applied Mechanics, June, pp. 310-311.

Van Vlack (1964), Elements of Materials Science, 2nd Edition, Addision-Wesley, Reading, MA.

White, J.E. and Sengbush, R.L. (1953), "Velocity Measurements in Near-Surface Formation," Geophysics, Vol. 18, pp. 54-69.

White, J.E. (1965) Seismic Waves, McGraw-Hill, New York.

Whitman, R.V., Miller, E.T. and Moore, P.J. (1964), "Yielding and Locking of Confined Sand," Journal of the Soil Mechanics and Foundations Division, Proceedings, ASCE, Vol. 90, No. SM4, pp. 57-84, July.

Woods, R.D. (1978), "Measurement of Dynamic Soil Properties," Proceedings of the Earthquake Engineering and Soil Dynamics Conference, ASCE, Pasadena, CA, June 19-21, Vol. 1, pp. 91-178.

Yanagisawa, E. (1978), "Relation Between the Dynamic Shear Modulus and Void Ratio in Granular Media," Proceedings US-Japan Seminar on Continuum Mechanical and Statistical Approaches in the Mechanics of Granular Materials, Cowin and Satake, editors, pp. 64-70.

Yamagisawa, E. (1983), "The Influence of Void Ratio and Stress Condition on the Dynamic Shear Modulus of Grandular Media," Advances in the Mechanics and the Flow of Granular Materials, Vol. II, M. Shahinpoor, ed., Trans. Tech. Publications, Clausthal-Zellerfled, Fed. Republic of Germany.

Youd, T.L. (1972), "Compaction of Sands by Repeated Shear Straining," Journal of the SMFD, ASCE, 98, SM7, July, pp. 709-725.

Yu, P. and Richart, F.E., Jr. (1984), "Stress Ratio Effects on Shear Modulus of Dry Sands," Journal of Geotechnical Engineering, Vol. 110, No. 3, March, pp. 331-345.

Type of Packing	Other Name	Symbol Used in this report	Coordination Number (Number of Contacts Per Spheres)	Spacing of Layers	Volume of Unit Prism	Density	Porosity n	Void Ratio e
Simple Cubic	-----	sc	6	2R	$8R^3$	$\pi/6$	0.4764	0.9098
Body Centered Cubic	-----	bcc	8	$4R/\sqrt{3}$	$64R^3/3^{3/2}$	0.2165π	0.32	0.47
Cubical Tetrahedral	-----	ct	8	2R	$4\sqrt{3}\,R^3$	$\pi/3\sqrt{3}$	0.3954	0.65
Tetragonal-Sphenoidal	-----	ts	10	$R\sqrt{3}$	$6R^3$	$2\pi/9$	0.3019	0.4325
Hexagonal Closed Packed	tetrahedral	hcp	12	$R\sqrt{2}$	$4\sqrt{2}\,R^3$	$\pi/3\sqrt{2}$	0.2595	0.3504
Face Centered Cubic	pyramidal	fcc	12	$2R\sqrt{2/3}$	$4\sqrt{2}\,R^3$	$\pi/3\sqrt{2}$	0.2595	0.3504

Table 1. Properties of Regular Arrays of Equal Spheres (Deresciewicz, 1958, Van Vlack, 1964)

Coordination Number	Symbol	Porosity	Void Ratio	Cell Number
4	[1,1,2]	0.7181	2.5473	1
	[1,0,3]	0.6599	1.9403	2
	[2,0,2]	0.6599	1.9403	3
5	[1,2,2]	0.6933	2.2605	4
	[2,1,2]	0.6298	1.7012	5
	[1,2,2]≡[1,3,1]	0.5969	1.4808	6
	[1,1,3]	0.5790	1.3753	7
	[1,0,4]	0.5582	1.2635	8
	[2,0,3]	0.5373	1.1612	9
6	[2,2,2]	0.6298	1.7017	10
	[2,2,2]	0.5578	1.2614	11
	[1,2,3]	0.5574	1.2594	12
	[1,3,2]	0.5546	1.2452	13
	[2,2,2]≡[3,0,3]≡[1,4,1]	0.4764	0.9098	14
	[2,0,4]	0.4746	0.9033	15
7	[1,2,4]≡[2,2,3]	0.5132	1.0542	16
	[2,3,2]	0.5063	1.0255	17
	[3,1,3]	0.4918	0.9677	18
	[1,4,2]≡[1,5,1]	0.4389	0.7822	19
8	[2,2,4]	0.4642	0.8664	20
	[1,5,2]	0.3985	0.6625	21
	[2,2,4]	0.3954	0.6540	22
	[3,2,3]≡[2,4,2]≡[1,6,1]	0.3954	0.6529	23
	[4,0,4]	0.3198	0.4702	24
9	[1,4,4]	0.3866	0.6303	25
	[2,5,2]≡[1,6,2]	0.3520	0.5432	26
10	[2,4,4]≡[1,6,3]	0.3343	0.5022	27
	[2,5,3]	0.3127	0.4550	28
	[4,2,4]≡[2,6,2]	0.3019	0.4327	29
11	[2,6,3]	0.2813	0.3908	30
12	[3,6,3]≡[4,4,4]	0.2595	0.3504	31

Table 2 Feasible Regular Arrays or "Cells" (Shahinpoor, 1981)
Coordination No. = N = No. of Contacts per Sphere
[u,m,ℓ] gives No. of Contacts of Spheres with Layer Above, Same Layer and Layer Below: $N = u + m + \ell$

Young's Modulus	$E_s = 11 \times 10^6$ psi
Poisson's Ratio	$\nu_s = 0.15$
Coefficient of Intergranular Friction	$f = 0.5$

Table 3 Properties of Quartz Used in this Report

[Note that Lambe and Whitman (1969) reported a different value $\nu_s = 0.31$ for quartz, which in turn was used for the calculations in Dobry et al. (1982). The lower value $\nu_s = 0.15$ used herein is more realistic and was obtained from White (1964) and Ko and Scott (1967)]

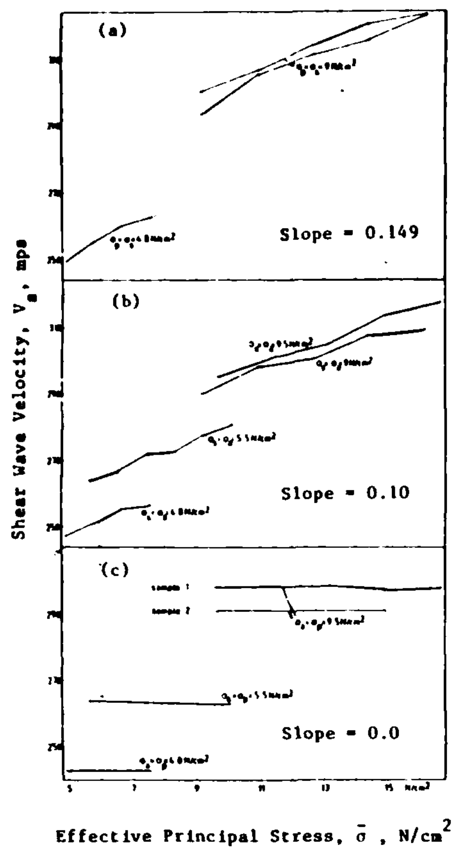

Fig. 1 Variation of V_s with Principal Stress in (a) Direction of Wave Propagation, (b) Direction of Polarization (Particle Motion) and (c) Out-of-Plane Direction (Roesler, 1979)

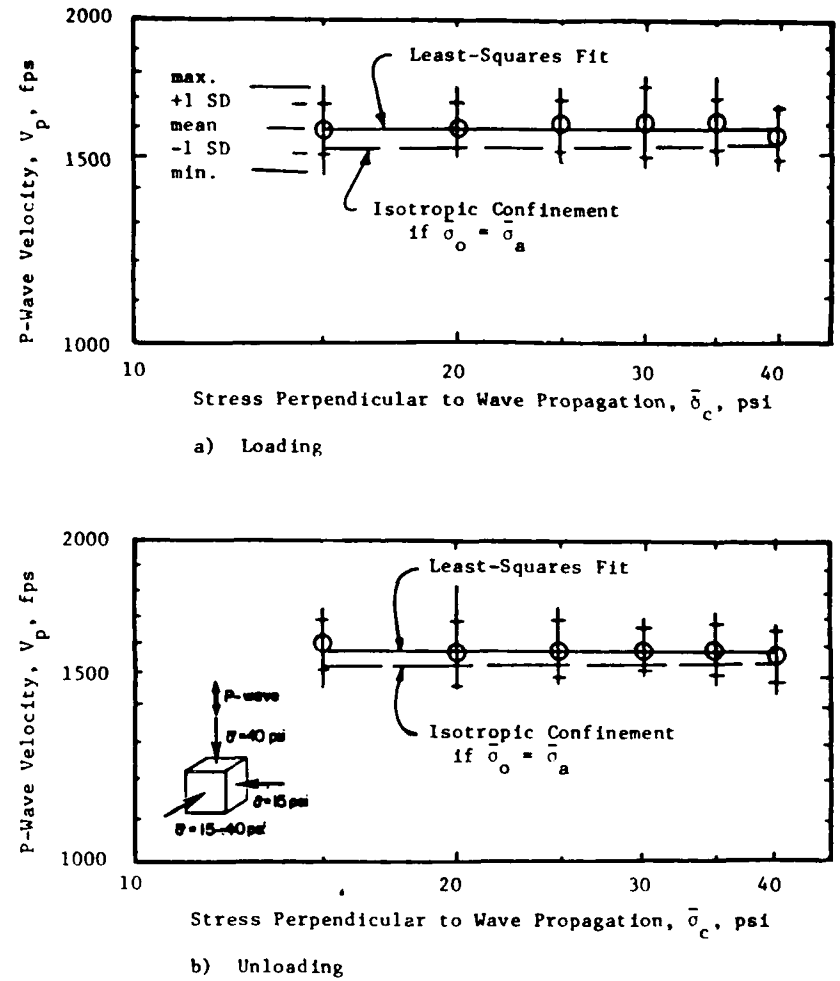

Fig. 2 Effect on V_p of Principal Stress σ_c Perpendicular to Wave Propagation for Biaxial Loading Case (Kopperman et al., 1982)

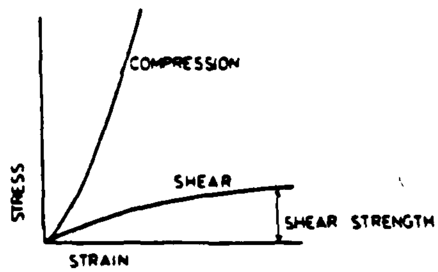

Fig. 3 - Stress-Strain Curves for Monotonic Loading of Dry Granular Soils.

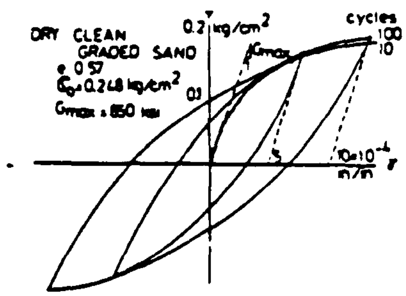

Fig. 4 - Stress-Strain Hysteresis Loops for Reversed Loading (Hardin and Drenevich, 1972).

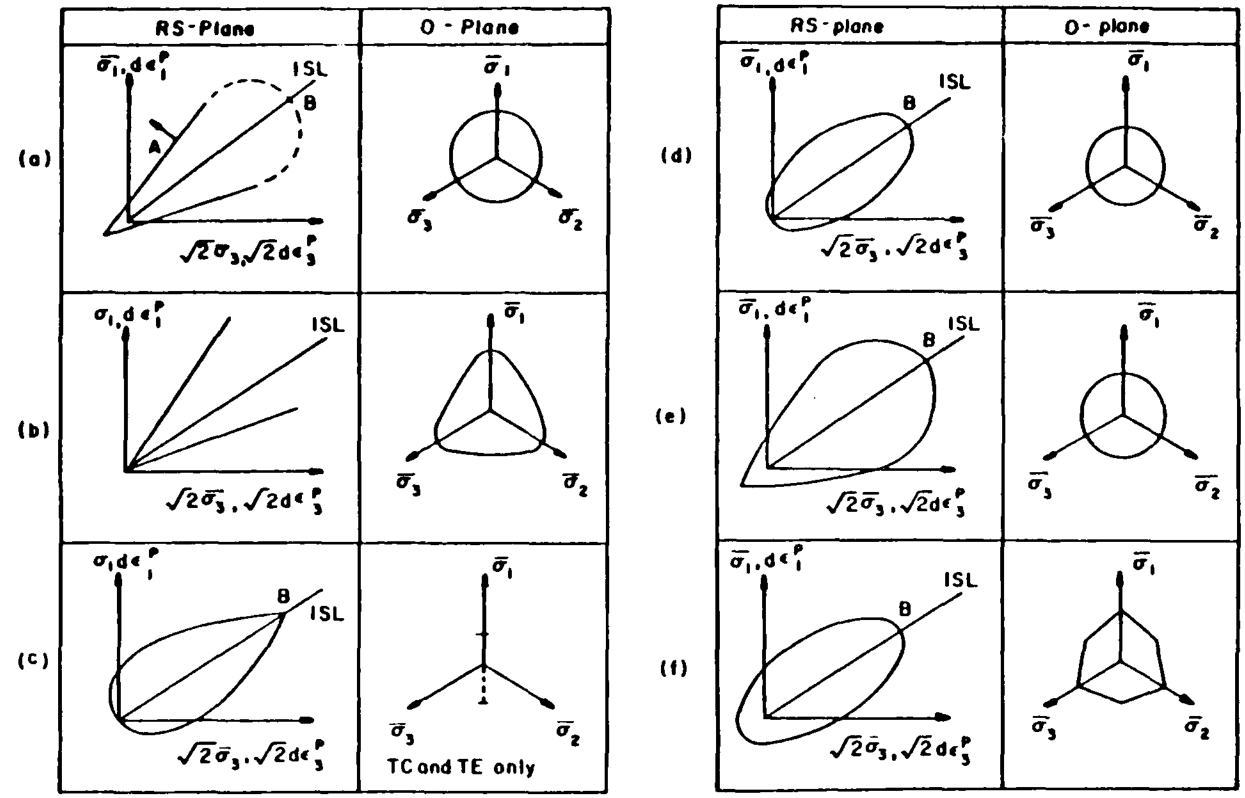

Fig. 5 - Plastic Potential Surfaces: (a) Drucker, et al.; (b) Lade and Duncan; (c) Original Clam-Clay; (d) Modified Cam-Clay; (e) DiMaggio and Sandler; (f) Zienkiewicz, et al. (Hardin, 1978).

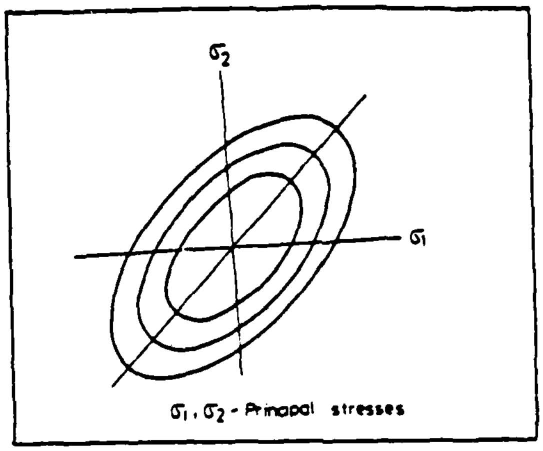

Fig. 6 - Isotropic Hardening Model (Chen, 1975).

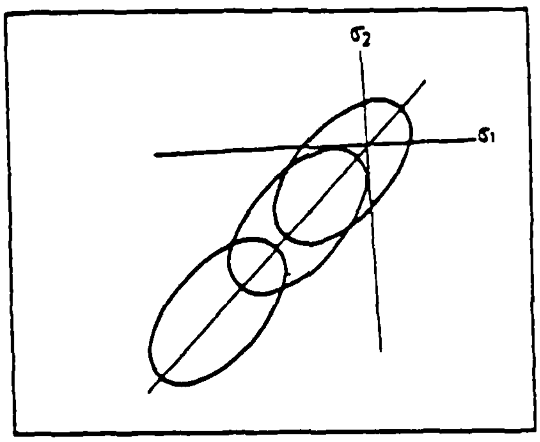

Fig. 7 - Kinematic Hardening Model (Chen, 1975).

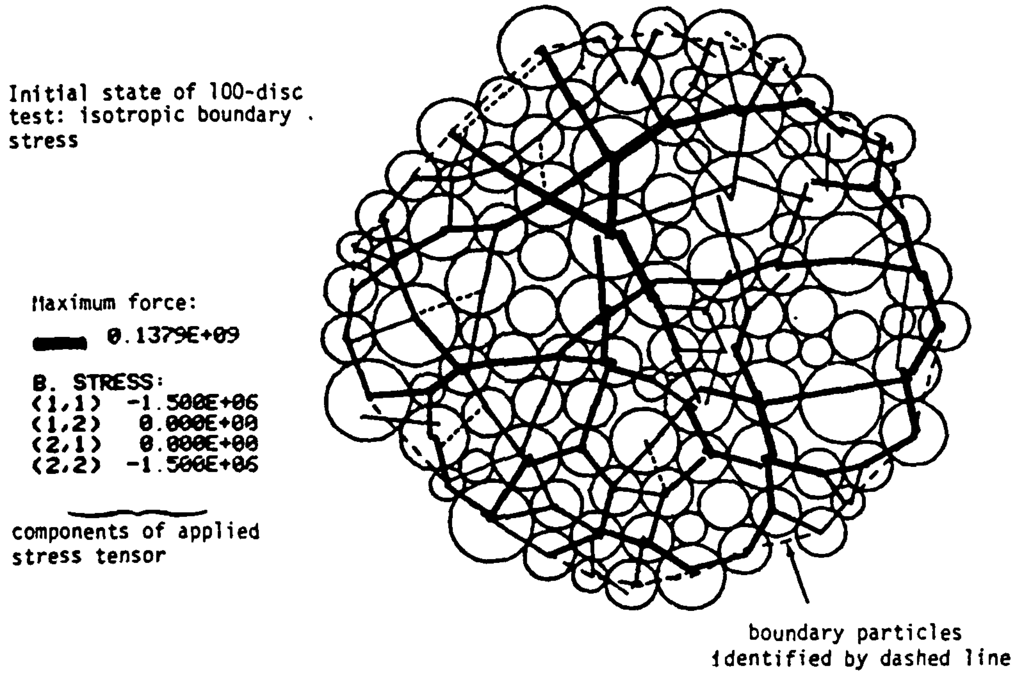

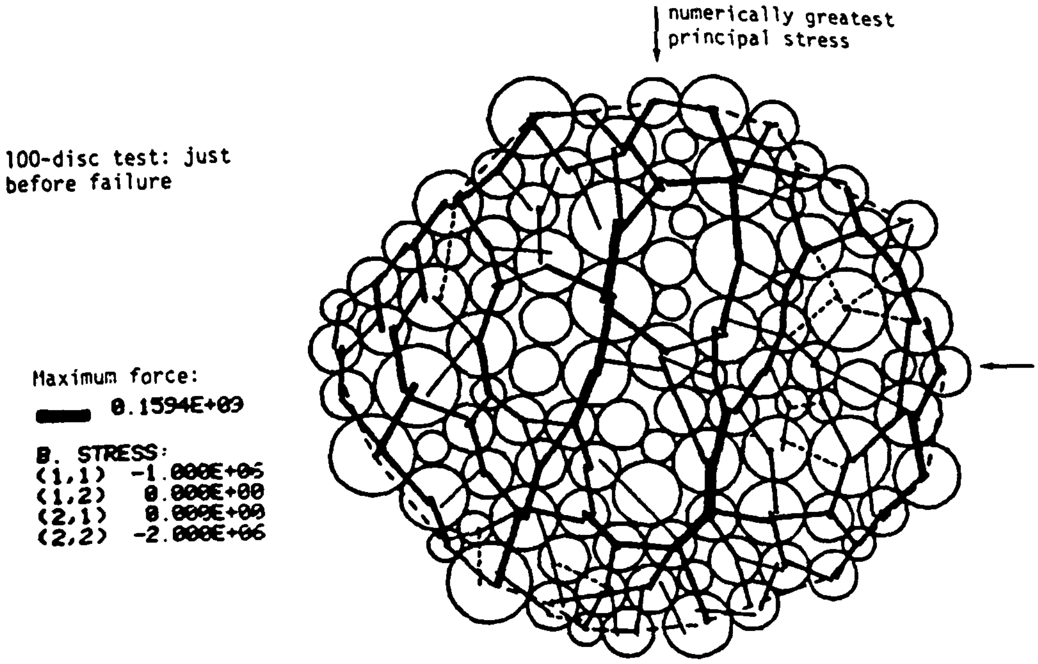

Fig. 8 Finite Difference Simulation of a Triaxial Test on a 100-disc Model (Cundall and Strack, 1983)

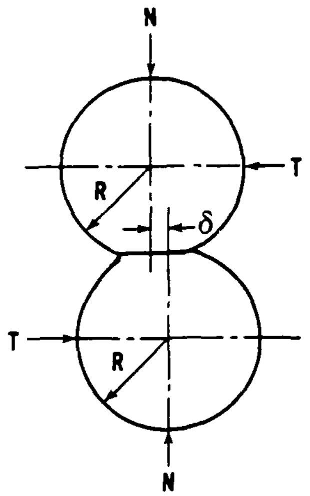

Fig. 9 Elastic Spheres Under Normal and Tangential Loads

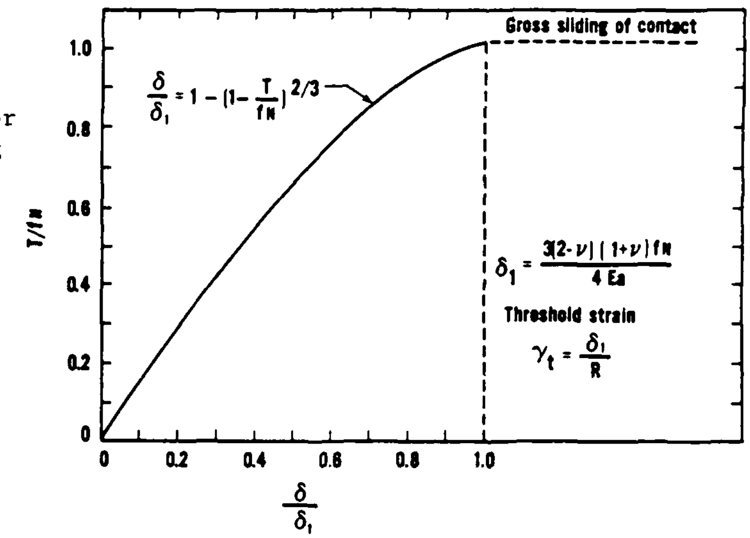

Fig. 10 Tangential Force - Displacement Relation for N Constant, T Increasing (Dobry and Grivas, 1978)

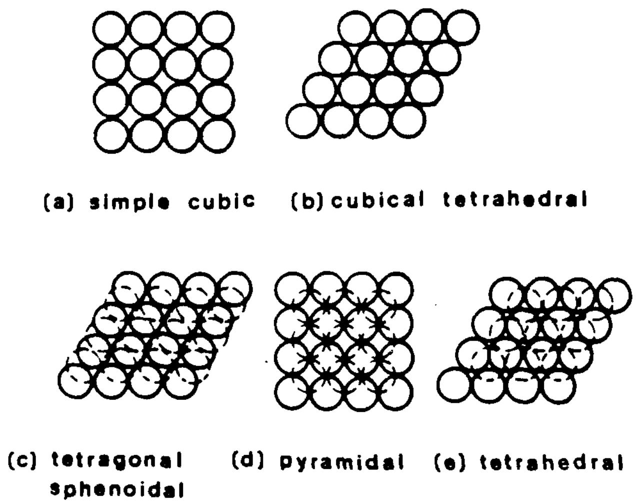

Fig. 11 Regular Arrays of Equal Spheres (Deresciewicz, 1958)

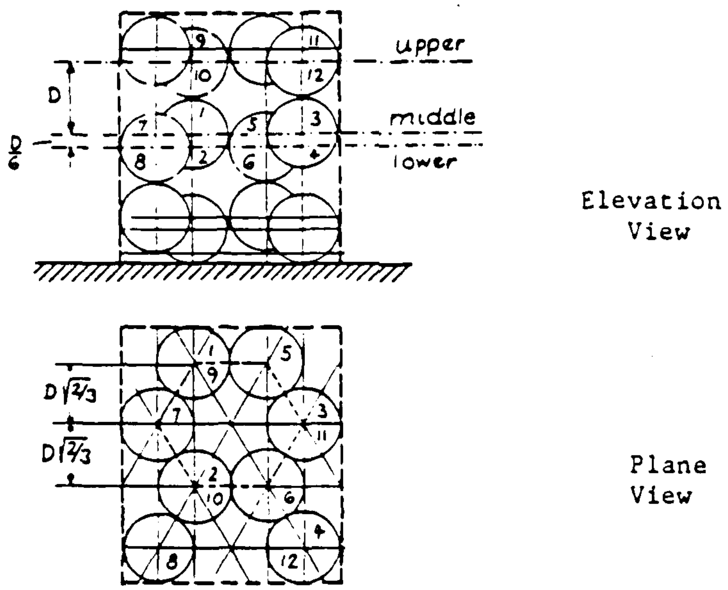

Fig. 12 Regular Array No. 2 (see Table 2)
[1,0,3]; N = 4
n = 0.6599; e = 1.9403

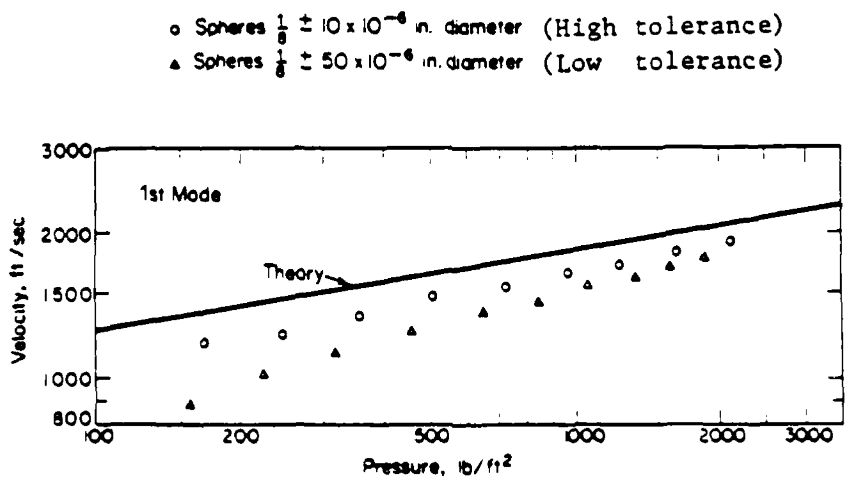

Fig. 13 - Rod Wave Velocity Measurements in Regular Dense Array of Steel Spheres Isotropically Loaded (Duffy and Mindlin, 1957, figure presented by Richart et al., 1970)

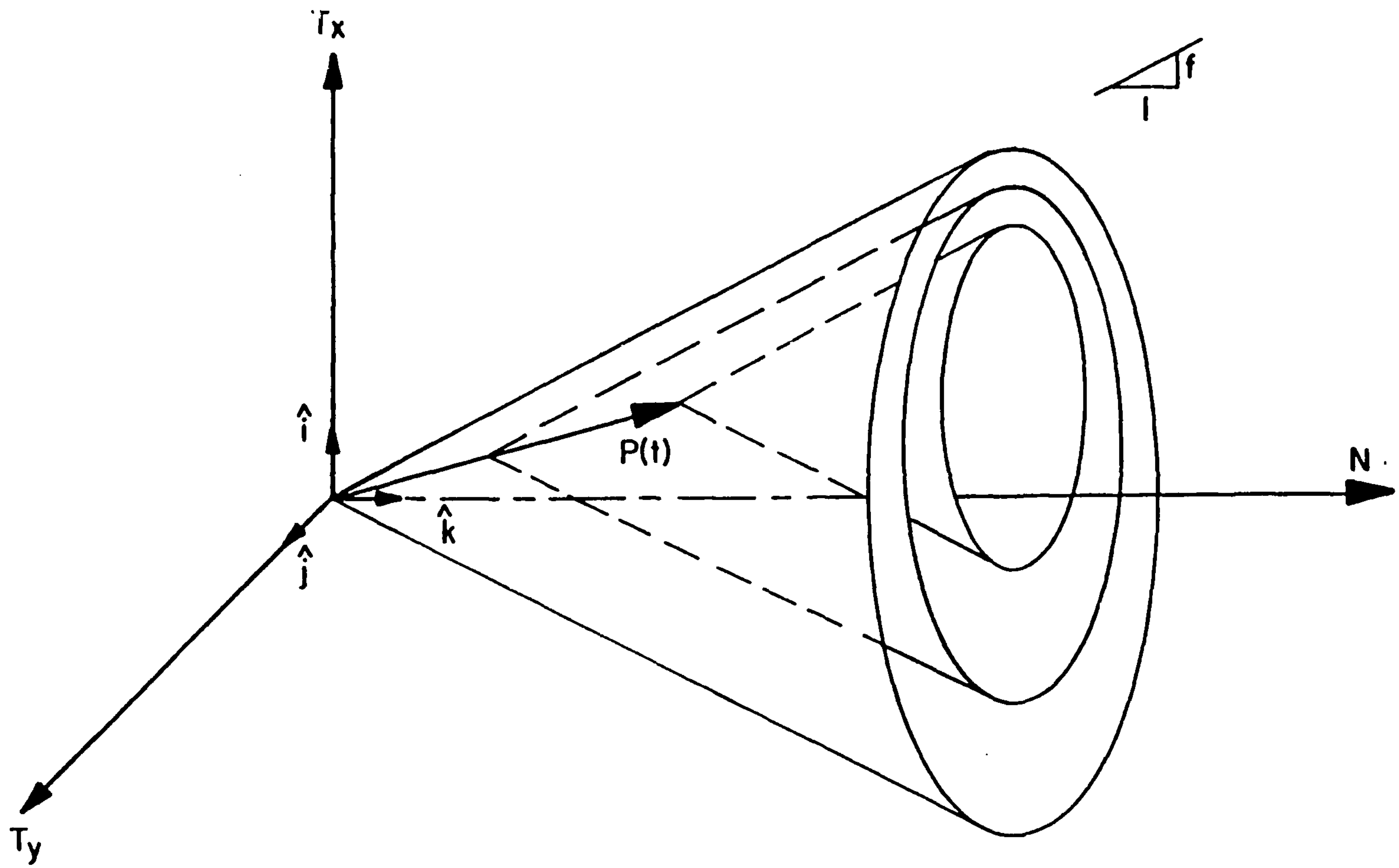

Fig. 14 - Contact Force Space and Conical Yield Surfaces, Elastic-Plastic Incremental Solution of Mindlin's Problem (Seridi and Dobry, 1984).

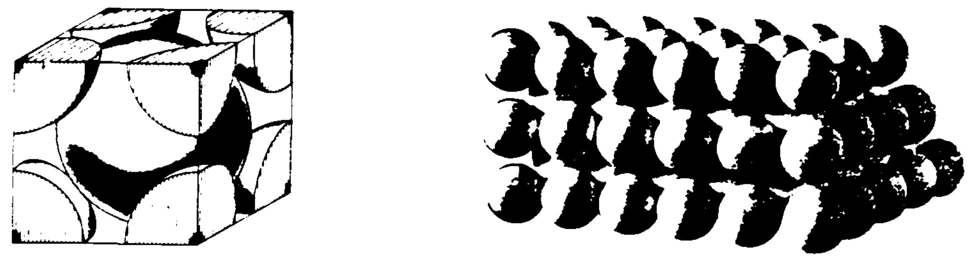

a) Body-centered cubic unit cell b) Body-centered cubic structure

Fig. 15 (Van Vlack, 1964)

a) Face-centered cubic unit cell b) Face-centered cubic structure

Fig. 16 (Van Vlack, 1964)

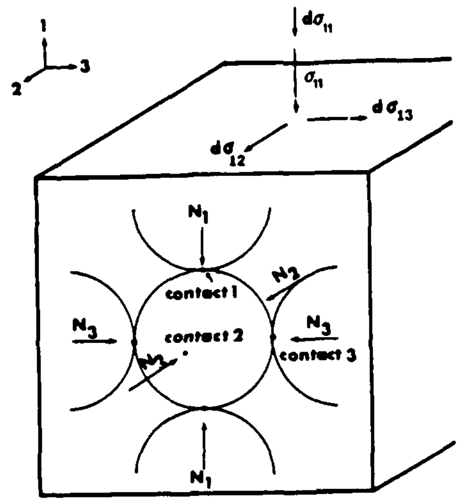

Fig. 17 Regular Simple Cubic Array of Equal Spheres

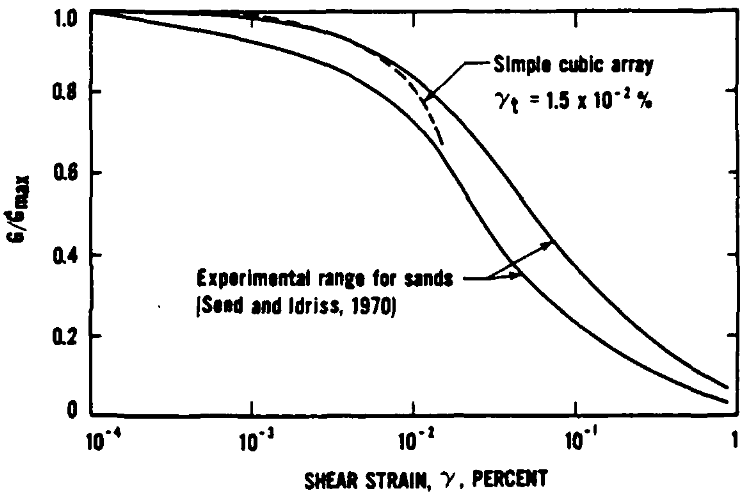

Fig. 18 Secant Shear Modulus Reduction Versus Shear Strain: Comparison Between Calculated G/G_{max} for Simple Cubic Array and Experimental Range for Sand (Dobry et al., 1982)

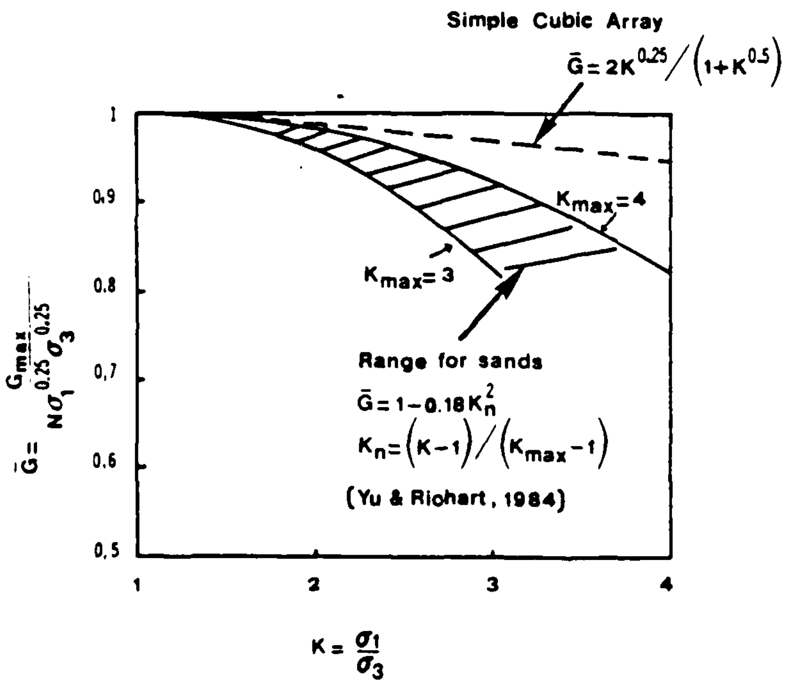

Fig. 19 Influence of Stress Ratio, $K = \sigma_1/\sigma_3$ on G_{max}: Comparison Between Prediction From Simple Cubic Array and Experimental Range for Sand

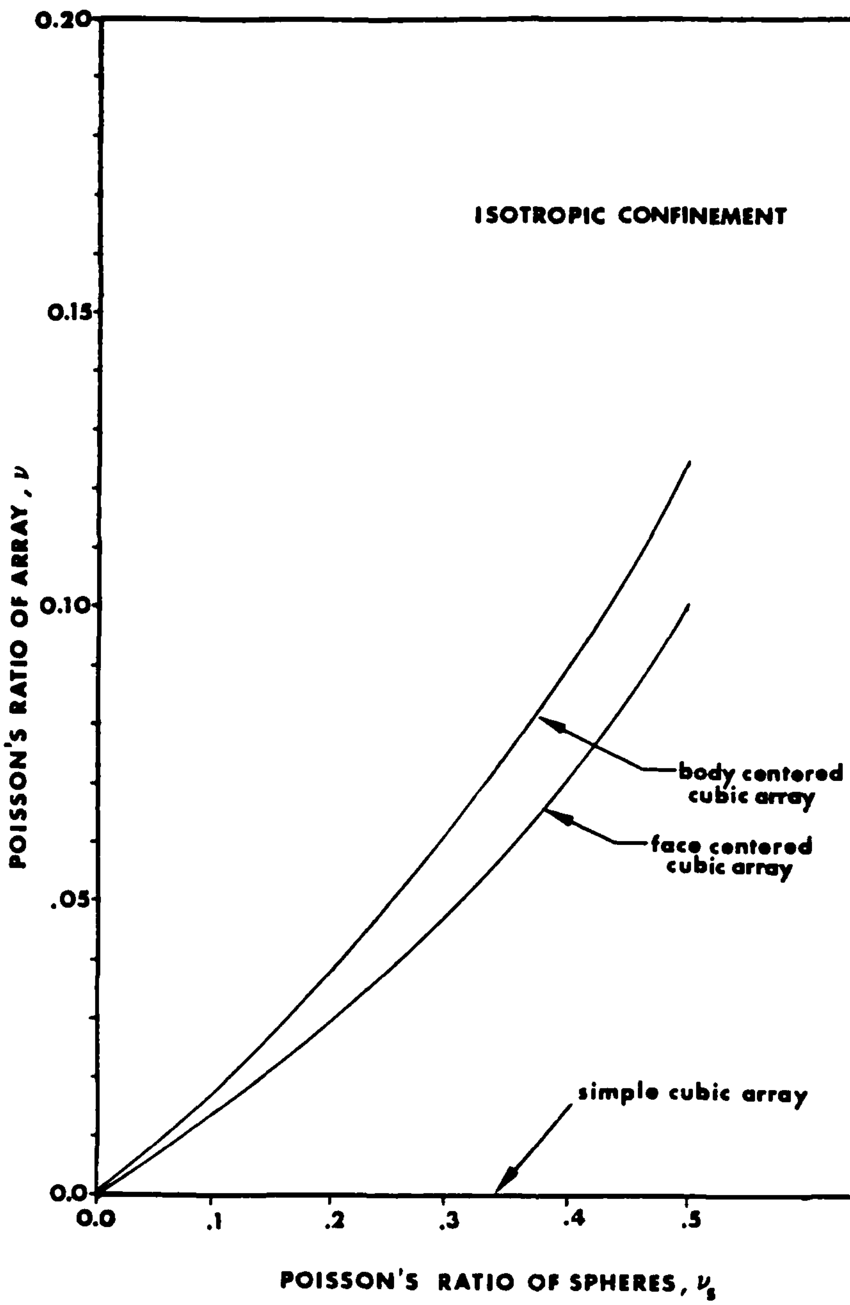

Fig. 20 Poisson's Ratio of Regular Cubic Arrays, ν, as a Function of the Poisson's Ratio of the Spheres, ν_s

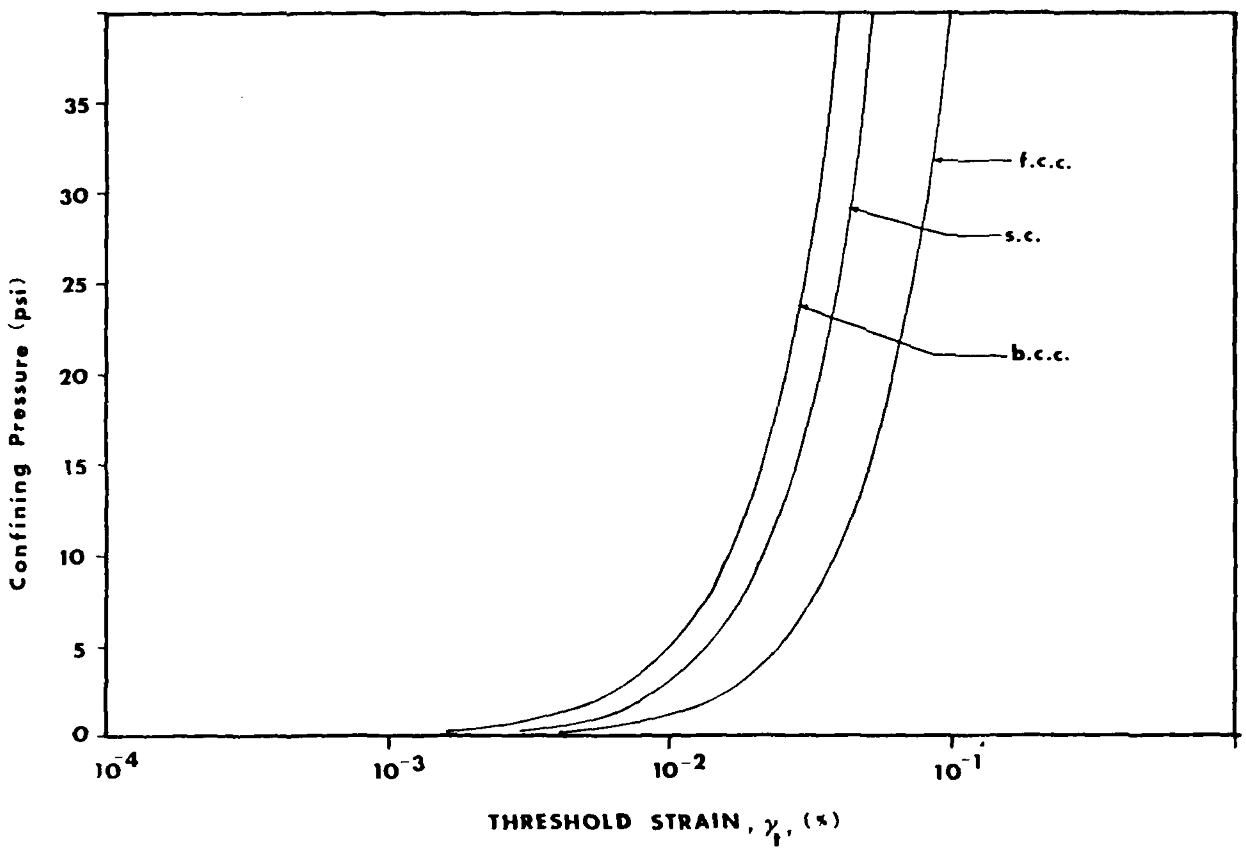

Fig. 21 Threshold Strain for Simple Cubic (sc) Body Centered Cubic (bcc) and Face Centered Cubic (fcc) Arrays of Quartz Spheres

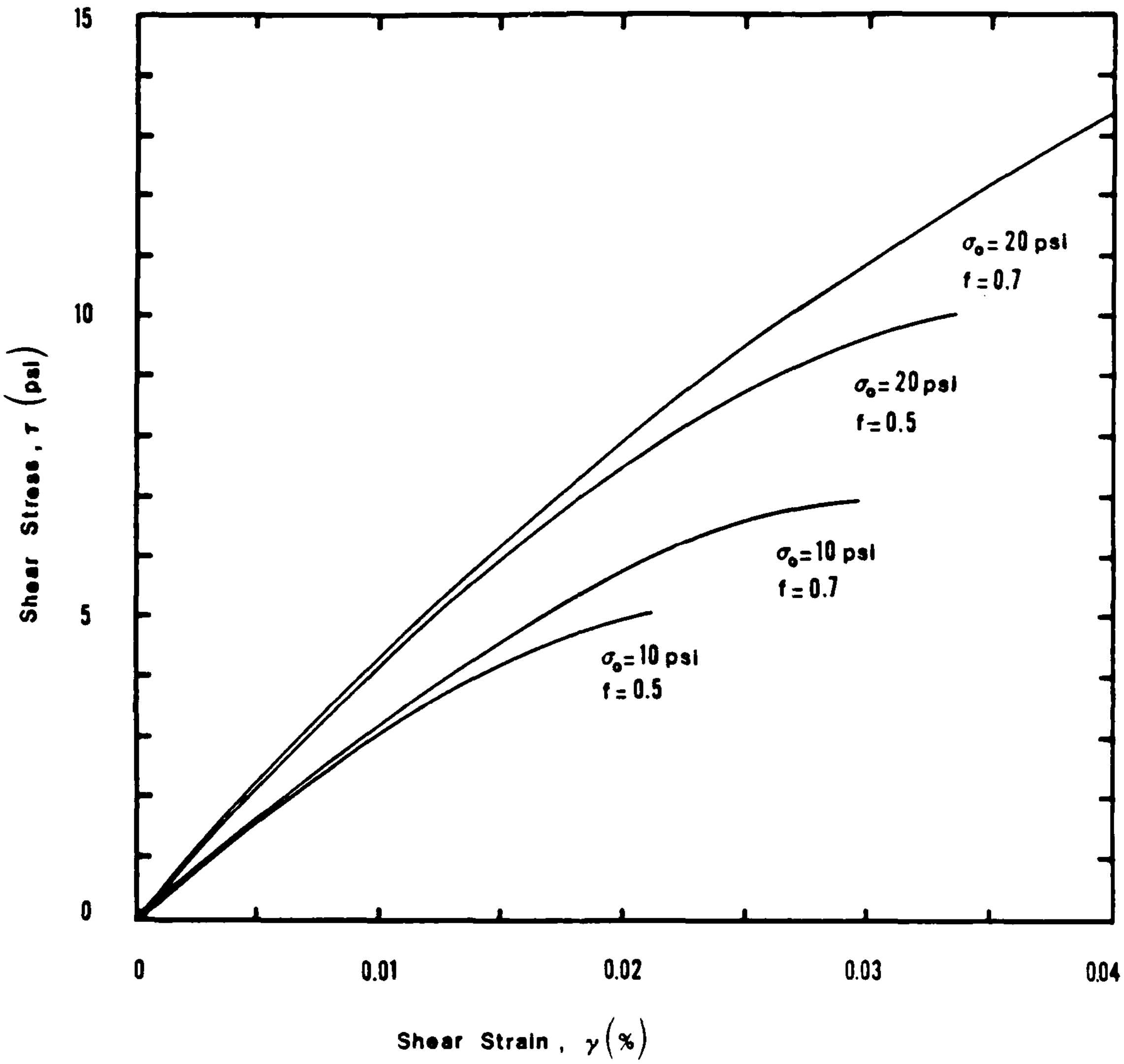

Fig. 22 Shear Stress-Strain Curves for Simple Cubic Arrays of Quartz Spheres

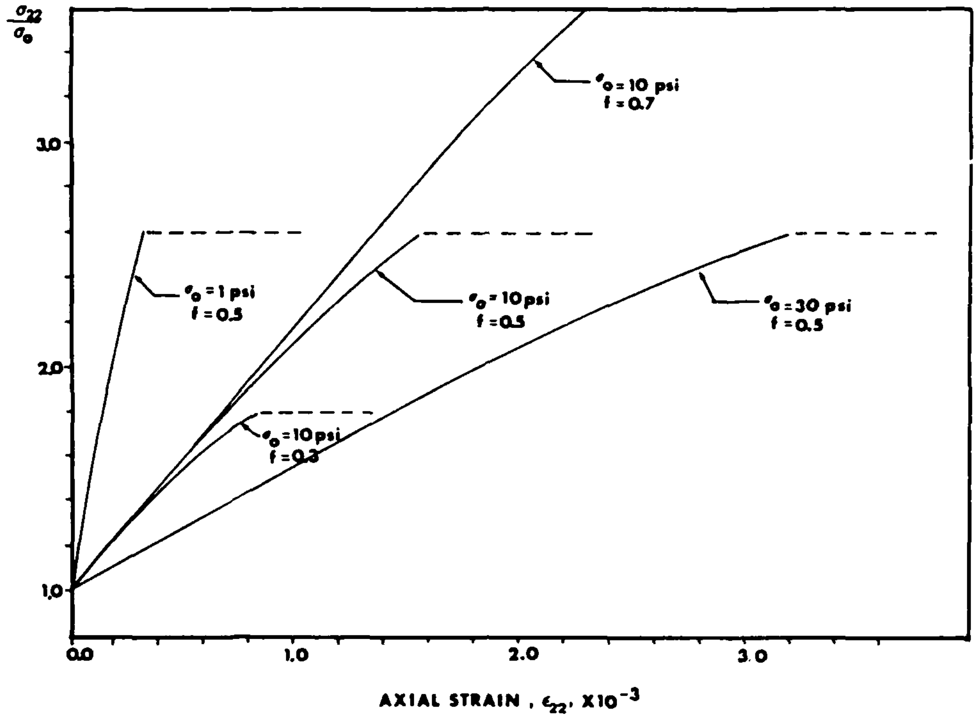

a) Triaxial Compression of Body Centered Cubic Arrays of Quartz Spheres

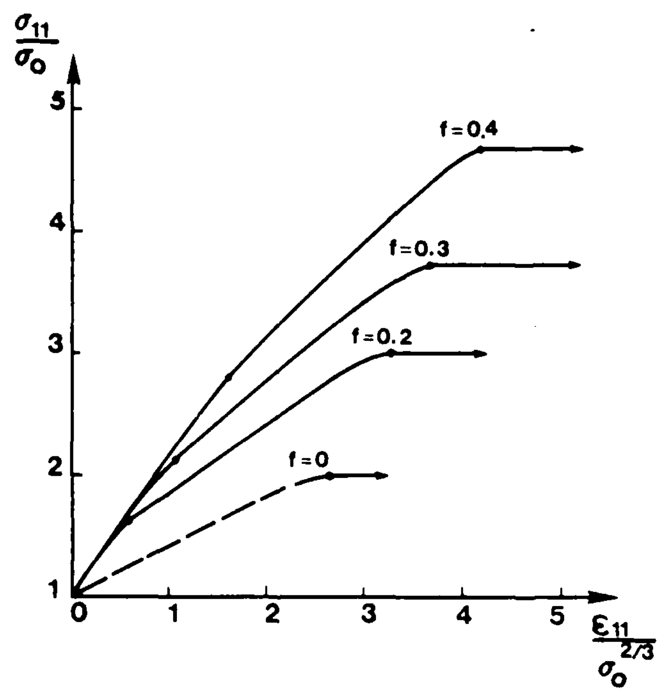

b) Triaxial Compression of Face Centered Cubic Arrays of Glass Spheres (Brauns 1968)

Fig. 23 Triaxial Compression of Regular Arrays

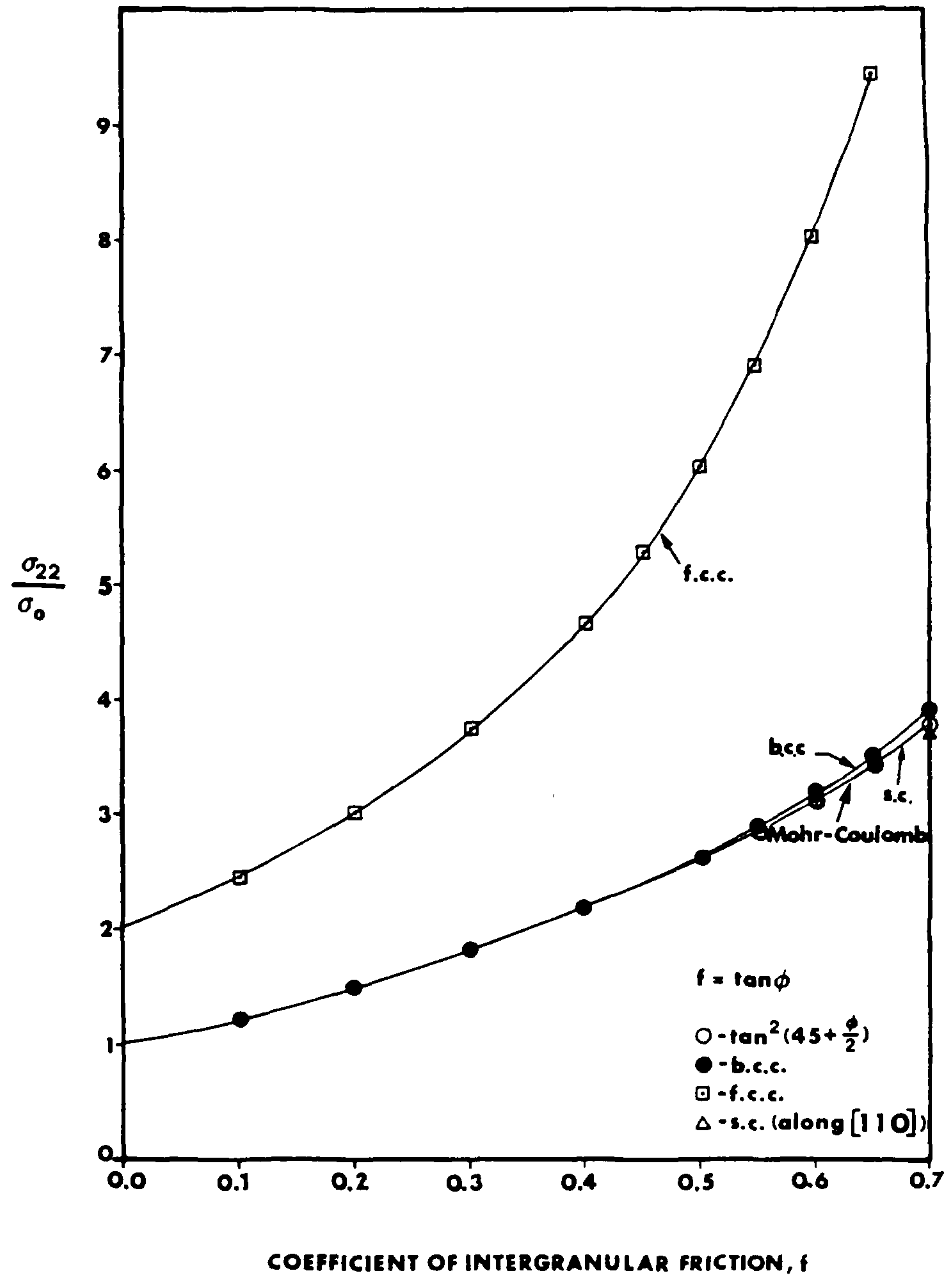

Fig. 24 Triaxial Loading: Obliquity, $\frac{\sigma_{22}}{\sigma_o}$, at Failure Versus Coefficient of Intergranular Friction, f, for Three Regular Cubic Arrays

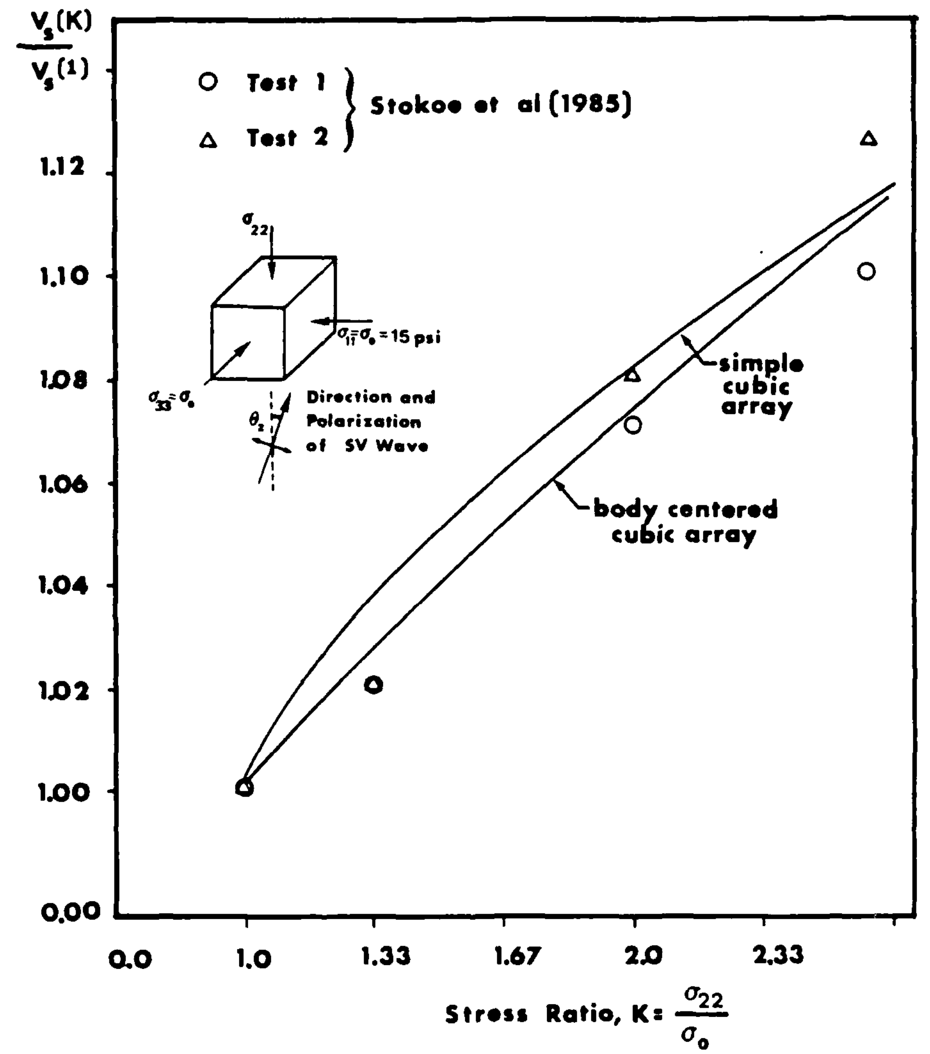

Fig. 25 Shear Wave Velocity V_S Versus Stress Ratio K for Biaxial Confinement and θ_z = 0: Analytical and Experimental Results

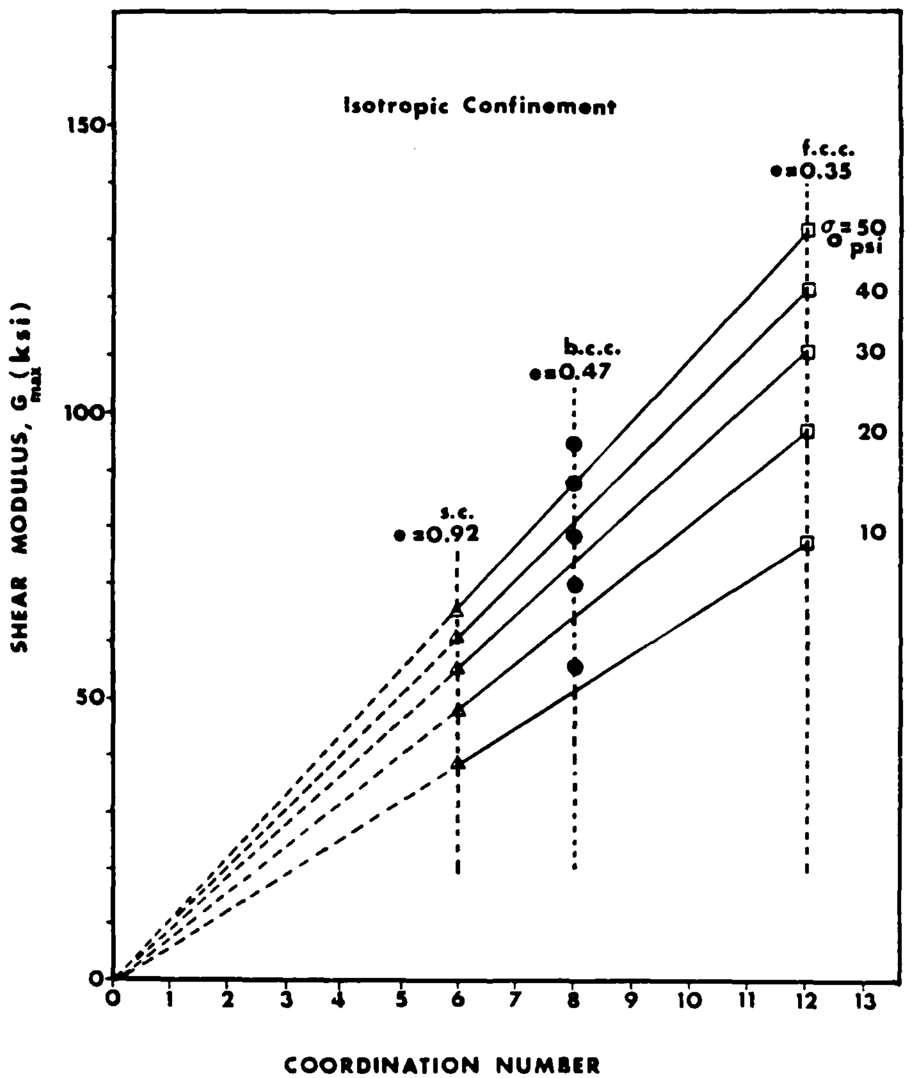

Fig. 26 Shear Modulus versus Coordination Number (= number of Contacts per Sphere) for Regular Cubic Arrays of Quartz Shpheres

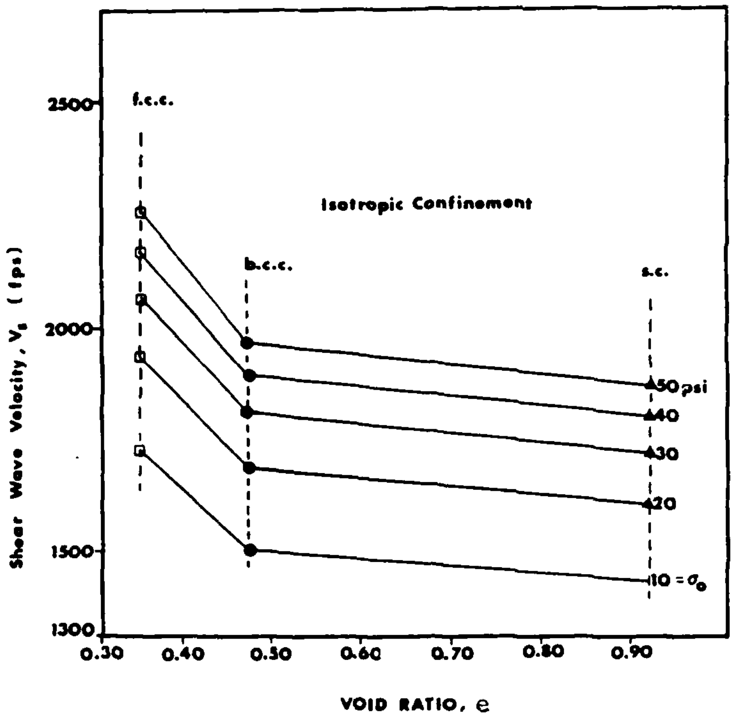

a) Analytical Results for Regular Cubic Arrays of Quartz Spheres

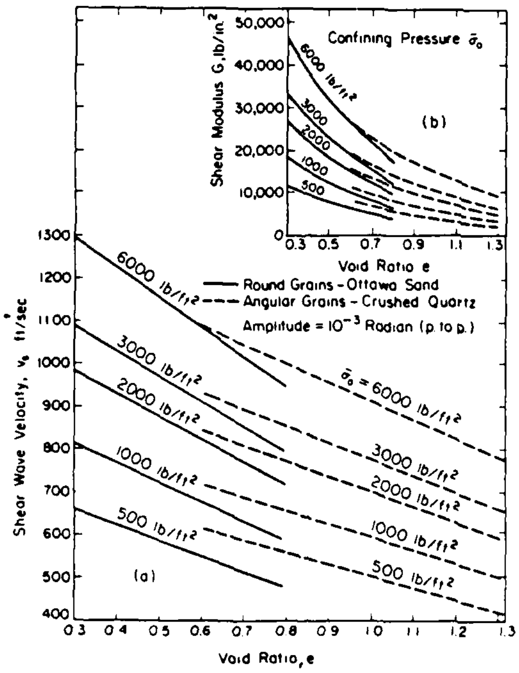

b) Experimental Results for Quartz Sands (Richart et al, 1970)

Fig. 27 Shear Wave Velocity versus Void Ratio-Comparison between Predictions from Regular Cubic Array and Measurements in Quartz Sands

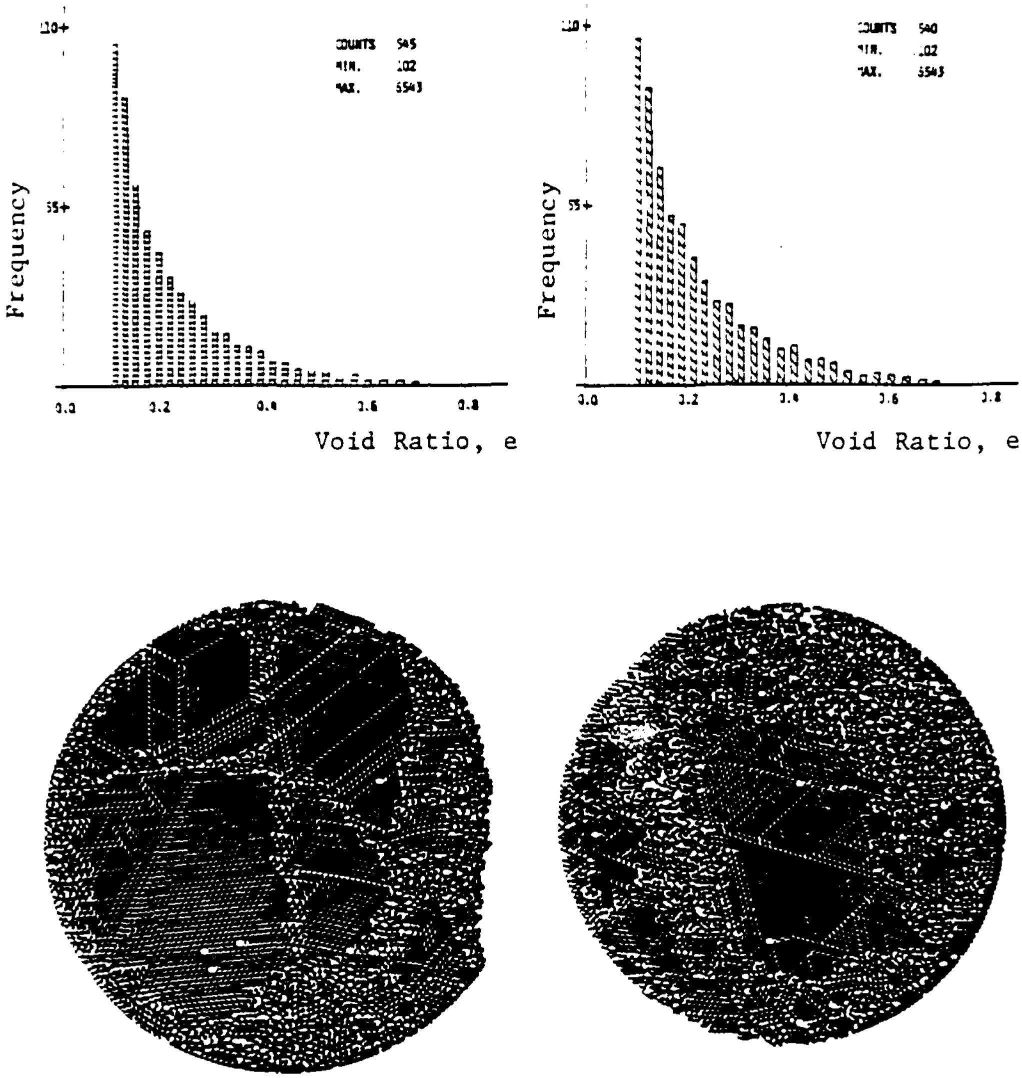

Fig. 28 Histogram and Random Two-Dimensional Packing of Equal Sized Spherical Steel Balls (After Shahinpoor and Shahrpass, 1982)

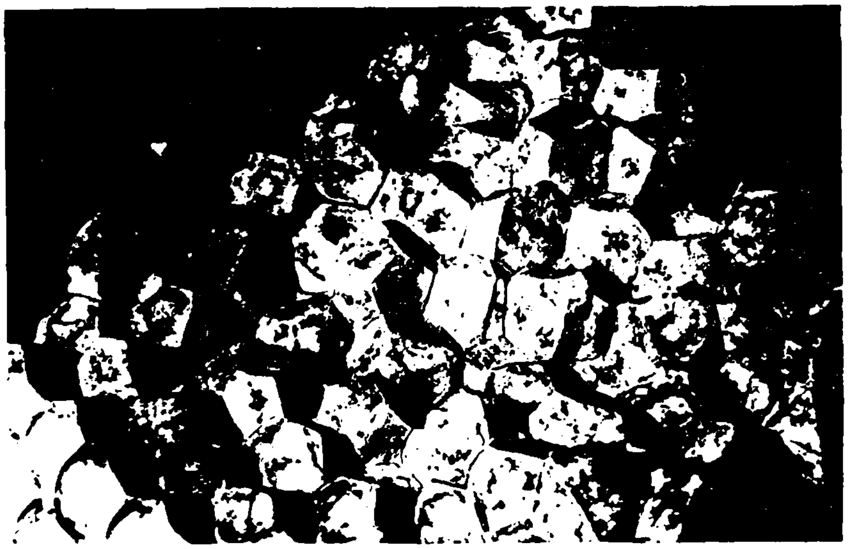

Fig. 29 Cut-away Artist View of a Space Filling Configuration of Voronoi Polyhedra Containing Regular Arrays of Spheres (Finney, 1983)

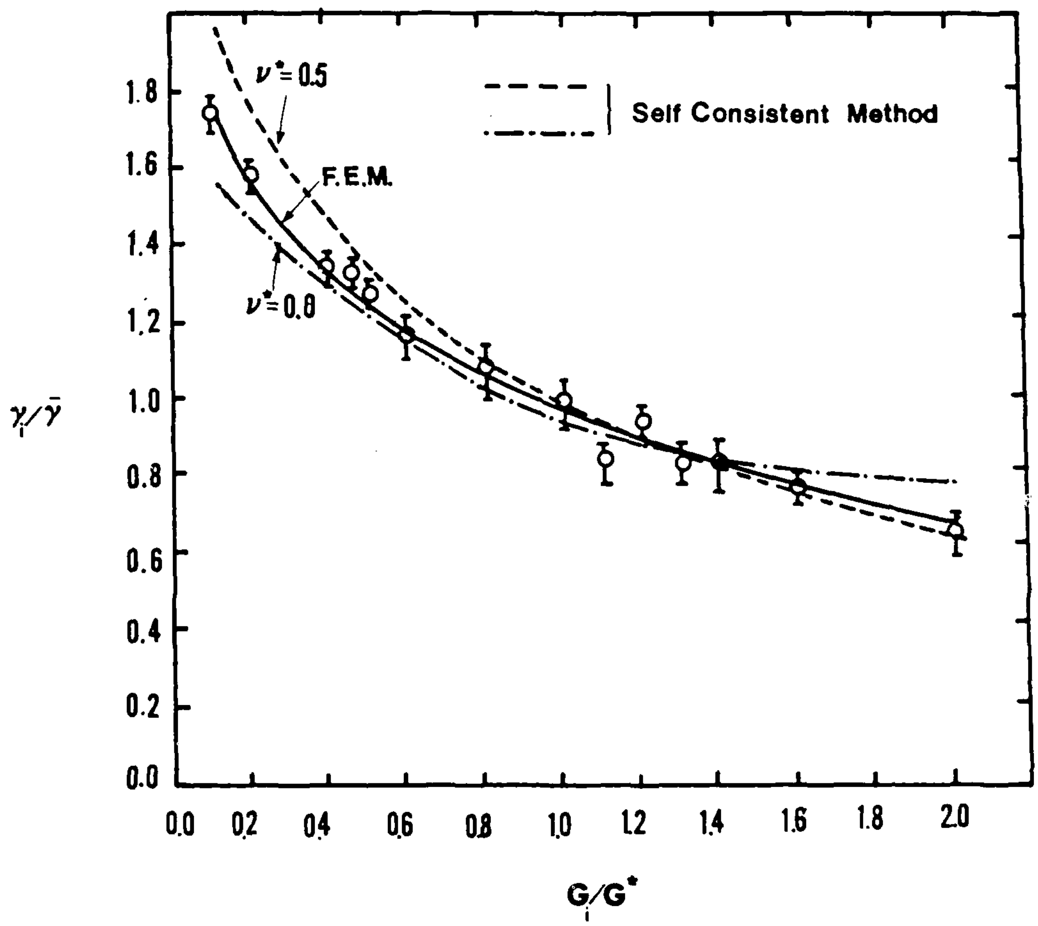

Fig. 30 Shear Strain Experienced by Each Inclusion, γ_i, as a Function of its Shear Stiffness, G_i. Comparison Between Finite Element (FEM) and Self Consistent Method Results

AD-A174 442 A SELF CONSISTENT ESTIMATE OF THE ELASTIC CONSTANTS OF A RANDOM ARRAY OF..(U) RENSSELAER POLYTECHNIC INST TROY NY DEPT OF CIVIL ENGINEERING.. E PETRAKIS ET AL. 2/2

UNCLASSIFIED JUL 86 RPI-CE-86-04 AFOSR-TR-86-1050 F/G 8/13 NL

MICROCOPY RESOLUTION TEST CHART
NATIONAL BUREAU OF STANDARDS-1963-A

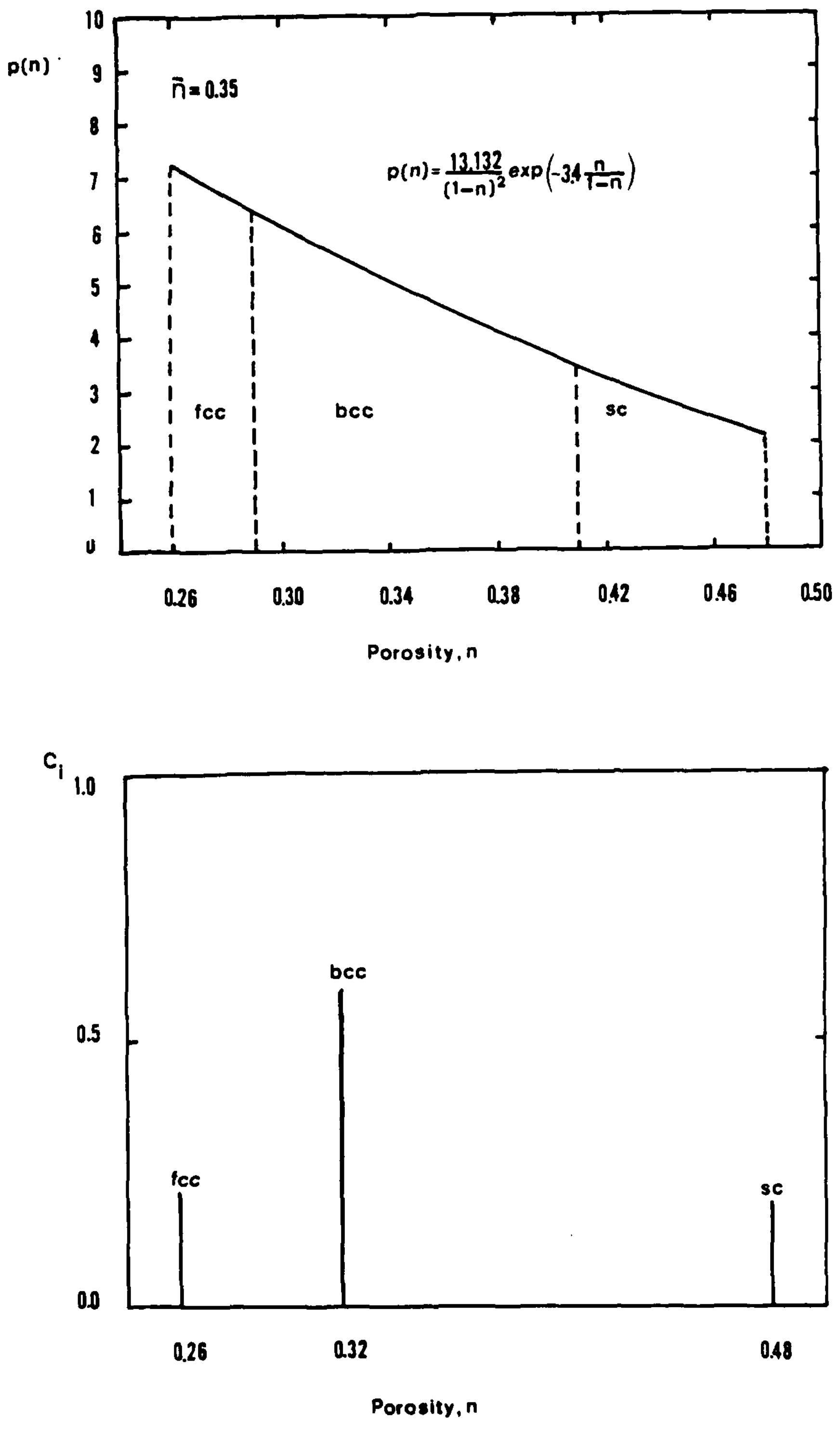

Fig. 31 - Discretazation of Probability Density Function of Porosity, P(n), to Represent Medium of Macroscopic Porosity, $\bar{n}$ = 0.35, by a Combination of Three Regular Cubic Arrays

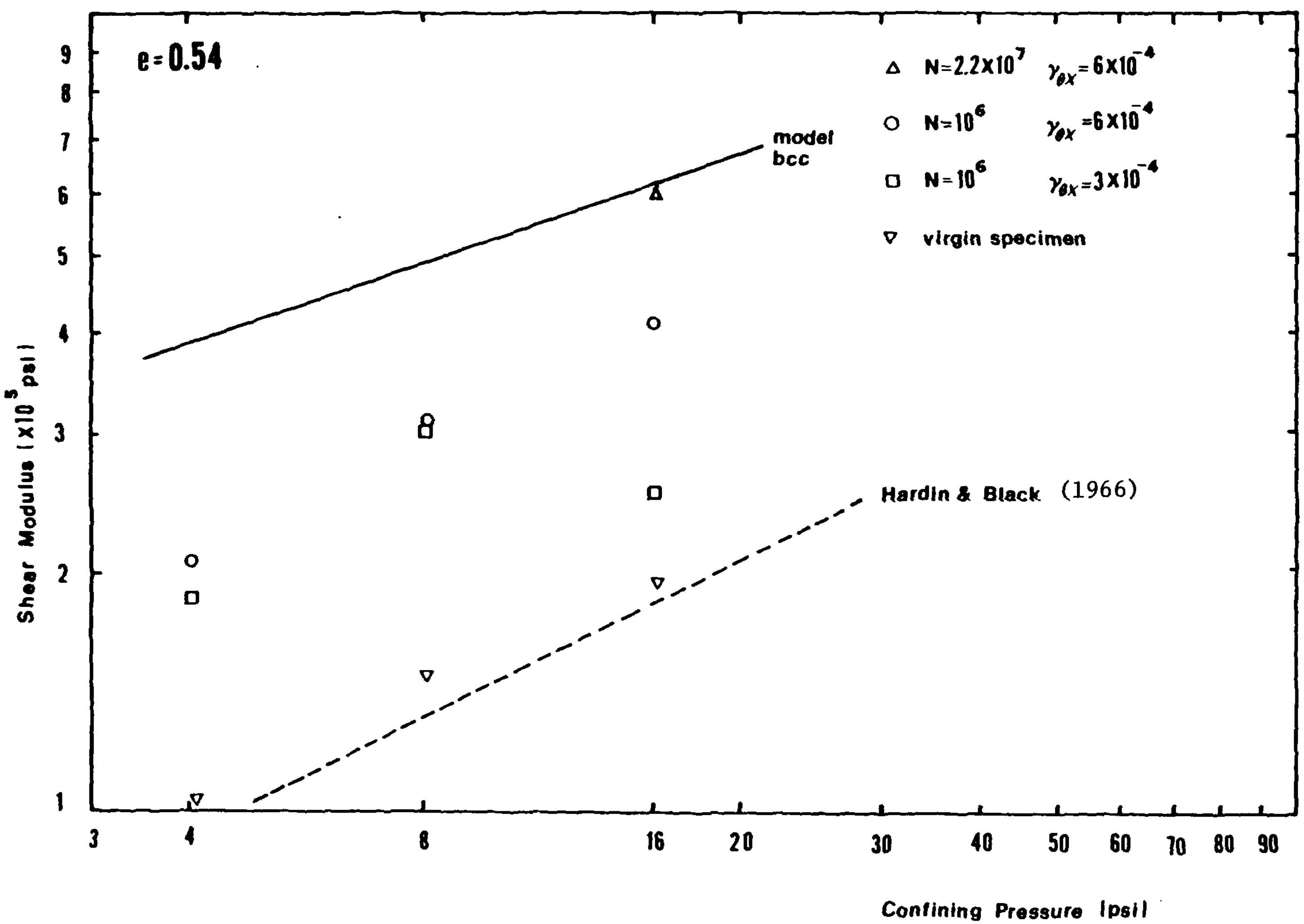

Fig. 32 Shear Modulus, G_{max}, versus Isotropic Confining Pressure. Analytical and Experimental Results for e = 0.54

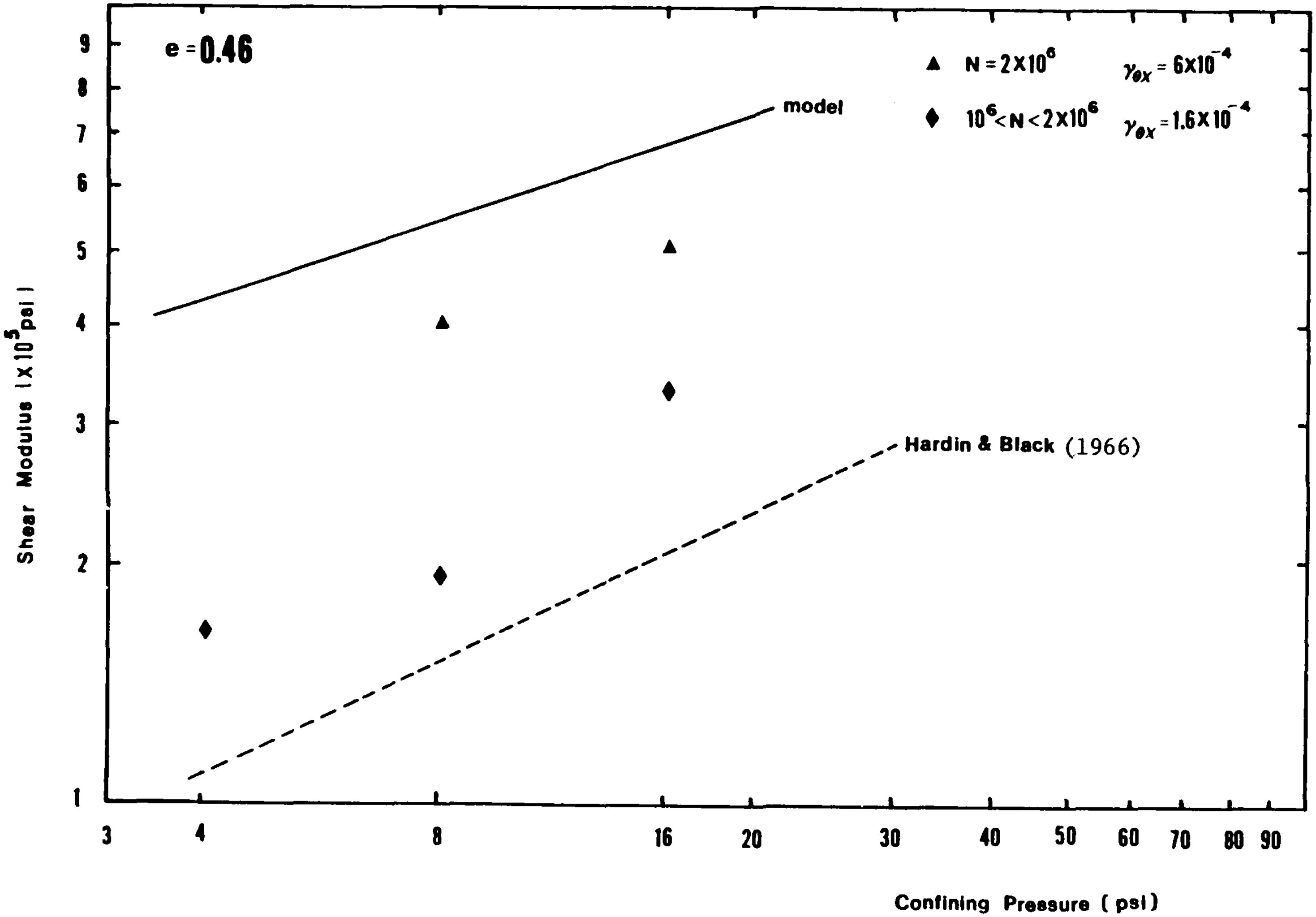

Fig. 33 Shear Modulus, G_{max}, Versus Isotropic Confining Pressure. Analytical and Experimental Results for e = 0.46

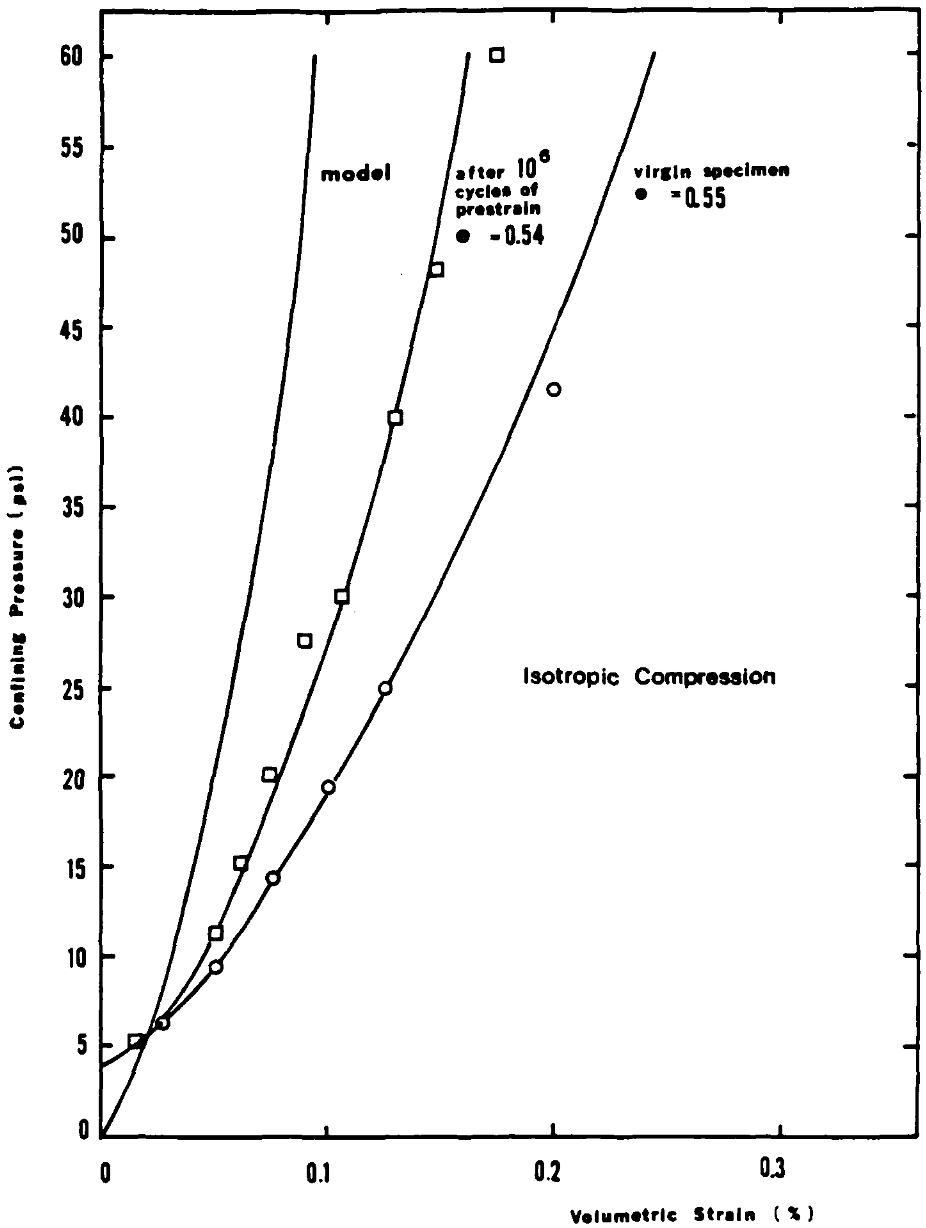

Fig. 34 Confining Pressure versus Volumetric Strain - Analytical and Experimental Results for e = 0.54

APPENDIX A - STRESS-STRAIN RELATIONS FOR A BODY CENTERED CUBIC ARRAY

Following a procedure similar to that used for the simple cubic array by the authors and by others, incremental stress-strain relations for various states of initial stress can be obtained for the body centered cubic array.

A.1 Relation Between Stress and Contact Forces

Consider first a medium composed of identical spheres, Fig. 15b, arranged in a body centered cubic array. Take as an element of the medium the cube shown in Fig. 15a. This "elementary" cube (or representative volume), (Fig. A1), is chosen to contain a sufficient portion of the medium to define the arrangement. Clearly, each sphere in the medium is in contact with 8 other spheres.

Increments of the force dP_{ij} act on the forces of the cube, Fig. A1, and they are assumed to be distributed among the spheres in proportion to their stiffness, that is to their section exposed on the faces of the cube.

The incremental stress components are defined as follows:

$$d\sigma_{ij} = \frac{1}{4}\, dP_{ij}/(\frac{16R^2}{3}) \qquad \text{(A1)}$$

where $\frac{16R^2}{3}$ is the gross area of the face of the cube.

At each contact between spheres, the normal and tangential components of the incremental force are again designated by dN_{ij}; with dN_{ii} being the normal component and dN_{ij} being two the tangential components.

Once more, the first step in deriving the incremental stress-strain relationships is to define the expressions for the increments in the forces at the contacts between the spheres in the cube, Fig. 15a, dN_{ij}, in terms of the increments of the applied stress $d\sigma_{ij}$. However, since this array is statically

determinate for initial isotropic and transversely isotropic triaxial loading, only the equilibrium conditions are sufficient for the solution of this sub-problem. However, this case is much more involved than the simple cubic array and tedious calculations have to be performed.

Fig. A2 shows one octant of a sphere at the apex H as well as the point of contact with the "central" sphere and the applied and contact forces. This octant of the sphere at H will be treated as the representative octant. Now equilibrium equations have to be written for each spherical octant at every apex and the contact forces will have to be solved for each case separately. For example for apex H, (Fig. A2), the equilibrium equations are:*

$$\sum F_{x_1} = 0 \Rightarrow \frac{1}{\sqrt{3}} dN'_{33} + \frac{1}{\sqrt{2}} dN'_{31} - \frac{1}{\sqrt{6}} dN'_{32} + \frac{1}{4} dP_{11} + \frac{1}{4} dP_{13} + \frac{1}{4} dP_{12} = 0 \tag{A2}$$

$$\sum F_{x_2} = 0 \Rightarrow \frac{1}{\sqrt{3}} dN'_{33} + \frac{2}{\sqrt{6}} dN'_{32} + \frac{1}{4} dP_{22} + \frac{1}{4} dP_{12} + \frac{1}{4} dP_{32} = 0 \tag{A3}$$

$$\sum F_{x_3} = 0 \Rightarrow \frac{1}{\sqrt{3}} dN'_{33} - \frac{1}{\sqrt{2}} dN'_{31} - \frac{1}{\sqrt{6}} dN'_{32} + \frac{1}{4} dP_{13} + \frac{1}{4} dP_{33} + \frac{1}{4} dP_{23} = 0 \tag{A4}$$

the solution of which is:

$$dN'_{31} = -\frac{\sqrt{2}}{8} (dP_{11} - dP_{33} + dP_{12} - dP_{23}) \tag{A5}$$

$$dN'_{32} = -\frac{\sqrt{6}}{24} (dP_{11} - 2dP_{22} + dP_{33} - dP_{12} + 2dP_{13} - dP_{23}) \tag{A6}$$

$$dN'_{33} = -\frac{\sqrt{3}}{12} (dP_{11} + dP_{22} + dP_{33} + 2dP_{12} + 2dP_{13} + 2dP_{23}) \tag{A7}$$

* The primed symbols refer to the local coordinate system.

At this point the state of stress can be defined and the constitutive law may be determined for each case (isotropic or cross-anisotropic triaxial confinement).

A.2 Isotropic State of Stress:

Applying increments of force along the three principal directions, dP_{11}, dP_{22}, dP_{33} and one at a time, on top of the isotropic confining stress, an inremental force-deformation relationship can be developed. For example, in the case of application of dP_{11} (Fig. A1) we have:

$$d\delta_{11} = -\left(\frac{1}{6} C_n + \frac{1}{3} C_t\right) dP_{11} \tag{A8}$$

$$d\delta_{22} = +\frac{1}{6} (C_n - C_t)\, dP_{11} \tag{A9}$$

$$d\delta_{33} = \frac{1}{6} (C_n - C_t)\, dP_{11} \tag{A10}$$

where C_n, C_t are the normal and tangential Compliances at the contact.

Similarily applying dP_{22}:

$$d\delta_{11} = \left(\frac{1}{6} C_n - \frac{1}{6} C_t\right) dP_{22} \tag{A11}$$

$$d\delta_{22} = -\left(\frac{1}{6} C_n + \frac{1}{3} C_t\right) dP_{22} \tag{A12}$$

$$d\delta_{33} = \left(\frac{1}{6} C_n - \frac{1}{6} C_t\right) dP_{22} \tag{A13}$$

To determine now the relation between changes in angle and forces we have to look at the difference between displacements (Fig. A1). For example, dP_{12} being applied, we have:

$$d\gamma_{23} = \frac{\delta_{33}\big|_A - \delta_{33}\big|_E}{a_{bcc}} + \frac{\delta_{22}\big|_A - \delta_{22}\big|_D}{a_{bcc}} \quad \text{etc.} \tag{A14}$$

where a_{bcc} is the length of edge of the cube. Now:

$$\delta 33\Big|_A - \delta 33\Big|_E = 2\left(-\frac{1}{\sqrt{3}}\,\delta_{33} + \frac{1}{\sqrt{2}}\,\delta_{13} + \frac{1}{\sqrt{6}}\,\delta_{23}\right) \tag{A15}$$

$$\delta 22\Big|_A - \delta 22\Big|_D = 0 \quad \text{etc.} \tag{A16}$$

Consequently:

$$d\gamma_{12} = \left(\frac{2}{3}\,C_n + \frac{1}{3}\,C_t\right)\,dP_{12} \tag{A17}$$

Evaluating the compliances

$$C_n = \frac{1-\nu_s}{2G_s a_o} \quad \text{which yields}$$

$$C_n = \frac{(1-\nu_s)^{2/3}}{(4\sqrt{3}G_s{}^2\sigma_o)^{1/3}} * \frac{1}{R} \tag{A18}$$

Similarily

$$C_t = \frac{2-\nu_s}{2(1-\nu_s)^{1/3}} * \frac{1}{(4\sqrt{3}G_s{}^2\sigma_o)^{1/3}} * \frac{1}{R} \tag{A19}$$

in the case that $\nu_s \neq 0$

$$d\delta_{11} = \left(\frac{1}{6}\,C_n + \frac{1}{3}\,C_t\right)\,dP_{11}$$

Substituting for C_n, C_t eqns. (A18, A19) we obtain:

$$d\delta_{11} = \frac{1}{6}\,\frac{(1-\nu_s)^{2/3}}{(4\sqrt{3}G_s{}^2\sigma_o)^{1/3}}\,\frac{1}{R}\,dP_{11} + \frac{1}{6}\,\frac{2-\nu_s}{(1-\nu_s)^{1/3}}\,\frac{1}{(4\sqrt{3}G_s{}^2\sigma_o)^{1/3}}\,\frac{1}{R}\,dP_{11} \tag{A20}$$

then:

$$d\varepsilon_{11} = \frac{2}{3\sqrt{3}} \frac{1}{(4\sqrt{3}G_s{}^2\sigma_o)^{1/3}} \left[(1-\nu_s)^{2/3} + \frac{2-\nu_s}{(1-\nu_s)^{1/3}}\right] d\sigma_{11} \tag{A21}$$

$$d\sigma_{11} = \frac{3\sqrt{3}\,(4\sqrt{3}G_s^2\ \sigma_o)^{1/3}}{2\left[(1-\nu_s)^{2/3} + \frac{2-\nu_s}{(1-\nu_s)^{1/3}}\right]}\ d\varepsilon_{11} \tag{A22}$$

Similarily

$$d\varepsilon_{22} = \frac{1}{3\sqrt{3}} \frac{1}{(4\sqrt{3}G_s{}^2\sigma_o)^{1/3}} \left[2(1-\nu_s)^{2/3} - \frac{2-\nu_s}{(1-\nu_s)^{1/3}}\right] d\sigma_{11} \tag{A23}$$

$$d\varepsilon_{33} = d\varepsilon_{22} \tag{A24}$$

Also from eqns. (A17, A18) and (A19) we have that

$$d\varepsilon_{12} = \frac{4}{3\sqrt{3}} \frac{1}{(4\sqrt{3}G_s{}^2\sigma_o)^{1/3}} \left[(1-\nu_s)^{2/3} + \frac{1}{4}\frac{2-\nu_s}{(1-\nu_s)^{1/3}}\right] d\sigma_{12} \tag{A25}$$

Finally, the incremental stress-strain law for the isotropic case may be w itten as follows

$$\begin{aligned} d\varepsilon_{11} &= C_{1111}\ d\sigma_{11} + C_{1122}\ d\sigma_{22} + C_{1133}\ d\sigma_{33} \\ d\varepsilon_{22} &= C_{1122}\ d\sigma_{11} + C_{2222}\ d\sigma_{22} + C_{2233}\ d\sigma_{33} \\ d\varepsilon_{33} &= C_{1133}\ d\sigma_{11} + C_{3322}\ d\sigma_{22} + C_{3333}\ d\sigma_{33} \quad \text{etc.} \end{aligned} \tag{A26}$$

where $C_{ijk\ell}$ are the expressions (compliances) in the stress-strain relations, as for example, in eqn. (A21), (A22). In matrix form

$$\begin{bmatrix} d\varepsilon_{11} \\ d\varepsilon_{22} \\ d\varepsilon_{33} \\ d\varepsilon_{12} \\ d\varepsilon_{13} \\ d\varepsilon_{23} \end{bmatrix} = \begin{bmatrix} C_{1111} & C_{1122} & C_{1133} & 0 & 0 & 0 \\ C_{2211} & C_{2222} & C_{2233} & 0 & 0 & 0 \\ C_{3311} & C_{3322} & C_{3333} & 0 & 0 & 0 \\ 0 & 0 & 0 & C_{1212} & 0 & 0 \\ 0 & 0 & 0 & 0 & C_{1313} & 0 \\ 0 & 0 & 0 & 0 & 0 & C_{2323} \end{bmatrix} \begin{bmatrix} d\sigma_{11} \\ d\sigma_{22} \\ d\sigma_{33} \\ d\sigma_{12} \\ d\sigma_{13} \\ d\sigma_{23} \end{bmatrix} \tag{A27}$$

In order for the bcc array to be isotropic under isotropic loading the following condition must be satisfied:

$$C_{1212} = C_{1313} = C_{2323} = C_{1111} - C_{1122} \tag{A28}$$

$$C_{2211} = C_{1122} = C_{1133} = C_{2233} - C_{3311} = C_{3322} = C_{1122} \tag{A29}$$

The above conditions are satisfied only when $\nu_s = 0$; furthermore, in this case of the bcc array, as in the sc array, $C_{1122} = 0$ and the compliance matrix is diagonal.

In this case:

$$C_{1111} = C_{2222} = C_{3333} = \frac{2}{\sqrt{3}} \left(\frac{1}{4\sqrt{3}\ G_s{}^2\ \sigma_o}\right)^{1/3} \tag{A30}$$

Since the compliance matrix is diagonal, its inverse, the stiffness matrix is easily computed by inverting each term: i.e.

$$\begin{bmatrix} d\sigma_{11} \\ d\sigma_{22} \\ d\sigma_{33} \\ d\sigma_{12} \\ d\sigma_{13} \\ d\sigma_{23} \end{bmatrix} = \frac{\sqrt{3}}{2} (4\sqrt{3}\, G_s^{\,2}\ \sigma_o)^{1/3} \begin{bmatrix} 1 & & & & & \\ & 1 & & & & \\ & & 1 & & & \\ & & & 1 & & \\ & & & & 1 & \\ & & & & & 1 \end{bmatrix} \begin{bmatrix} d\varepsilon_{11} \\ d\varepsilon_{22} \\ d\varepsilon_{33} \\ d\varepsilon_{12} \\ d\varepsilon_{13} \\ d\varepsilon_{23} \end{bmatrix} \tag{A31}$$

and clearly the shear modulus of the array, G, is $G = \frac{3}{4} (4\ \ 3\ G_s^{\,2}\ \sigma_o)^{1/3}$ (A32)

At this point the Poisson's Ratio of the bcc array may be computed as follows:

$$\nu_{bcc} = \frac{|\varepsilon_{33}|}{|\varepsilon_{11}|} = \frac{|\varepsilon_{22}|}{|\varepsilon_{11}|} \tag{A33}$$

$$\nu_{bcc} = \left| \frac{(1-\nu_s)^{2/3} - \dfrac{2-\nu_s}{2(1-\nu_s)}}{(1-\nu_s)^{2/3} \quad \dfrac{2-\nu_s}{(1-\nu_s)}\ 1/3} \right| \tag{A34}$$

For different values of ν_s, the Poisson's Ratio of the bcc array, ν_{bcc}, may be computed; a plot of ν_{bcc} versus the Poisson's ratio of the spheres, ν_s, appears in Fig. (21) together with the variation of ν_{sc} and ν_{fcc} with ν_s for easy comparison.

A.3 Transversely Isotropic State of Stress (Triaxial Loading)

As in the case of the simple Cubic Array, the application of an anisotropic stress increment will result in a variation of the contact forces and, consequently, of the corresponding contact stiffnesses. Therefore, in order to obtain the stress strain relationships, the derivation must be performed once more distinguishing between compliances at contacts with different loading histories.*

Consider now the case of cross-anisotropic stress ("triaxial test") imposed after the array has been subjected to an initial hydrostatic stress. That is: (Fig. A3)

$$\text{at} \quad t = t_o \quad \sigma_{11} = \sigma_{22} = \sigma_{33} = \sigma_o \tag{A35}$$

$$t = t_1 \quad \sigma_{11} = \sigma_{33} = \sigma_o \tag{A36}$$

$$\sigma_{22} = \sigma_o + \sigma_a \tag{A37}$$

The contact forces during this Anisotropic Loading are:

$$dN'_{31} = \pm \frac{\sqrt{2}}{8} [dP_{11} - dP_{33}] \tag{A38}$$

$$dN'_{32} = \pm \frac{\sqrt{6}}{24} [dP_{11} - 2dP_{22} + dP_{33}] \tag{A39}$$

$$dN'_{33} = \pm \frac{\sqrt{3}}{12} [dP_{11} - dP_{22} + dP_{33}] \tag{A40}$$

in the case of transversely isotropic loading the above equations simplify to

---

*The computation of the compliances for the case of anisotropic loading for both the sc and the bcc arrays has been done in order for the results to be used only for the special case of wave propagation. This way, the load was assumed to reverse direction, and for this the elastic tangential compliances were used. In the general case, the load could either increase or decrease monotonically and different compliances in each case would apply.

$$dN'_{31} = 0 \tag{A41}$$

$$dN'_{32} = \pm \frac{\sqrt{6}}{12} dP_a \tag{A42}$$

$$dN'_{33} = \pm \frac{\sqrt{3}}{12} dP_a \tag{A43}$$

This is the case of the two spheres in contact where the normal force is increasing from N_o to $N_o + N^*$ and the tangential force from 0 to T^*, with $\beta = \frac{dT}{dN} > f$ (Mindlin and Deresiewicz, 1953)

$$\beta = \frac{dT}{dN} = \frac{dN'_{32}}{dN'_{33}} = \sqrt{2} > f \tag{A44}$$

(usually $0.5 \leq f \leq 0.8$ for sands)

in this case the Normal Compliance, C_n, is:

$$C_n = \frac{1-\nu_s}{2G_s a}$$

where $$a^3 = \frac{3(1-\nu_s)}{8G_s} R(N_o + N) \tag{A45}$$

and finally

$$a^3 = \frac{3(1-\nu_s)}{2G_s} R^3 \sigma_o \left[1 + \frac{1}{3} \left(\frac{\sigma_a}{\sigma_o}\right)\right] \tag{A46}$$

then

$$C_n = \left[\frac{(1-\nu_s)^2}{4\sqrt{3}\, G_s{}^2 \sigma_o}\right]^{1/3} \left[1 + \frac{1}{3}\left(\frac{\sigma_a}{\sigma_o}\right)\right]^{-1/3} \frac{1}{R} \tag{A47}$$

The Tangential Compliance, C_t, is:

$$C_t = \frac{2-\nu_s}{4G_s a}\{-\theta + (1+\theta)[1-(1-\theta)\frac{L^*-L}{2(1+\theta L)}]^{1/3}\} \quad \text{(A48)}$$

where $\theta = \frac{f}{\beta}$, $L = \frac{T}{fNo}$ and $L^* = \frac{T^*}{fNo}$

However, in this case, since the load decrement is small, then $L^* - L \rightarrow 0$, therefore

$$C_t \rightarrow \frac{2-\nu_s}{4G_s a} \quad \text{(A49)}$$

in this case

$$C_t = \frac{2-\nu_s}{2(1-\nu_s)^{1/3}} [\frac{1}{4\ 3\ G_s{}^2\sigma_o}]^{1/3} [1 + \frac{1}{3}(\frac{\sigma_a}{\sigma_o})]^{-1/3} \frac{1}{R} \quad \text{(A50)}$$

The constitutive law for this particular loading may be developed in the same manner as in the case of the isotropic loading, i.e.

$$d\delta_{22} = [\frac{1}{6} C_n + \frac{1}{3} C_t]\ dP_{22} \quad \text{(A51)}$$

finally

$$d\varepsilon_{22} = \frac{2}{3\sqrt{3}} (\frac{1}{4\sqrt{3}\ G_s{}^2\sigma_o})^{1/3} [1 + \frac{1}{3}(\frac{\sigma_a}{\sigma_o})]^{-1/3} [(1-\nu_s)^{2/3} + \frac{2-\nu_s}{(1-\nu_s)^{1/3}}]\ d\sigma_{22}$$

(A52)

for $\nu_s = 0.0$

$$d\varepsilon_{22} = \frac{2}{\sqrt{3}} (\frac{1}{4\sqrt{3}\ G_s{}^2\sigma_o})^{1/3} [1 + \frac{1}{3}(\frac{\sigma_a}{\sigma_o})]^{-1/3}\ d\sigma_{22} \quad \text{(A53)}$$

in the case of isotropic loading and $\nu_s = 0$, the above reduces to

$$d\varepsilon_{22} = \frac{2}{\sqrt{3}} \left(\frac{1}{4\sqrt{3}\, G_s^2 \sigma_o}\right)^{1/3} d\sigma_{22} \tag{A54}$$

which is the same obtained before, eqn. (A30). Analogously

$$d\varepsilon_{11} = \frac{-2}{\sqrt{3}} \left(\frac{1}{4\sqrt{3}\, G_s^2 \sigma_o}\right)^{1/3} \left[1 + \frac{1}{3}\left(\frac{\sigma_a}{\sigma_o}\right)\right]^{-1/3} \left[(1-\nu_s)^{2/3} - \frac{2-\nu_s}{2(1-\nu_s)^{1/3}}\right] d\sigma_{22} \tag{A55}$$

for $\nu_s = 0$ this reduces to zero.

The Shear Compliance is computed as follows:

$$d\delta_{ij} = \left[\frac{2}{3} C_n + \frac{1}{3} C_t\right] dP_{ij} \tag{A56}$$

$$d\varepsilon_{ij} = \frac{2}{3\sqrt{3}} \left(\frac{1}{4\sqrt{3}\, G_s^2 \sigma_o}\right)^{1/3} \left[1 + \frac{1}{3}\left(\frac{\sigma_a}{\sigma_o}\right)\right]^{-1/3} \left[4(1-\nu_s)^{2/3} + \frac{2-\nu_s}{2(1-\nu_s)^{1/3}}\right] d\sigma_{ij} \tag{A57}$$

for $\nu_s = 0$ this reduces to

$$d\varepsilon_{ij} = \frac{2}{3\sqrt{3}} \left(\frac{1}{4\sqrt{3}\, G_s^2 \sigma_o}\right)^{1/3} \left[1 + \frac{1}{3}\left(\frac{\sigma_a}{\sigma_o}\right)\right]^{-1/3} d\sigma_{ij} \tag{A58}$$

for $\sigma_a = 0$ this reduces to eqn. (A31). Therefore, for the case of $\nu_s \neq 0$

$$C_{1111} = C_{2222} = C_{3333} = \frac{2}{3\sqrt{3}} \left(\frac{1}{4\sqrt{3}\, G_s^2 \sigma_o}\right)^{1/3} \left[1 + \frac{1}{3}\left(\frac{\sigma_a}{\sigma_o}\right)\right]^{-1/3} *$$

$$* \left[(1-\nu_s)^{2/3} + \frac{2-\nu_s}{(1-\nu_s)^{1/3}}\right] \tag{A59}$$

$$C_{1122} = C_{2233} = C_{3311} = \frac{-2}{\sqrt{3}} \left(\frac{1}{4\sqrt{3}\ G_s{}^2\sigma_o}\right)^{1/3} \left[1 + \frac{1}{3}\left(\frac{\sigma_a}{\sigma_o}\right)\right]^{-1/3} *$$

$$* \left[(1-\nu_s)^{2/3} - \frac{2-\nu_s}{2(1-\nu_s)^{1/3}}\right] \tag{A60}$$

$$C_{1212} = C_{1313} = C_{2323} = \frac{1}{3\sqrt{3}} \left(\frac{1}{4\sqrt{3}\ G_s{}^2\sigma_o}\right)^{1/3} \left[1 + \frac{1}{3}\left(\frac{\sigma_a}{\sigma_o}\right)\right]^{-1/3} *$$

$$* \left[4(1-\nu_s)^{2/3} + \frac{2-\nu_s}{(1-\nu_s)^{1/3}}\right] \tag{A61}$$

In this case the material will be isotropic under <u>cross</u> <u>anisotropic</u> loading only if in the compliance matrix

$$C_{1111} - C_{1122} = C_{1212}$$

Performing the calculations we see that indeed,

$$C_{1111}-C_{1122} = \frac{1}{3\sqrt{3}}\left(\frac{1}{4\sqrt{3}\ G_s{}^2\sigma_o}\right)^{1/3} \left[1 + \frac{1}{3}\left(\frac{\sigma_a}{\sigma_o}\right)\right]^{-1/3} \left[4(1-\nu_s)^{2/3} + \frac{2-\nu_s}{(1-\nu_s)^{1/3}}\right] = C_{1212}$$

Therefore, the bcc array is isotropic under cross anisotropic loading*; this is a serious deficiency of the model and should be attributed to the symmetry of the array.

In the case that $\nu_s = 0$, the array is still isotropic but this time the compliance matrix is again diagonal:

---

*for the conditions specified previously.

$$\begin{bmatrix} d\varepsilon_{11} \\ d\varepsilon_{22} \\ d\varepsilon_{33} \\ d\varepsilon_{12} \\ d\varepsilon_{13} \\ d\varepsilon_{23} \end{bmatrix} = \frac{2}{\sqrt{3}}\left(\frac{1}{(4\sqrt{3}\,G_0^2\ \sigma_o)}\right)^{1/3}\left[1+\frac{1}{3}\left(\frac{\sigma_a}{\sigma_o}\right)\right]^{-1/3} \begin{bmatrix} 1 & 0 & 0 & 0 & 0 & 0 \\ & 1 & 0 & 0 & 0 & 0 \\ & & 1 & 0 & 0 & 0 \\ & & & 1 & 0 & 0 \\ & & & & 1 & 0 \\ & & & & & 1 \end{bmatrix} \begin{bmatrix} d\sigma_{11} \\ d\sigma_{22} \\ d\sigma_{33} \\ d\sigma_{12} \\ d\sigma_{13} \\ d\sigma_{23} \end{bmatrix} \quad \text{(A62)}$$

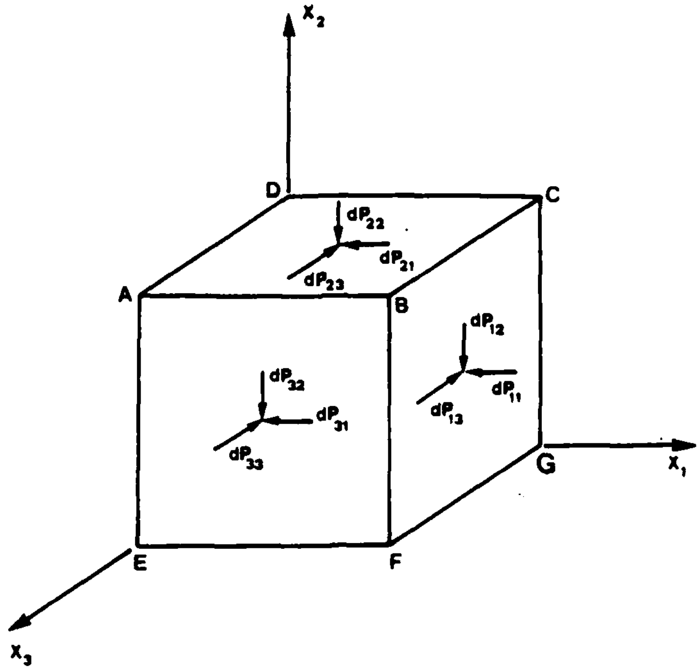

Fig. A1 Representative Unit Volume and Applied Incremental Forces

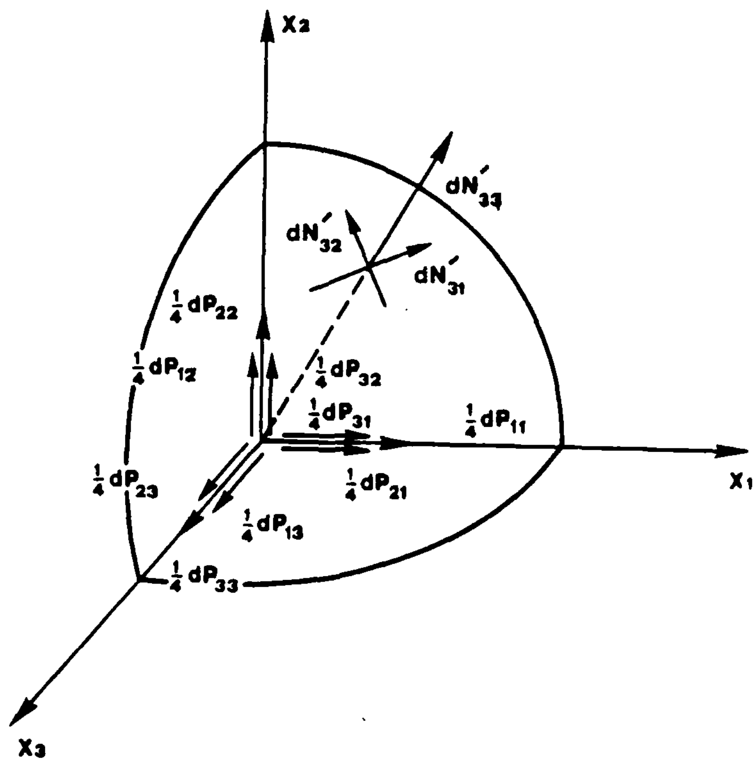

Fig. A2 Octant of Sphere with Center at Apex H of the Representative Unit Volume of a bcc Array, with Applied and Contact Forces Shown

APPENDIX B SIMULATION OF TRIAXIAL AND PURE SHEAR LOADING IN CUBIC ARRAYS

The three regular cubic arrays will be subjected to a finite loading in such a way so as to cause failure when applied along a principal direction. In the case of the simple cubic array, this corresponds to a pure shear loading, since for a triaxial loading the array locks. Conversely, the body centered cubic and the face centered cubic array will be subjected only to a triaxial loading, since for a pure shear loading the array also lock.

In order to obtain a finite stress strain relation in every case, the compliances need to be integrated along the loading path. Once this is done, finite displacements are computed and then the strains are obtained in the same manner as in the infinitesimal constitutive laws.

Finally, the load is increased until failure (gross sliding) occurs in the array; in the statically determinate arrays gross sliding at a contact translates into failure of the cubic array. In the statically indeterminate face centered cubic (fcc) array, the medium does not fail immediately, but first the number of contacts reduces from 12 to 8 when the fcc array becomes statically determinate, and then sliding at one contact becomes failure.

B1 The Simple Cubic Array Subjected to Pure Shear Loading

Consider the Simple Cubic Array shown in Fig. 17 and consider a force T acting in the x_1 direction (Fig. A1). The s.c. array is subjected to an initial isotropic force N_o and the value of T increases monotonically from zero to T*, where T* is the value of T that causes failure in the array, while N_o remains constant. In this case the tangential displacement is given by Mindlin (1949):

$$\delta = \frac{3(2-\nu_s)}{8G_s a} fN_o \left[1 - \left(1 - \frac{T}{fN_o}\right)^{2/3}\right] \tag{A63}$$

where $a^3 = \dfrac{3(1-\nu_s)N_oR}{8G_s}$

is the radius of contact.

Now $\gamma =$; substituting the expression for a^3 into eqn. (A63) and after transforming the forces into stresses we obtain:

$$\gamma = \frac{3(2-\nu_s)}{(1-\nu_s)^{1/3}} * f\left[\frac{\sigma_o^2}{12G_s^2}\right]^{1/3} * \left[1 - \left(1 - \frac{\tau}{f\sigma_o}\right)^{2/3}\right] \tag{A64}$$

The above equation has been plotted in Fig. 22 for different values of σ_o and f; obviously failure occurs when

$$\tau^* = f\sigma_o \tag{A65}$$

and at this point the value of the strain is*

$$\gamma_f = \gamma_t = \frac{3(2-\nu_s)}{(1-\nu_s)^{1/3}} * f\left(\frac{\sigma_o^2}{12G_s^2}\right)^{1/3} \tag{A66}$$

Substituting the properties of quartz (Table 3) in eqn. (A66) we obtain

$$\gamma_t = 4.5 \times 10^{-3} (\sigma_o)^{2/3} \tag{A66a}$$

with σ_o in psi.

B2 The Body Centered Cubic Array Subjected to Triaxial Loading

Consider the bcc array shown in Fig. 15, and consider a force Pa acting in the x_2 direction, Fig. A1). The bcc array is subjected to an initial isotropic stress σ_o and the stress $\sigma_{22} = \sigma_a$ is increased monotonically from 0

* The value of $\nu_s = 0.15$ used here was obtained from White (1964) and other sources, and is different from $\nu_s = 0.31$ used in a previous report (Dobry et al., 1982). The value $\nu_s = 0.15$ is more representative of quartz; as a result, the values of the threshold strain γ_f computed using Eq. A66 and $\nu_s = 0.15$ are slightly different from those originally obtained by Dobry et al. (1982).

to a value σ_a at which sliding occurs in the array. In this case, the loading path is as follows

$$\text{at } t = t_o \qquad P_{11} = P_{22} = P_{33} = P_o \tag{A67}$$

$$\text{at } t = t_1 \qquad P_{11} = P_{33} = P_o \tag{A68}$$

$$P_{22} = P_o + P_a \tag{A69}$$

The contact forces are (eqns, A5, A6, A7)

$$dN'_{31} = \pm \frac{\sqrt{2}}{8}\left[dP_{11} - dP_{33}\right] = 0 \tag{A70}$$

$$dN'_{32} = \pm \frac{\sqrt{6}}{24}\left[dP_{11} - 2dP_{22} + dP_{33}\right] = \frac{6}{12}\, dPa \tag{A71}$$

$$dN'_{33} = \pm \frac{\sqrt{3}}{12}\left[dP_{11} + dP_{22} + dP_{33}\right] = \frac{3}{12}\, dPa \tag{A72}$$

and the ratio between the increment of the tangential force and the increment of the normal force, β, is

$$\beta = \frac{dT}{dN} = \frac{dN'_{32}}{dN'_{33}} = \sqrt{2} \tag{A73}$$

In this case $\beta > f$, the coefficient of interparticle friction, therefore the values of the compliances are: (Mindlin and Deresiewicz, 1953)

a) Normal Compliance, C_n

$$C_n = \frac{1-\nu_s}{2G_s a} \tag{A74}$$

this expression for C_n being valid no matter what the loading history of the spheres is. Now

$$a = a_o\,(1 + \Theta L)^{1/3} \tag{A75}$$

where

$$a_o = \frac{3(1-\nu_s)}{8\mu_s} N_o\, R = \frac{3(1-\nu_s)}{8\mu_s}\frac{\sqrt{3}}{4} P_o * R \tag{A76}$$

Also $\theta = \frac{f}{\beta}$

$$L = \frac{T}{fN_o}$$

The vertical displacement, δ_{22}, has two components; a δ'_{33} and a δ'_{23} component:

$$\delta_{22} = \frac{2}{\sqrt{3}}\delta'_{33} + \frac{2}{\sqrt{6}}\delta'_{23} \tag{A77}$$

the δ'_{33} component is computed as follows:

$$C_n = \frac{d\delta'_{33}}{dN} = \frac{1-\nu_s}{2G_s a_o}\,(1 + \theta L)^{-1/3} \tag{A78}$$

$$\frac{d\delta'_{33}}{dN} = \frac{1-\nu_s}{2G_s a_o}\left(1 + \frac{f}{\beta}\,\frac{\beta N}{fN_o}\right)^{-1/3} \tag{A79}$$

$$\delta'_{33} = \int_o^N \frac{1-\nu_s}{2G_s a_o}\left[1 + \frac{N}{N_o}\right]^{-1/3} dN \tag{A80}$$

finally

$$\delta'_{33} = 2\sqrt{3}\,R(1-\nu_s)^{2/3}\left(\frac{\sigma_o{}^2}{4\sqrt{3}G_s{}^2}\right)^{1/3}\left[\left(1 + \frac{1}{3}\,\frac{\sigma_a}{\sigma_o}\right)^{2/3} - 1\right] \tag{A81}$$

The δ'_{23} component will be computed from the tangential compliance since it is a tangential displacement; the tangential compliance is (Mindlin and Deresiewicz, 1953):

$$C_t = \frac{2-\nu_s}{4G_s a}\left[\theta + (1 - \theta)\left(1 - \frac{L}{1+\theta L}\right)^{-1/3}\right] \tag{A82}$$

Simplifying:

$$C_t = \frac{2-\nu_s}{4G_s a} \frac{1}{(1+\Theta L)^{1/3}} \left[\theta + (1-\theta)\left(1 - \frac{L}{1+\theta L}\right)^{-1/3}\right] \tag{A83}$$

and finally

$$C_t = \frac{2-\nu_s}{4G_s a} * \frac{\theta}{\left(1+\theta \frac{T}{T_o}\right)^{1/3}} + \frac{2-\nu_s}{4G_s a} (1 - \theta)\left[\left(1 + \frac{T}{T_o} (\theta-1)\right]^{-1/3} \tag{A84}$$

now

$$\frac{d\delta_{23}'}{dT} = C_{t_o} \theta\left[1 + \theta \frac{T}{T_o}\right)^{-1/3} + C_{t_o} (1-\theta)\left[1 + \frac{T}{T_o} (\theta-1)\right]^{-1/3} \tag{A85}$$

where

$$C_{t_o} = \frac{2-\nu_s}{4G_s a_o}$$

Now

$$\delta_{23}' = \int_o^T T_o C_{t_o} \theta\left(1+\theta \frac{T}{T_o}\right)^{-1/3} dT + C_{t_o} T_o(1-\theta)\left[1+(\theta-1) \frac{T}{T_o}\right]^{-1/3} \frac{dT}{T_o} \tag{A86}$$

finally

$$\delta_{23}' = \frac{3}{2} \left(\frac{2-\nu_s}{4G_s a_o}\right) fN_o\left\{\left[\left(1 + \frac{T}{\beta N_o}\right)^{2/3} -1\right] - \left[\left(1 + \left(\frac{f}{\beta} -1\right) \frac{T}{fN_o}\right)^{2/3} - 1\right]\right\} \tag{A87}$$

Simplifying further and expressing the displacement in terms of stresses we obtain:

$$\delta_{23}' = \sqrt{3} fR \frac{2-\nu_s}{(1-\nu_s)^{1/3}} \left[\frac{\sigma_o^2}{4\sqrt{3}\, G_s^2}\right]^{1/3} \left\{\left[\left(1+ \frac{\sqrt{2}}{3\beta} \frac{\sigma_a}{\sigma_o}\right)^{2/3} -1\right] - \left[\left(1+\left(\frac{f}{\beta} -1\right)\frac{\sqrt{2}}{3f} \frac{\sigma_a}{\sigma_o}\right)^{2/3} -1\right]\right\}$$

(A88)

In order to compute the vertical displacement of the array, δ_{22}, we have to substitute equations (A81) and (A88) into eqn. (A77):

$$\delta_{22} = \frac{2}{\sqrt{3}}\delta_{33}' + \frac{2}{\sqrt{6}}\delta_{23}' \tag{A89}$$

$$\delta_{22} = 4R(1-\nu_s)^{2/3}\left(\frac{\sigma_o^2}{4\sqrt{3}\,G_s^2}\right)^{1/3}\left[\left(1+\frac{1}{3}\frac{\sigma_a}{\sigma_o}\right)^{2/3}-1\right] +$$

$$+\sqrt{6}\,fR\frac{2-\nu_s}{(1-\nu_s)^{1/3}}\left(\frac{\sigma_o^2}{4\sqrt{3}\,G_s^2}\right)^{1/3}\left\{\left[\left(1+\frac{\sqrt{2}}{3\beta}\frac{\sigma_a}{\sigma_o}\right)^{2/3}-1\right]-\left[\left[1+\left(\frac{f}{\beta}-1\right)\frac{\sqrt{2}}{3f}\frac{\sigma_a}{\sigma_o}\right]^{2/3}-1\right]\right\}$$

(A90)

From the above equation, A90, the stress-strain relation may be computed for the bcc array under isotropic loading, and it is:

$$\varepsilon_{22} = \left(\frac{\sigma_o^2}{4\sqrt{3}\,G_s^2}\right)^{1/3}\left\{\sqrt{3}(1-\nu_s)^{2/3}\left[\left(1+\frac{1}{3}\frac{\sigma_a}{\sigma_o}\right)^{2/3}-1\right]+\frac{3\sqrt{2}}{4}f\frac{2-\nu_s}{(1-\nu_s)^{1/3}}\ *\right.$$

$$\left. *\left[\left[\left(1+\frac{\sqrt{2}}{3\beta}\frac{\sigma_a}{\sigma_o}\right)^{2/3}-1\right]\left[\left(1+\left(\frac{f}{\beta}-1\right)\frac{\sqrt{2}}{3f}\frac{\sigma_a}{\sigma_o}\right)^{2/3}-1\right]\right]\right\} \tag{A91}$$

The above equation is plotted in Fig. 23 for various values of σ_o and f. At this point, the value of σ_a/σ_o which causes failure in the array must be determined. Failure is defined as sliding at the contacts; this time since the bcc array is statically determinate failure in one contact implies failure of the array. Furthermore, because of the symmetry of the array, failure will occur simultaneously at all contacts. Sliding will occur when

$$\frac{T}{N_o+N} = f \tag{A92}$$

We know that

$$T = \frac{\sqrt{6}}{12} A\ \sigma_a \tag{A93}$$

$$N = \frac{\sqrt{3}}{12} A\ \sigma_a \tag{A94}$$

$$N_o = \frac{\sqrt{3}}{4} A\ \sigma_o \tag{A95}$$

where A is the area of the face of the bcc array. Then:

$$T = f(N_o + N) \tag{A96}$$

$$\frac{\sqrt{6}}{12} A\ \sigma_{22} = f\left(\frac{\sqrt{3}}{12} A\ \sigma_a + \frac{\sqrt{3}}{4} A\ \sigma_o\right) \tag{A97}$$

$$\frac{\sqrt{2}}{3} \sigma_{22} = f\left(\frac{1}{3} \sigma_a + \sigma_o\right) \tag{A98}$$

$$\frac{\sigma_{22}}{\sigma_o} \left[\frac{\sqrt{2}}{3} - \frac{f}{3}\right] = f \tag{A99}$$

and finally, σ_a/σ_o at failure, $(\sigma_a/\sigma_o)_t$ is

$$\left(\frac{\sigma_a}{\sigma_o}\right)_f = \frac{3f}{\sqrt{2}-f} \tag{A100}$$

If $\sigma_{22} = \sigma_o + \sigma_a$ (total stress), then

$$\left(\frac{\sigma_{22}}{\sigma_o}\right)_f = \frac{f}{\frac{\sqrt{2}}{3} - \frac{f}{3}} + 1 \tag{A101}$$

in terms of total stress (Fig. 24)

In order to compute the strain at failure, ε_{22_f}, we must substitute the equation for $(\sigma_{22}/\sigma_o)_f$, eqn. (A100) into the stress-strain relation, eqn. (A91). Doing this we obtain

$$\varepsilon_{22_f} = \left(\frac{\sigma_o^2}{4\sqrt{3}\,G_s^2}\right)^{1/3} \{\sqrt{3}(1-\nu_s)^{2/3}\left[\left(1+\frac{f}{\sqrt{2}-f}\right)^{2/3}-1\right] + \frac{3\sqrt{2}}{4} f \frac{2-\nu_s}{(1-\nu_s)^{1/3}} *$$

$$* \left[\left[\left(1+\frac{f}{\sqrt{2}-f}\right)^{2/3}-1\right]-\left[1+\left(\frac{f}{\beta}-1\right)\frac{\sqrt{2}}{\sqrt{2}-f}\right)^{2/3}-1\right]\right]\} \qquad \text{(A102)}$$

for the properties of quartz (Lamb and Whitman, 1964, Ko and Scott, 1967, White, 1964)

$G_s = 4.783 \times 10^6$ psi

$\nu_s = 0.15$

$f = 0.5$

the strain at failure is

$$\varepsilon_{22_f} = 3.438 \times 10^{-3}\ \sigma_o^{2/3} \text{ (in percent)} \qquad \text{(A103)}$$

and $\gamma_t = \varepsilon_{22_f}$ for $\nu_s = 0$.

which is the threshold strain γ_t for the array. Thus an equation is plotted in Fig. 21 together with the other expressions for γ_t for the other arrays for easy comparison.

B3 The Face Centered Cubic Array Subjected to Triaxial Loading

The triaxial loading of a Face Centered Cubic Array was solved by Brauns and Leussink (1970). In this work, the stress-strain relationship is not obtained for the whole range of values of σ_{22}/σ_o but only for those which make the array statically determinate. It is extremely hard to determine the values of compliances for cross anisotropic loading (Duffy and Mindlin, 1957); therefore once sliding occurs and the number of contacts decreases from 12 to 8, the array becomes statically determinate and it is possible to compute a stress-strain relation up to the point that the array fails (range b - Fig.

B2). Once the array has failed, simple geometric considerations make the computation over the strain range c possible (Fig. B2).

Consider the fcc array in Fig. B1a and the cross anisotropic loading as shown. The free body diagram of the octant of sphere A is shown in Fig. B1b. The equilibrium conditions yield

$$N + T = \sqrt{2}\, R^2\, \sigma_1 \tag{A104}$$

$$N - T + N_1 = 2\sqrt{2}\, R^2\, \sigma_3 \tag{A105}$$

Also the sum of the displacements around a closed path must vanish (Duffy and Mindlin, 1957), which yields

$$a_1 - a + \delta = 0 \tag{A106}$$

The normal compliance is found to be

$$C_n = \frac{da}{dN} = \frac{1-\nu_s}{[3(1-\nu_s)G_s{}^2RN]^{1/3}} \tag{A107}$$

and the Tangential Compliance

$$C_t = \frac{d\delta}{dT} = \frac{2-\nu_s}{2[3(1-\nu_s)G_s{}^2RN]^{1/3}} * \left[f\,\frac{dN}{dT} - \frac{1 - f\,\frac{dN}{dT}}{[1 - \frac{T}{fN}]^{1/3}}\right] \tag{A108}$$

The strain is

$$\epsilon_{11} = \frac{1}{2R}\,(a + \delta) \tag{A109}$$

Integrating the compliances and substituting the results into eqn. (A109), we find after transforming the forces into stresses that the strain, ϵ_{11}, is given by

$$\varepsilon_{11} = \left[\frac{3\sqrt{2}(1-\nu_s)}{8G_s}\right]^{2/3} * \left\{2\left[\frac{1}{1+f}\left(\frac{\sigma_{11}}{\sigma_{33}}\right)\right]^{2/3} - \left[2 - \frac{1-f}{1+f}\left(\frac{\sigma_{11}}{\sigma_{33}}\right)\right]^{2/3} - 1\right\} \sigma_{33}^{2/3} \quad \text{(A110)}$$

this expression being valid only for the range of $(\sigma_{11}/\sigma_{33})$ in which the array is statically determinate, that is 8 contacts per sphere (range b in Fig. B1).

Failure is defined again as sliding, but this time when the whole array fails, that is when the number of contacts from 8 reduces to none.

Using the same criteria as in the other arrays, the critical stress ratio at which the array fails is

$$\left(\frac{\sigma_{11}}{\sigma_{33}}\right)_f = 2 \frac{1+f}{1-f} \quad \text{(A111)}$$

The above equation is plotted in Fig. 24.

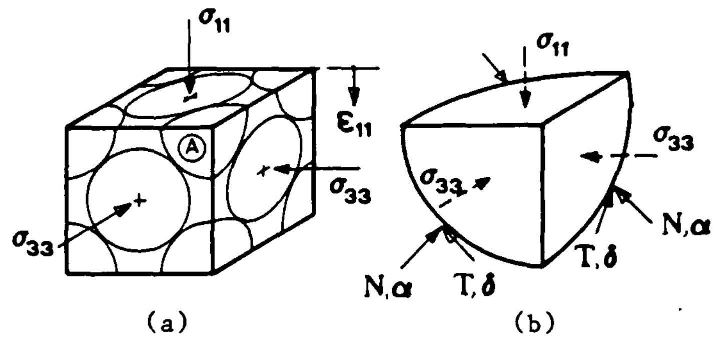

Fig. B1 a) Representative Unit Volume of an fcc Array with State of Stress
b) Sphere Centered at Apex A with Applied Stresses, Contact Forces and Displacements (Brauns and Leussink, 1970)

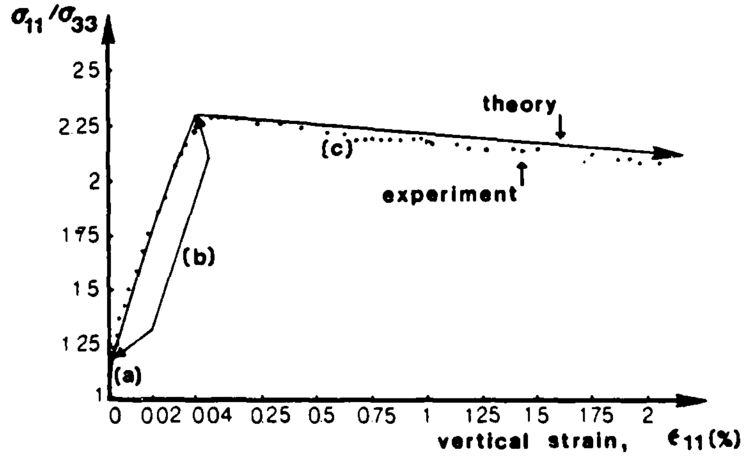

Fig. B2 Triaxial Compression of an fcc Array of Glass Spheres: Analytical and Experimental Results (Brauns and Leussink, 1970)

END

12-86

DTIC